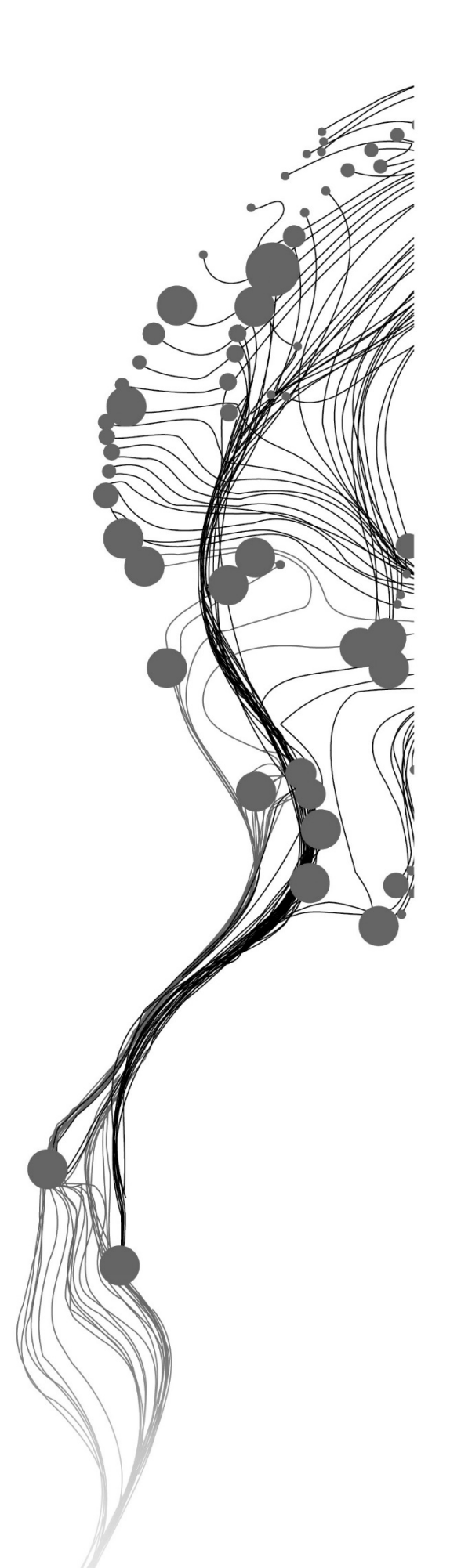
COMBINING SATELLITE-BASED ET TIME SERIES WITH INTEGRATED MODELING OF A WETLAND

NGABO JEAN LEONCE 5th JUNE, 2021

SUPERVISORS:

First supervisor: Dr.Z. Vekerdy (Water Resources Department)
Second Supervisor: Dr.M.W. Lubczynski (Water Resources Department)



COMBINING SATELLITE-BASED ET TIME SERIES WITH INTEGRATED MODELING OF A WETLAND

NGABO JEAN LEONCE

Enschede, The Netherlands, 5th June, 2021

Thesis submitted to the Faculty of Geo-Information Science and Earth Observation of the University of Twente in partial fulfilment of the requirements for the degree of Master of Science in Geo-information Science and Earth Observation.

Specialization: Water Resources and Environmental Management

SUPERVISORS:

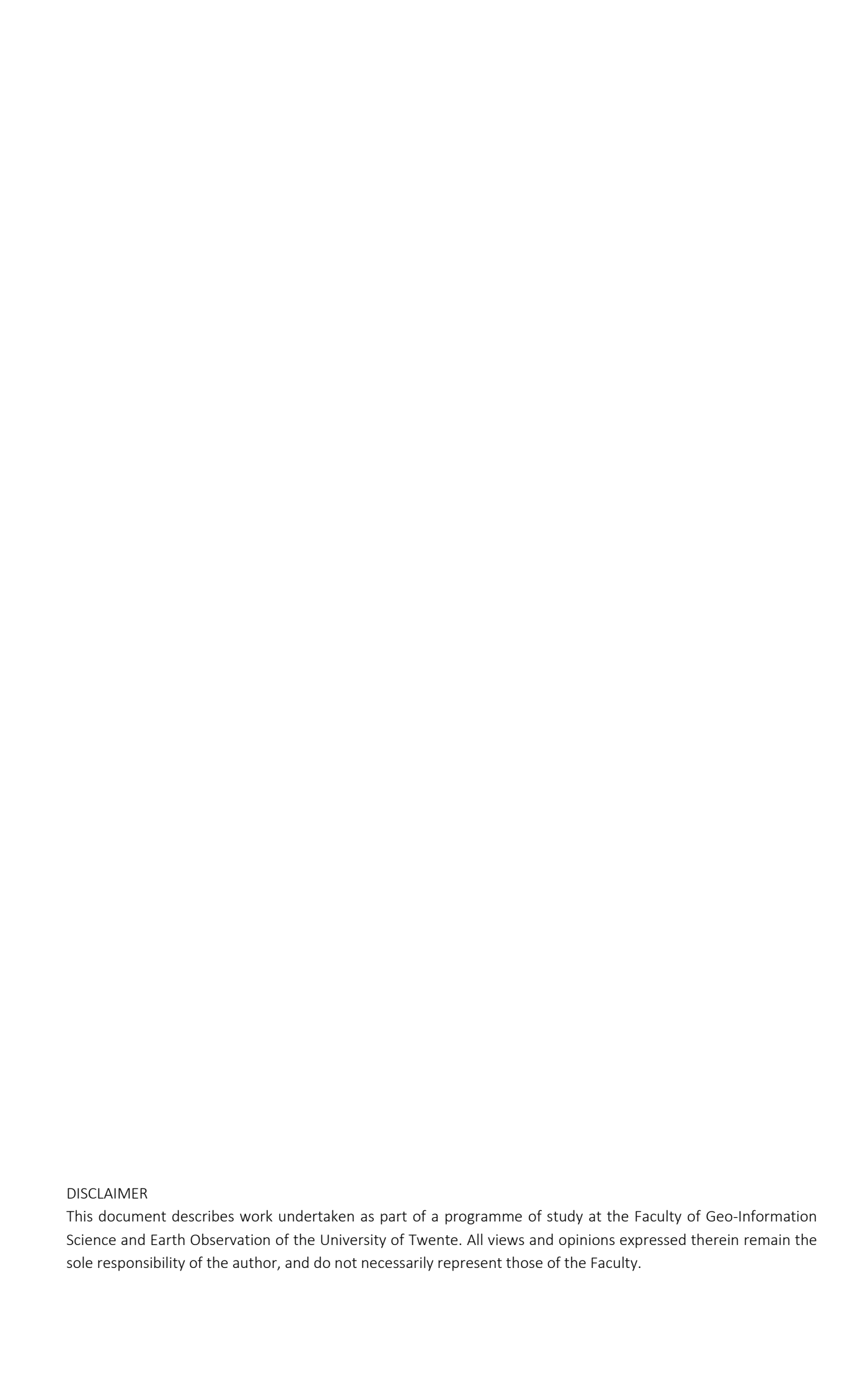
First supervisor: Dr. Z. Vekerdy (Water Resources Department)

Second Supervisor: Dr.M.W. Lubczynski (Water Resources Department)

THESIS ASSESSMENT BOARD:

Dr.Ir.C. van der Tol (Chair)

Dr.hab.Prof.P.J. Gurwin (External Examiner, University Wraclow, Poland)



ABSTRACT

Aamsveen, a fen wetland located to the South-East of Enschede, on the border of Netherlands and Germany. It is considered a recreational area and people frequently visit the area due to the aesthetic view of different vegetation species present in the area. Heath, grass, evergreen, and deciduous trees are the predominant vegetation of the wetland. The surface and groundwater interactions play a key role in the hydrology of the wetland. Different studies have been carried out in the region to analyze the interactions between the surface and groundwater such as a previous one by Emmanuel (2019).

The aim of this research is to develop a method that integrates satellite-based ET time series in integrated groundwater modelling using the example of Aamsveen. It was achieved by improving the existing integrated groundwater model of Aamsveen by defining the spatial and temporal distributaion of the potential evapotranspiration (ET_p) which was not perfectly considered in the previous wetland model (Emmanuel's model). Two different methods that provide ET_p (satellite-based ET_p and K_c-based ET_p) were adopted and compared to each other to define which one is suitable for improving the current wetland model. Besides, a new approach to calibrate and validate the wetland model was developed and applied. The approach consisted of integrating satellite-based actual evapotranspiration (ET_a) in the calibration and validation. It was done by matching the simulated ET_a that includes interception to the satellite-based ET_a for a calibration period of 4 years (1st January 2012 to 31st December 2015). Then the model was validated from 1st January 2016 to 31st December 2018 using also satellite-based ET_a. This new method was additional to the normal calibration method with state variables (groundwater heads and streamflow) which was used in the Emmanuel's model. A comparison of the Emmanuel's model and the current model was carried out.

The results demonstrated that satellite-based ET_p (MOD16A2) time series values after bias correction were in the same range as k_c -based ET_p with an R^2 of 0.95 and RMSE of 0.8 mm. However, in terms of representing the spatial variability of Aamsveen, K_c -based ET_p was showing more details than the MOD16A2 product. Therefore, K_c -based ET_p data were used in the wetland model. In the calibration, the simulated ET_a plus canopy interception was matched to MOD16A2 ET_a with an R^2 of 0.84 and RMSE of 0.0005. The comparison of both models (the current model and Emmanuel's model) showed that the highest outflow component from the area is ET_a although the rates are different. The ET_a plus interception in the Emmanuel's model was 63.2% of rainfall (P) while in the present model, ET_a with interception is 56.2% of P in the same calibration period (1st January 2012 to 31st December 2015).

Keywords: Aamsveen, Actual evapotranspiration (ETa), potential evapotranspiration (ETp)

ACKNOWLEDGEMENTS

First and foremost, I thank God for his grace and countless blessings. He has given me knowledge, health, and strength to be able to complete my thesis.

I would like to thank my family, especially my parents for being always there for me, their advice and encouragement have driven me all along through this challenging period. I will always do my best to make them proud.

I would like to express my gratitude to the Kingdom of the Netherland that has financially supported me to undertake this MSc program.

My sincere gratitude to Dr. Zoltan Vekerdy, my first supervisor for his tremendous support and guidance throughout my research phase. Despite his tight schedule, he managed to get time for me with regular discussions which have been important to accomplish this MSc thesis. Maybe I have not met his expectations but honestly, I have significantly gained a lot and improved my thinking attitude through the meetings we had. I will forever be thankful for that.

I am also very thankful to Dr. Maciek Lubczynski, my second supervisor for his explanations and tips that were crucial in understanding my research. He helped me to have control of the integrated groundwater model of Aamsveen by providing a better approach. I was lucky to have him as my lecturer and supervisor.

I would like to think Ir. Arno Van Lieshout (Course director of the department of water resources and environmental management) for the meetings we had. He advised and helped me to choose the right topic that was related to my background. I thank also Mr. Bas Retsios for helping me in coding and solving ILWIS related problems.

Special thanks to Stephen George Emmanuel and Mostafa Gomaa Mohamed Daoud, former ITC students. They have done their best to share their experience and knowledge, especially in groundwater modeling. Honestly, I have enjoyed having discussions with them.

Last but not least, I think all my classmates for supporting me through this tough period. Special thanks to Ranit who has been very helpful when developing and adjusting codes that were used in this research.

TABLE OF CONTENTS

1.	INTRODUCTION		
	1.1.	Background	1
	1.2.	Problem statement	2
	1.3.	Research objectives	3
	1.4.	Research novelty	3
2.	THEC	PRETICAL BACKGROUND	4
3.	STUDY AREA		
٠.	3.1.	Location	
	3.2.	Topography and landcover	
	3.3.	Monitoring Network in Aamsveen	
4.	RESEARCH METHODS		
	4.1.	Estimating the spatial and temporal distribution of ETp	11
	4.2.	Implementation of the model	16
	4.3.	Comparison between current and Emmanuel's model	29
5.	RESU	LTS AND DISCUSSIONS	30
	5.1.	Validation and bias correction for MOD16A2 product	30
	5.2.	ET ₀	32
	5.3.	Defining K _c	32
	5.4.	Comparison between MOD16A2 ET _p and K _c based ET _p	36
	5.5.	Interception rates	39
	5.6.	Calibration Results	40
	5.7.	Validation Results	48
	5.8.	Water balance	52
	5.9.	Temporal and spatial variability of water fluxes	55
	5.10.	Comparison of the current study with the study Emmanuel (2019)	58
	5.11.	calibration and validation experience with satellite-based ETa	60
6.	CONCLUSION AND RECOMMANDATION		
	6.1.	Conclusion	61
	6.2.	Recommendation	62

LIST OF FIGURES

Figure 1: Aamsveen Catchment (left) and Aamsveen land cover map (right)	8
Figure 2: Monitoring Network in Aamsveen	9
Figure 3: Flowchart of the research	10
Figure 4: MODIS land cover (left) vs the land map of Aamsveen (right), both represent 25 th Septo	
Figure 5: Winter image demonstrating how heathland is turning into bushland in Aamsveen	
Figure 6: Conceptual model of Aamsveen defined by Emmanuel (2019)	
Figure 7: Aamsveen sand (left) thickness map and peat thickness defined by Emmanuel (2019)	
Figure 8: Root depth map	
Figure 9: Observed stream flow for validation	28
Figure 10: MOD16A2 ET _p validation results	31
Figure 11: Time series ET_0 produce by Penman-Monteith model using ILWISILWIS	32
Figure 12: Time series average NDVI value for heath, Deciduous, and built-up area	33
Figure 13: Summer (left) and winter (right) average variation of NDVI for heath	34
Figure 14: Summer (left) and winter (right) average variation of NDVI for deciduous	34
Figure 15: Time series pixel comparison between MOD16A2 and Kc based ETp (average daily ET_{p}	
values taken every eight days)	36
Figure 16: Correlation between MOD16A2 and K_{c} based ETp	36
Figure 17: Spatial pattern comparison between MOD16A2 ETp and K_c based ETp that represent	
summer period (all images represent 12th of August each year from 2012 to 2015)	37
Figure 18: Spatial pattern comparison between MOD16A2 ETp and K_{c} based ETp that represent $ u$	vinter
period (all images represent 2 nd of February each year from 2012 to 2015)	38
Figure 19: Interception rate for summer (left) and winter (right)	39
Figure 20: Spatial variability of HK for layer 1 (left) and layer 2 (right)	41
Figure 21: Spatial variability of SY for layer 1(left) and layer 2 (right)	42
Figure 22: Spatial variability of VK for layer 1 (left) and layer 2 (right)	43
Figure 23: B35A0178 (calibrated vs observed heads)	44
Figure 24: B35A0835 (calibrated vs observed heads)	44
Figure 25: B35A0836 (calibrated vs observed heads)	
Figure 26: B35A0837 (calibrated vs observed heads)	
Figure 27: B35A0890 (calibrated vs observed heads)	
Figure 28: Comparison between simulated and observed streamflow	
Figure 29: Comparison between simulated ETa + interception and MODIS16A2 ETa	
Figure 30: Scatter plot for MOD16A2 ETa and Simulated ETa + Interception (calibration)	
Figure 31: B35A0178 (validated and observed heads)	
Figure 32: B35A0835 (validated and observed heads)	
Figure 33: B35A0837 (validated and observed heads)	
Figure 34: B35A0836 (validated and observed heads)	
Figure 35: B35A0890 (validated and observed heads)	
Figure 36: Comparison between validated streamflow and simulated streamflow	
Figure 37: Comparison between MOD16A2 and simulated ETa (validation)	51

Figure 38: Scatter plot between MOD16A2 and Simulated ETa + Interception (validation)	. 51
Figure 40: Temporal variability of important groundwater fluxes	. 55
Figure 41: Spatial variability of R_g (left), ET $_a$ excluding interception (Middle) and I_{exf} (right)	. 56
Figure 42: Sensitivity analysis on groundwater heads	. 57
Figure 43: Sensitivity analysis on ET _a + interception	. 57
Figure 44: Previously calibrated groundwater head for piezometer B35A0837 by Emmanuel (2019)	. 58
Figure 45: Previously simulated streamflow at Aamsveen camping Area by Emmanuel (2019)	. 59
Figure 46: Budget comparison between Emmanuel's model and the current model of Aamsveen	. 59

LIST OF TABLES

Table 1: Interception rate of different land cover classes (Miralles et al., 2010)	20
Table 2: SFR package input data	25
Table 3: Initial hydraulic and storage parameters of the present model	27
Table 4: average bias fixing factor	30
Table 5: K_c values for different land cover classes for the growing	35
Table 6: K_c values for different land cover classes for the inactive season	35
Table 7: Results of calibrated parameters	40
Table 8: Accuracy assessment between observed and simulated heads	46
Table 9: Accuracy assessment for the validated heads	50
Table 10: Water budget components of Aamsveen	53
Table 11: Surface and unsaturated zone budget	54
Table 12: Saturated zone budget	54
Table 13: Entire model budget	54

1. INTRODUCTION

1.1. Background

Wetlands are water-inundated areas that create and contribute to the development of diverse communities of trees and animal species that live and depend in these productive areas (Mitsch & Gossilink, 2000). These delicate ecosystems occupy only 6.2% -7.6% of the earth's surface (Liu et al., 2020). Nevertheless, they are essential and valuable areas that preserve water, provide food, and shelter for wild animals (Mitsch & Gossilink, 2000). They are considered the kidneys of the Earth due to their capability to purify water (Wu & Chen, 2020). Furthermore, wetlands naturally protect people from flood risks by retaining water after heavy rainfall (Wu et al., 2020). However, in the last 100 years, half of the world's wetlands disappeared and the wetlands areas are still decreasing due to the current drought events and land-use changes mainly triggered by anthropogenic activities (Zedler & Kercher, 2005). Consequently, animal and plant species that are part of the wetlands' ecosystem are threatened due to their continuous destruction. Humanity is failing to effectively protect, develop, and properly manage these vulnerable areas of such importance.

Different policies and strategies have been implemented to protect fragile natural areas including wetlands. For example, a network of protected and improved natural areas in the European Union (EU) is known as Natura 2000. Aamsveen is an example of such a protected wetland. Various actions have been adopted regarding species habitat development and conservation in terms of quantity and quality to preserve the wetland (Bell et al., 2018). Examples of such actions include termination of exploitation activities in the wetland, creating a proper drainage system, construction of retaining reservoirs, etc. These activities need to be endorsed with more scientific approaches for the sustainable monitoring and management of wetlands. Deep insight and accurate estimation of the governing hydrological fluxes such as evapotranspiration, runoff, precipitation are very crucial for the restoration and long-term management of wetlands. Therefore, an effective and efficient technology or method is needed to rapidly detect, quantify, and scientifically analyze a change in a wetland's water regime and the corresponding ecosystem.

1

1.2. Problem statement

The health of wetlands depends on the balance of the inflow and outflow fluxes. Modeling wetlands to determine this balance requires integrated modeling of the groundwater and surface water systems. Earth observation can support the quantification of evapotranspiration in a spatially-temporally distributed manner, which can be used for defining the forcings and supporting the calibration. Aamsveen, a small wetland on the border of Germany and the Netherlands is the study area of this research, and different research studies have been conducted earlier in the region. This study will complement those studies. Humans intervened in this area from time to time to restore and preserve the wetland by terminating peat extraction in 1969, changing the open channel of the main stream with underground pipes in 1983, a new channel construction around the wetland, etc. Studies have also been carried out to assess the impact of these changes on the wetland. Lianghui (2015) was checking if the wetland was restored by analyzing the change in vegetation extent by assessing NDVI of different years and the groundwater level variations. She realized that changes were not significant as they were expected, therefore recommends more detailed studies. Nyarugwe (2016) concluded that the groundwater level was increasing in the wetland but could not provide details on surface-groundwater interaction. Later, Bakhtiyari (2017) improved the analysis by developing a model and provided details on surface-groundwater interaction using a steady-state model. However, a steady-state model is not sufficient to rely on for a wetland with highly dynamic fluxes varying both temporally and spatially. Therefore the study of Emmanuel (2019) analyzed the variations in surface-groundwater interaction with a transient model. He defined the water balance from this integrated model of the wetland and quantified the most important fluxes in different stress periods. He concluded that actual evapotranspiration is larger than the inflow, and this why the wetland is drying. In his transient model, the spatial and temporal variability of potential evapotranspiration (ET_p) were not fully incorporated. The landcover map produced did not consider the bushland which has been growing and dominating the heathland recently (i.e, the native vegetation of the wetland is disappearing). Besides, The model was calibrated insufficiently with in situ data considering both the spatial and temporal aspects of the groundwater, but It is not exactly understood how good the simulation of the actual evapotranspiration is.

Nowadays, remote sensing is emerging as an effective and efficient tool to sustainably control and preserve wetlands (Dahl et al., 2006). Different satellite-based evapotranspiration products are available with detailed spatial and temporal information of any area of interest. Therefore, the present research develops a method to integrate satellite-based evapotranspiration with the integrated groundwater model of Aamsveen.

1.3. Research objectives

The main objective of this research is to develop a method that utilizes satellite-based evapotranspiration time series in integrated groundwater modeling, using the example of Aamsveen.

The specific objectives of the research are:

1. To improve the ET_p of the existing integrated model of Aamsveen by defining the spatial-temporal distribution of the ET_p.

<u>Research question 1.</u> How much does the defined spatial and temporal ET_p influence the simulation of the dynamics of the groundwater heads, stream flows, and groundwater fluxes?

2. Calibrate and validate the integrated groundwater model with satellite-based ET_a

Research question 2. Is the calibration and validation of the wetland model possible with three components (groundwater heads, stream flow, and satellite-based ET_a)?

3. Comparison of the improved transient model of Aamsveen to the previous one of Emmanuel (2019).

Research question 3. How much did the modifications affect the simulation results?

1.4. Research novelty

Different studies have been conducted in the Aamsveen and they all highlighted that the region is drying. Emmanuel's model which is the previous transient model of Aamsveen did not perfectly consider the spatial and temporal variation of ET_p . It was estimated by multiplying the crop coefficient (K_c) of different landcover classes with daily reference evapotranspiration (ET_0) obtained from the nearest KNMI meteorological station. The landcover map used in this calculation did not consider the bushes that have been growing in the wetland. Besides, the model was calibrated with four groundwater monitoring wells (piezometers) and one stream gage in an area of 23km^2 as demonstrated in Figure 2. These in situ data are insufficient to rely on. Therefore this research aims at improving the previous transient model by integrating spatial and temporal variation of ET_p , and calibrate and validate the existing Aamsveen model with satellite-based ET_a .

THEORETICAL BACKGROUND

Concepts and methods adopted in this research are briefly explained in this section using information retrieved from related literature.

2.1.1. Evapotranspiration (ET) terms

In hydrology, three terms related to evapotranspiration (reference, potential, and actual) are often misused and wrongly applied. Thus, for the sake of suitable analysis and usage, the following subsections clarify them.

2.1.1.1. Reference evapotranspiration (ET₀)

It is the rate of evapotranspiration from a reference crop mostly grass with 12 cm of uniform height with unlimited water supply in the soil (Doorenbos & Pruitt, 1977). It is usually estimated by using the FAO Penman-Monteith method (Allen et al, 1998). ET_0

2.1.1.2. Potential evapotranspiration (ET_p)

It is the maximum evapotranspiration from a vegetated area with an optimum supply of water in the soil. Normally, it is estimated by multiplying ET₀ with a crop coefficient (K_c) that is highly dependent on different species of crop and crop height (Perry et al., 2009)

2.1.1.3. Actual evapotranspiration (ET_a)

It is the real or exact amount of evapotranspiration under certain soil conditions and water availability. When enough water is available in the soil, ET_a is equal to ET_p . In contrast, ET_a is less when a limited amount of water is available in the soil.

2.1.2. Calculation of ET terms

 ET_a and ET_p can be directly retrieved from satellite-based products. They are estimated using algorithms developed from models such as the Penman-Monteith model, Priestley and Taylor model, etc. Moderate Resolution Imaging Spectrometer product (MOD16A2) is an example of a such satellite-based product that can directly provide ET_p and ET_a estimated using the Penman-Monteith model. According to the MOD16A2 algorithm, ET_p and ET_a is the sum of water evaporated from the soil surface, canopy interception, and transpiration from plant tissues. ET_p and ET_a are controlled by aerodynamics resistance and surface resistance parameters. These two parameters are assumed to be zero when estimating ET_p and more details can be found in Running et al. (2019).

In Egypt, Ayyad, Al Zayed, Ha, & Ribbe (2019) made a comparison of three different satellite products that directly provide ET_a. Those products are Earth Engine Evapotranspiration Flux (EEFLUX) with 30 m resolution, US Geological Survey (USGS) product (1 km resolution) which

uses Simplified Surface Energy balance model (SSEBop) to produce daily ET_a. The third product is the MOD16A2 with a 500 m resolution. The study was conducted to find the best performing product with reasonable estimates based on their advantages and limitations for optimal irrigation water management. However, no validation was conducted due to the unavailability of ground data.

Another widely used method to calculate ET_p is the multiplication of crop coefficient (K_c) to ET_0 which can be estimated using the Makkink equation, or Penman-Monteith model, etc. The K_c coefficient (value) depends on the vegetation type and development stages of that particular vegetation. Normally, vegetations have high K_c during the growth season and drops during the inactive season. One single vegetation can have one or more different k_c values depending on its growing seasons. It is important to accurately estimate K_c values for a reliable spatial and temporal variable ET_p .

Different studies have proved that the k_c value can be linked with vegetation indexes such as Leaf Area Index (LAI) or Normalized Difference Vegetation Index (NDVI). The latter is a good indicator of the health and growth of vegetations (Park et al., 2017). Generally, in the summer the K_c and NDVI values are higher than in the winter. It is because plants are photosynthetically active when enough energy or light is available. Analyzing NDVI variations is essential in determining changes in vegetation characteristics within a region throughout time. NDVI of a certain vegetation type can increase if either the density of the same plant is increasing or another different plant is growing in the same area.

Depending on the area and vegetation type, different linear regression models have been developed and demonstrated a strong correlation between simulated K_c (using remote sensing vegetation indices) and measured K_c . Park et al., (2017) (equation 2-1) combined LAI (leaf area index) and NDVI (normalized difference vegetation index) to derive Kc values for a mixed forest and got a correlation coefficient of 0.80. Choudhury et al., (1994) (equation 2-2) developed a generally linear relationship between K_c and NDVI on a vegetated surface and showed a correction of 0.81. Kamble et al., (2013) (equation 2-3) used an almost similar relationship as Choudhury et al., (1994) for an irrigated agriculture field and got a correlation of 0.91 between measured and simulated K_c .

$$K_c = (0.55 * NDVI) - 0.01 * LAI$$
 (2-1)

$$K_c = (1.46 * NDVI) - 0.26 \tag{2-2}$$

$$K_c = (1.46 * NDVI) - 0.17$$
 (2-3)

2.1.3. Integrated groundwater modelling of a wetland

In a wetland ecosystem, there is a surface-groundwater interaction that varies spatially and temporally resulting in a significant fluctuating hydrological flow pattern (Emmanuel, 2019). The flow regime of this sensitive ecosystem is governed by different fluxes including water inflow and outflow, infiltration, exfiltration, stream runoff, evapotranspiration, etc. These fluxes are responsible for a change in the water storage of the wetland. The quantity and quality of

water resources are affected by this continuous dynamic interaction of both surface and groundwater (Sophocleous, 2002). Modeling software is used to simulate and quantify all the above-mentioned fluxes. In groundwater modeling, commonly used models are numerical models though the analytical do exist as well. The analytical models are based on assumptions, highly simplified especially in considering the spatial heterogeneity, hence it is inappropriate for most practical groundwater problems (Rientjes, 2016). The advantage of using numerical models over analytical is that they can deal with the transient or steady-state with complex boundaries and complexity of a network of sources and sinks (Anderson et al., 2015a). Numerical models can be either a single domain or multi-domain. The single-domain considers only one part of hydrology for modeling, either surface or groundwater modeling where an arbitrary recharge is determined. In this case, the surface and groundwater are not dynamically linked. On the other hand, in the multi-domain models, the different parts of the hydrological system are dynamically linked. Some examples of numerical models are MODFLOW, IHM, SWATMOD, FEFLOW, etc (Anderson et al., 2015b). MODFLOW-NWT is the Newton formulation of MODFLOW-2005 that represents surface and groundwater interaction (Harbaugh, 2005). This version was built to handle the problem of non-linearity of the drying and wetting of cells. This problem occurs when the Unsaturated Zone Flow package (UZF1), Streamflow Routing package (SFR), and Lake (LAKE) package are used. The UZF1 quantifies the recharge from rainfall and interception loss, The SFR packages link rivers or streams. The lake package represents volumetric interaction between surface water bodies and groundwater (Anderson et al., 2015d).

Interception and rooting depth of different landcover classes are also required for integrated groundwater modelling. Interception is the amount of rainfall that remains on the vegetation canopy and returns to the atmosphere by evapotranspiration (Van Meter et al., 2016). The rooting depth is the deepest level in the soil that individual crop roots can reach (Lopez et al., 2017).

2.1.4. Integrating satellite-based ET and modelling

Scientific research had been conducted and confirmed that satellite-based products are reliable and suitable in the hydrological modeling domain. Lekula, Lubczynski, Shemang, & Verhoef (2018) demonstrated that satellite-based products can be an alternative source of data in data-sparse areas. Lekula & Lubczynski (2019) combined remote sensing and integrated hydrological modeling to analyze the water balance in the Central Kalahari Basin using the MODFLOW-NWT model where in-situ measurements monitoring networks (stream gauges and piezometers) were insufficient. The accuracy between the simulated and observed heads of their calibrated model was in the range of 0.02m to 2.70 m of MAE and 0.02m to 3.13m of RMSE. A large-scale ET_p time series (110 km resolution) downloaded from USGS FEWSNET was used as a driving force in their model. It was concluded that satellite-based ET_p can provide reasonable and good spatial and temporal details of any area of interest for integrated groundwater modeling.

3. STUDY AREA

3.1. Location

Aamsveen is located just a few kilometers from Enschede city center on the border of the Netherlands and Germany as shown in Figure 1. The whole catchment is around 23 km² and contains an inland wetland of around 4 km². It is a fen wetland and considered a recreational area since people frequently visit the area due to the aesthetic view of different vegetation species present in the area. The surface water network of the wetland is formed by two reservoirs and different interconnected streams. The main one is called Glanerbeek. This mainstream flows from the southwest to the northeastern part of the wetland and has a direct connection with the Aamsveen reservoirs (Emmanuel, 2019).

3.2. Topography and landcover

Aamsveen is a flat region. The elevation varies within the range of 38 to 54 meters. In Emmanuel's model, the landcover map of the region was improved by considering more landcover classes (9 classes) as shown in Figure 2. A sentinel-2A image of 25th September 2016 was used for the landcover classification. The area is dominated by grass and forests (evergreen and deciduous trees) with a percentage of 38% and 21% of the total area respectively. Heathland is also abundant in the region covering an area of 13%. The remaining area is covered by built-up area (17%), agriculture area (10%), and water (1%).

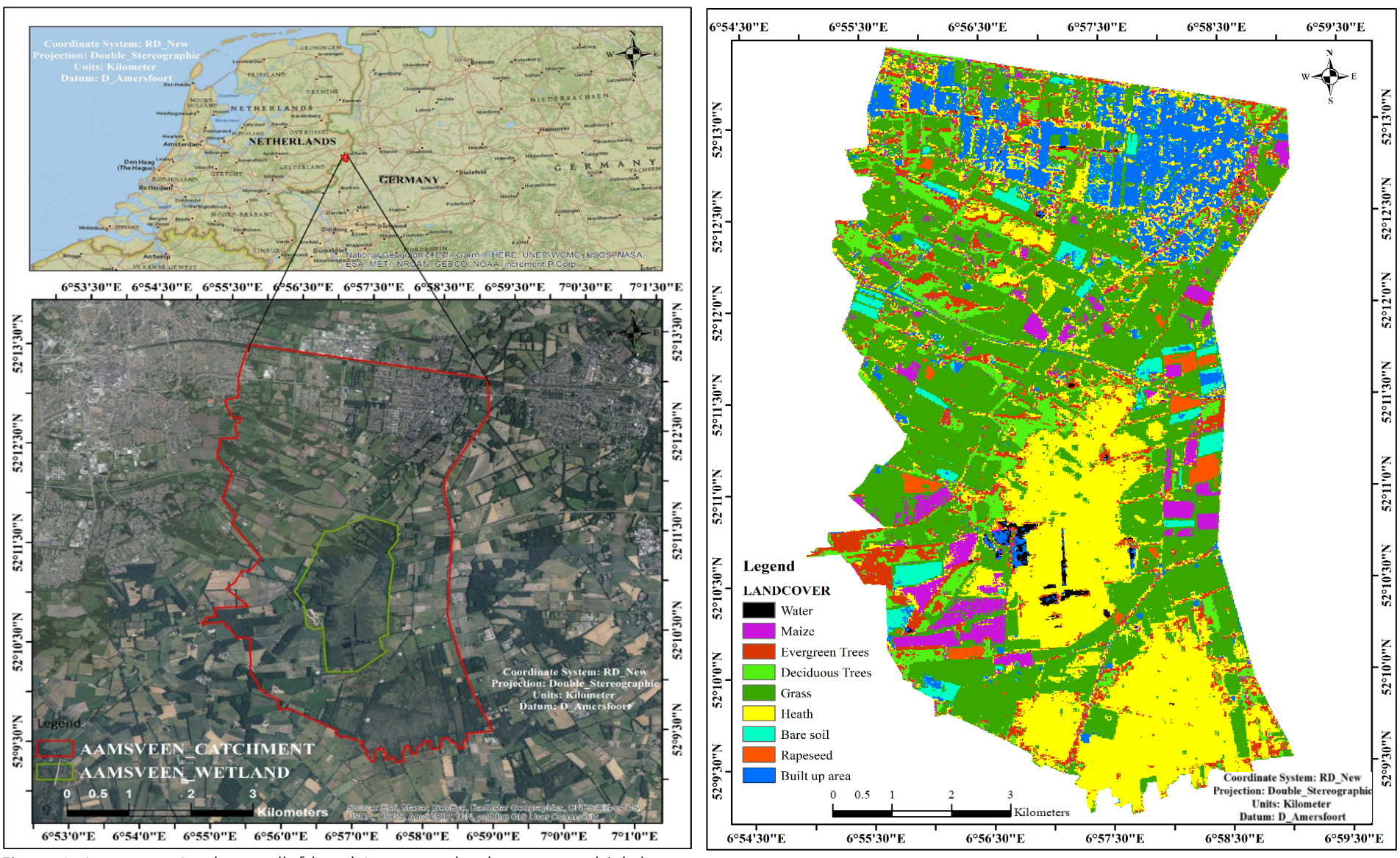


Figure 1: Aamsveen Catchment (left) and Aamsveen land cover map (right)

3.3. Monitoring Network in Aamsveen

Figure 2 demonstrates the monitoring network that consists of stream gauges and piezometers. In Emmanuel's model, the calibration was carried out using four piezometers presented in Figure 2 as old piezometers. They are all located in the wetland part of the modelled area. In the current model, the calibration was conducted using an additional piezometer named "New piezometer" in Figure 2 and it is located just outside the Aamsveen wetland. Figure 2 also provides the network of streams, drains, and reservoirs in the study area. The Digital Elevation Model (DEM) of the Aamsveen catchment was used to demonstrate upstream and downstream areas of the Aamsveen catchment.

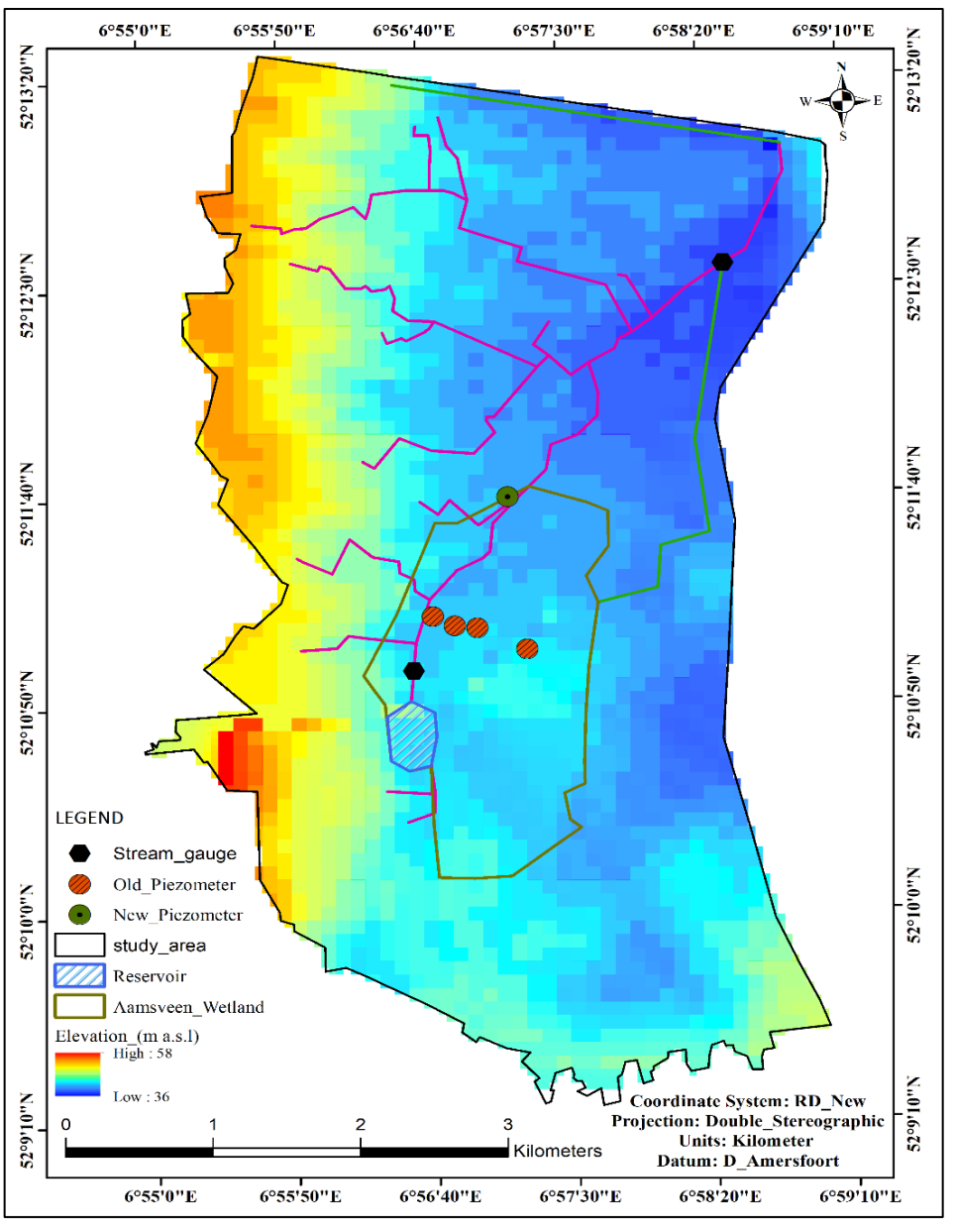


Figure 2: Monitoring Network in Aamsveen

4. RESEARCH METHODS

Figure 3 shows different methods applied accomplish the specific objectives. The data and information were obtained from four different sources; satellite data, field data, literature review, and modelgenerated data from the previous transient model of Aamsveen.

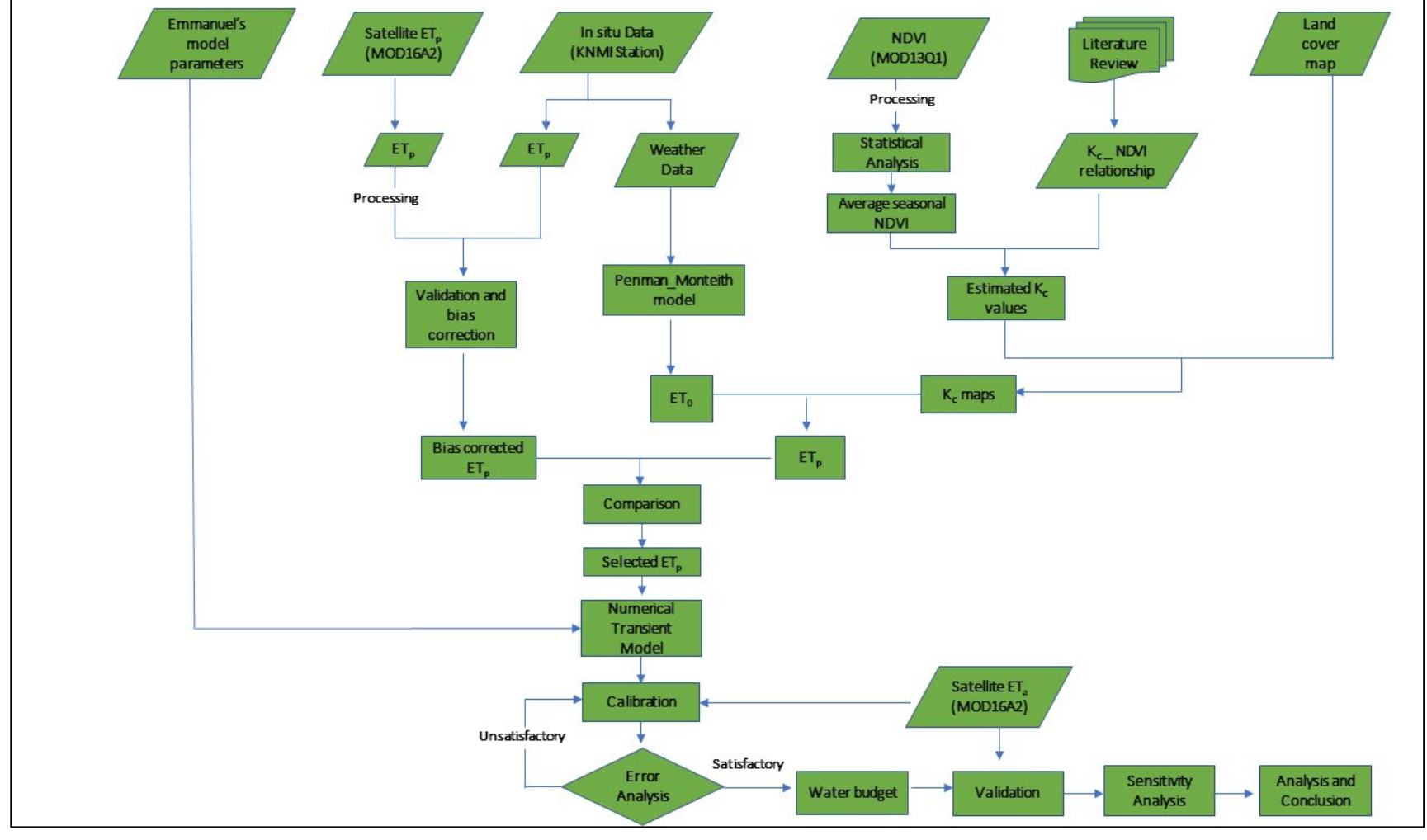


Figure 3: Flowchart of the research

4.1. Estimating the spatial and temporal distribution of ETp

To achieve the first specific objective, two different methods (satellite-based ET_p and K_c -based ET_p) that provide ET_p were analyzed and compared to each other to define which one is better for the existing integrated groundwater model of Aamsveen. The comparison was based on analyzing the temporal and spatial variations of ET_p .

4.1.1. Satellite-based ETp

The MOD16A2 product of MODIS, was used to retrieve ET_p of the study area. The product was selected because it can provide both ET_p and ET_a that are both needed for this research. In addition to that, it has high spatial resolution relatively to the other available satellite-based ET products outlined in section 2.1.2. However, a land cover map used in the MOD16A2 algorithm did not perfectly represent the vegetation of the study area. It contains some generic land cover classes and their spatial distribution does not match the existing land cover. This was noticed after the comparison with the land cover map used in Emmanuel's model shown in Figure 4.

4.1.1.1. Processing MOD16A2 product

The time series (1st January 2012- 31st December 2018) of the MOD16A2 product was downloaded using the AppEEARS tool. It's a tool developed by NASA to access MODIS data simply and efficiently (https://urs.earthdata.nasa.gov/). The images obtained were in tiff format with 8 days sum of ET_p (temporal resolution) and 500m (spatial resolution). The MOD16A2 product algorithm runs on a daily basis and a summation of ET_p is provided over every 8 day period (Running et al., 2019). For batch processing, a python script was developed and used to extract valid data of ET_p (ranges from -32767 to 32760). Then a scaling factor of 0.1 was multiplied to the valid data to obtain real values of ET_p in mm/8day.

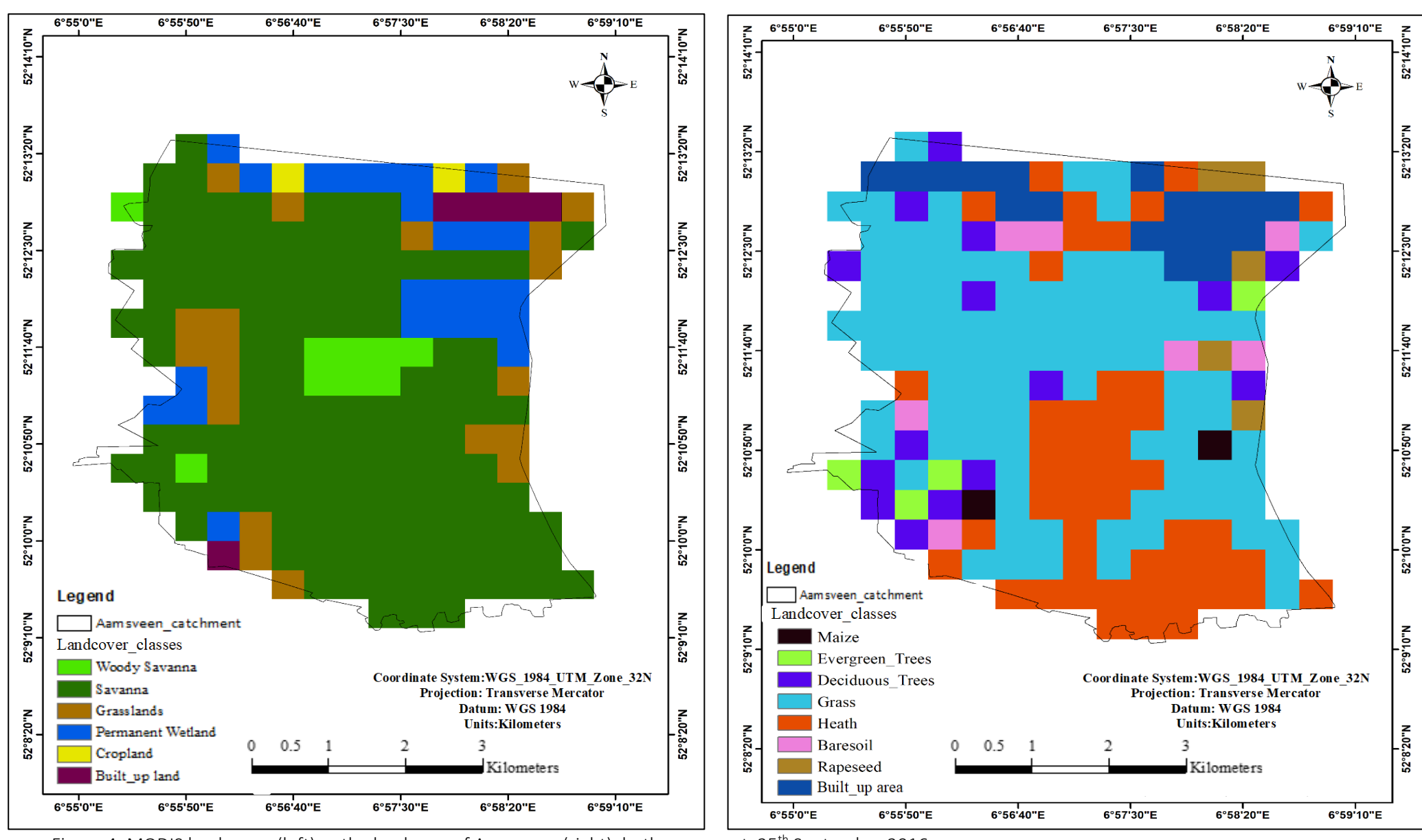


Figure 4: MODIS land cover (left) vs the land map of Aamsveen (right), both represent 25th September 2016

4.1.1.2. Validation of MOD16A2 product

Two in situ KNMI stations, TWENTHE, and HUPSEL located at about 6 km and 21 km from the Aamsveen, respectively, were used to validate the MOD16A2 ET_p product using the point to pixel method. The method consists of extracting time series ET_p values from the pixels where the stations are located (Fensholt & Sandholt, 2005).

During validation, statistical measures of accuracy were determined (RMSE and R²) and analysis was made. A systematic error (bias) with a periodicity or seasonal trend was noticed. Hence, a simple linear scaling approach was adopted for bias correction as demonstrated in equation 4-1. The approach uses an average seasonal bias correction factor (equation 4-2) based on the ratio between in situ data and satellite data (Teutschbein & Seibert, 2012).

$$ET_n^{\prime\prime} = b * ET_n^{\prime} \tag{4-1}$$

$$b = \left(\frac{ET_p^0}{ET_p'}\right) \tag{4-2}$$

Where

 $ET_p^{\prime\prime}$ (mm.day $^{ ext{-}1}$) Bias corrected ET_p^{\prime}

 ET_p' (mm.day⁻¹) MOD16A2 ET_p before bias correction

b (-) Average seasonal (summer, autumn, winter and spring) bias correction factor

 ET_n^0 (mm.day⁻¹) In situ ET_p obtained from KNMI stations.

After bias correction, MOD16A2 ET_p time series maps of the Aamsveen catchments were produced and compared to the time series K_c -based ET_p maps.

4.1.2. K_c based ET_p

In this approach, ET_p is estimated by multiplying K_c by ET_0 , as demonstrated in equation 4-3. The single crop coefficient approach was adopted in this research. Weather changes are included in ET_0 and vegetation characteristics and variations are included in the K_c factor (Allen et al., 1998).

$$ET_p = ET_0 * K_c \tag{4-3}$$

4.1.2.1. ET₀

ET₀ was obtained by using an extension of the Penman-Monteith model in the ILWIS software. It is simulated using weather data that include wind speed, net solar radiation, air temperature, and relative humidity.

The wind speed data (m.s⁻¹) were made available from the KNMI station (TWENTHE station). Using the attribute map function in ILWIS, wind speed data were converted into time series

raster images according to the model requirements. A 10 km*10 km raster pixel produced from the study area map, was created and time series values of wind speed were assigned to it.

Relative humidity data (maximum and minimum) and temperature data (maximum, minimum, and average) were obtained from the TWENTHE station. Daily net solar radiation data with 9km resolution were downloaded from ERA5.

4.1.2.2. Defining K_c

Based on field observation, as Figure 5 shows, in Aamsveen the heathland is turning into bushland. These changes can be monitored by considering either time-series satellite image-based classified land cover maps or time series NDVI values. In this study, the vegetation changes were defined using time series NDVI values as it would be more complex to monitor these variations with time-series satellite-based classified land cover maps. Very high spatial resolution time-series images would be required to accurately classify the growing bushes.

The approach of linking NDVI to K_c value as described in section 2.1.2 was used. The Choudhury et al., (1994) relationship was adopted because this equation was developed in a region having more or less similar characteristics as the Aamsveen catchment.

Time series of NDVI data (2012 - 2018) in CSV format with a spatial resolution of 250 m*250 m and best NDVI values of 16 days period were obtained from MOD13Q1 product through the Google Earth Engine. To prevent NDVI values of different land cover classes within the same pixel which would result in misinterpretations, a landcover map of Aamsveen was used as a reference (Figure 1). The retrieval of time series of NDVI values was conducted on important categories that include deciduous trees and heath (where bushes are increasingly dominating). Furthermore, ET_p values were assigned to the built-up areas, which was left out of consideration in Emmanuel's model. It was noticed that the built-up area is a combination of buildings, gardens, trees, etc. Therefore, NDVI values were also retrieved in those areas. Time series NDVI values of each of the above classes were obtained and statistical analysis was made.

From the NDVI statistical analysis, two seasons in the Aamsveen were noticed, an inactive season (October, November, December, January, February, and March) and a growing season (April, May, June, July, August, September). The regression coefficients were demonstrating an increase in NDVI of heathland throughout 2012 - 18 which is due to the growth of bushes. To estimate the K_c values of these specific classes, Choudhury et al., (1994) equation was used. Average NDVI values for winter months (representing the inactive season) and summer months (representing growing season) were used to estimate K_c values for the above classes. The obtained K_c values were assigned to the land cover map (Figure 1).



Figure 5: Winter image demonstrating how heathland is turning into bushland in Aamsveen

4.1.3. Comparison between MOD16A2 ET_p and K_c-based ET_p

A comparison between the bias-corrected MOD16A2 ET_p products (section 4.1.1.2) and the K_c -based ET_p (section 4.1.2) was made to define which data set to use in the modeling. The comparison was based on temporal and spatial variations of the ET_p for 2012-15.

For the spatial pattern comparison, the K_c -based ET_p time series of 20 m resolution were upscaled to 500 m resolution using the aggregate map function followed by resampling in ILWIS. To downscale MOD16A2 ET_p raster images (from 8 days to daily), time series daily values of ET_p from the two KNMI stations (TWENTHE and HUPSEL stations) were used. It was achieved by summing up the daily ET_p values every eight days. Then, daily ratios were obtained by dividing daily ET_p by the 8 days ET_p sums as demonstrated in equation 4-4.

$$B_i = ET_p^i / ET_p^{ii} \tag{4-4}$$

Where

 B_i The average daily downscaling ratio of a certain day

 ET_n^i (mm.day⁻¹) Daily ET_p value from the KNMI station

 ET_p^{ii} (mm.day⁻¹) 8 days sum of ET_p^i

The 12th of August (sunny day) maps of each year from 2012 to 2015 were chosen to represent the summer months and the 2nd of February (rainy day) to represent the winter months. These days of different seasons were selected because they were found to have high differences in spatial patterns

4.2. Implementation of the model

The second specific objective of this research was achieved in two steps. The first step consisted of improving the existing transient model of Aamsveen. The improvements were made on both the conceptual and numerical models. It was achieved by using the parameterization of Emmanuel's model and modified some of the parameters and forcing data. The second step was to calibrate and validate the model including satellite-based ET_a time series in the process. The data sets were split into two different data sets: a calibration data set that consists of 4 years (1st January 2012 -31st December 2015) and a validation data set that consists of 3years (1st January 2016- 31st December 2018).

4.2.1. Conceptual Hydrological Model of Aamsveen

The conceptual model is a qualitative representation of a system, indicating the hydrological and hydrogeological information about the area of interest (Anderson et al., 2015b). It mainly consists of defining model boundaries, hydro stratigraphic units, flow system pattern, direction, and flow rate. This information is later transferred into the numerical model which is described in section 4.2.3. In the current transient model, the same conceptual model (Figure 6) as previously defined by Emmanuel's model was applied, and about which more information can be found in his MSc thesis. However, the implementation of the hydro-stratigraphic units that define the model layers were improved. The model is normally made of two layers as previously defined, a peat layer shown in Figure 7 underlain by a sand layer. The latter was improved by considering more boreholes data to sufficiently represent the spatial distribution of the sand layer which is shown in Figure 8.

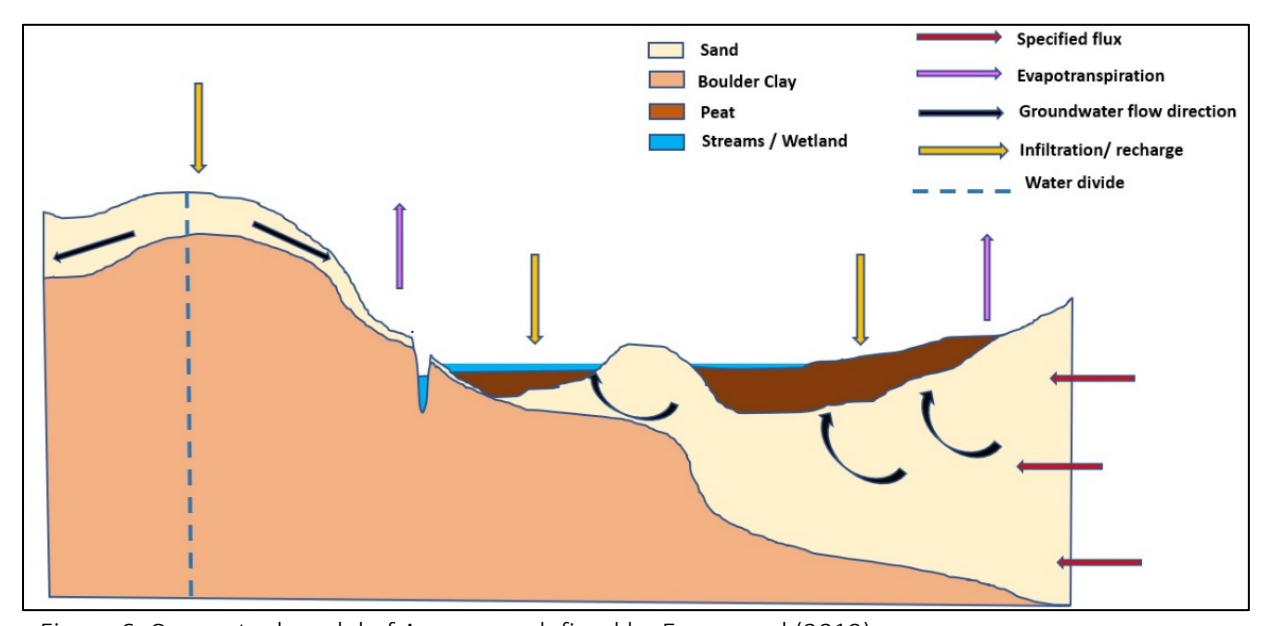


Figure 6: Conceptual model of Aamsveen defined by Emmanuel (2019)

4.2.2. Water balance

The water budget is quantitative information about all the inflow, outflow, and change in storage of all the hydrological components of a region over a certain period of time (Rientjes, 2016). All the water budget components are expressed in m.day⁻¹. The general water budget of the entire Aamsveen catchment can be written as:

$$P + SF = ET_a + I + Q_s + Q_{drain} \pm \partial S \tag{4-5}$$

Where:

P Rainfall

SF or Q_{in} Specified flow entering the system at the eastern boundary

I Canopy interception Q_{drain} Outflow through drains

 ∂S Total change in storage for both unsaturated and saturated zone

 $Q_{\rm s}$ Total surface runoff at the catchment outlet

ET_a can be divided into:

$$ET_a = ET_g + ET_{uz} + I (4-6)$$

Where

ET_g Groundwater ET

ET_{uz} Unsaturated zone ET

 Q_s can be written as

$$Q_s = Q_H + Q_D + Q_b \tag{4-7}$$

Where

 Q_H Hortonian runoff which occurs when precipitation is high than the infiltration rate

 Q_D Dunnian runoff which occurs when the surface is saturated

 Q_b Baseflow or outflow through streams

 ∂S can be written as:

$$\partial s = \partial s_q + \partial s_{uz} \tag{4-8}$$

Where

 ∂s_{g} Groundwater zone change in storage ∂s_{uz} Unsaturated zone change in storage

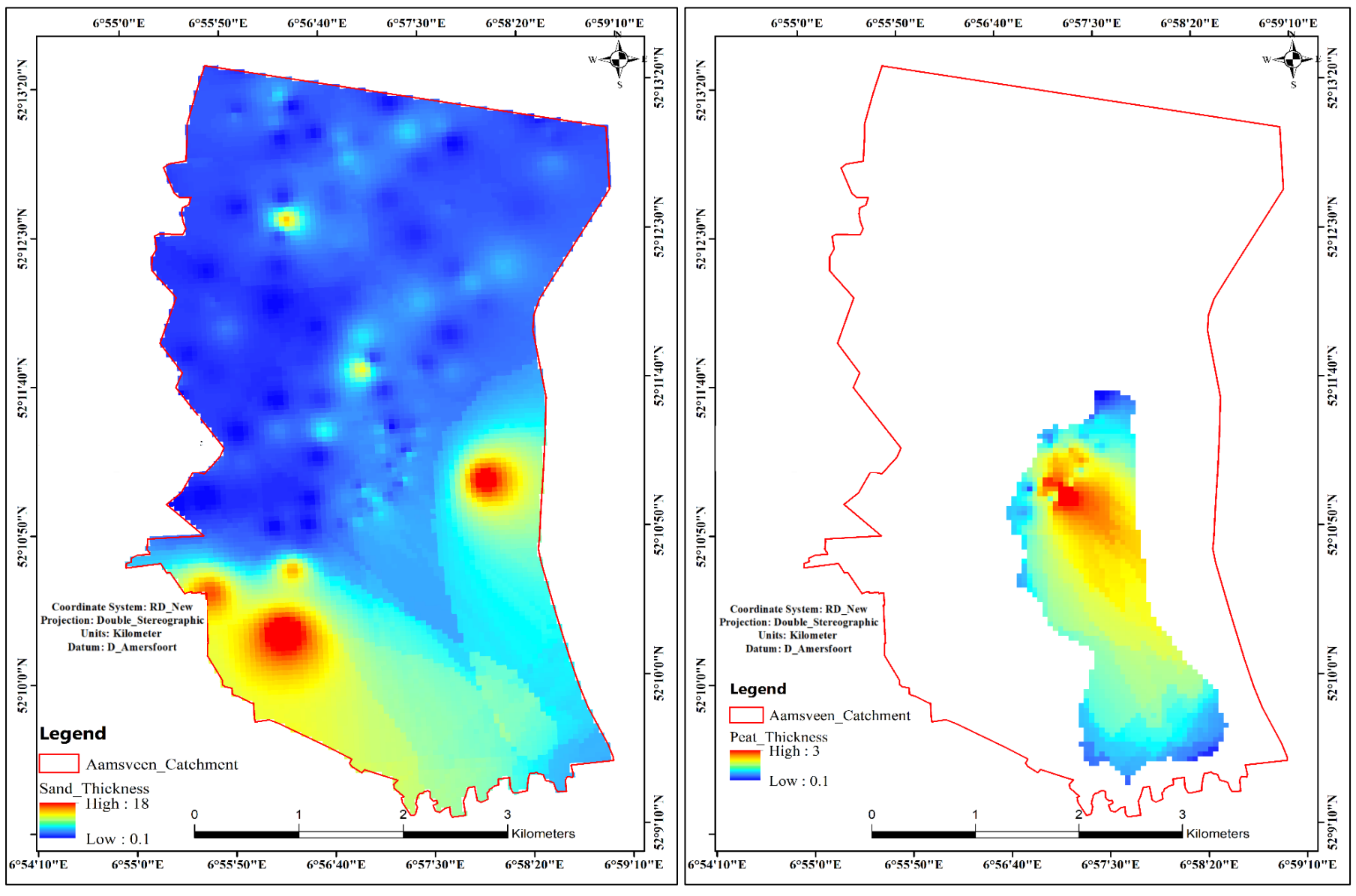


Figure 7: Aamsveen sand (left) thickness map and peat thickness defined by Emmanuel (2019)

 Q_h can also be split into:

$$Q_b = Q_{in(streams)} - Q_{out(streams)}$$
 (4-9)

Where

 $Q_{in(streams)}$ Stream leakages to the groundwater $Q_{out(streams)}$ Groundwater leakages to the stream

The surface and unsaturated zone budget can be written as

$$P_a = ET_{uz} + R_g + Q_{H+D} \pm \partial s_{uz} (4-10)$$

Where

 P_a Gross infiltration or applied infiltration in MODFOW-NWT I_{exf} Groundwater exfiltration is also known as surface leakage R_a Gross recharge also known as unsaturated zone recharge

The saturated zone budget can be written as

$$R_{uz} + Q_{in(res)} + Q_{in(s)} = ET_q + I_{exf} + Q_{out(res)} + Q_{out(s)} + Q_{out(drain)} \pm \partial S$$
 (4-11)

Where

 $Q_{in(res)}$ Reservoir leakages in the groundwater $Q_{in(s)}$ Stream leakages in the groundwater $Q_{out\,(res)}$ Groundwater leakages to the reservoir $Q_{out(s)}$ Groundwater leakages to stream $Q_{out\,(drain)}$ Groundwater leakages to drain

The net recharge (R_n) which is the amount of water that can recharge the saturated zone is expressed as

$$R_n = R_g - I_{exf} - ET_g (4-12)$$

4.2.3. Numerical Model

MODFLOW-2005 was adopted as it was previously used in the Emmanuel's model. It is a version of MODFLOW that simulates 3D surface and groundwater interactions of a complex hydrological system. MODFLOW-NWT solver was used to take into consideration the wetting and drying of cells in the system.

4.2.3.1. Spatial Discretization

The study area was discretized into a regular rectangular grid of 50*50m resolution, as in the Emmanuel's model, using the Dutch projection system (ESPG 28992).

4.2.3.2. Aquifer Geometry Design

Once the spatial discretization is done, the aquifer geometry is defined. It consists of defining the elevation of the top and bottom of each layer. The DEM (Digital Elevation Model) of the Aamsveen catchment was used as model top elevation. The bottom of the first layer was obtained by subtracting the peat thickness from the model top elevation. The bottom of the second layer was obtained by subtracting the thickness of the sand layer from the bottom of the first layer.

4.2.3.3. Forcing-related Parameters

The forcing-related parameters of the model are rainfall (P), canopy interception (I), and ET_p. They are all defined in the UZF package described in section 4.2.4.2.

In the present model, the canopy interception was modified. In the Emmanuel's model, the interception was defined using different literature values and some doubtfully high values (reaching 76%) were noticed. Consequently resulting in low water in the aquifer. According to Miralles et al. (2010) that provides the global standard interception rate of different land cover classes, the seasonal interception rate can reach a maximum of 30%, which was also confirmed by G. Pypker et al., 2012. Therefore the interception rates were redefined according to these global standard values and presented in Table 1.

Infiltration is the amount of water that enters the soil per unit of time. It is estimated in the UZF package by taking precipitation values minus canopy interception. Precipitation data were obtained from the KNMI station (TWENTHE station).

The spatial and temporal distributed ET_p time series maps (defined and described in section 4.1) were imported into the model through the UZF package.

Land cover type	Interception Rate (%)
Water	0
Maize	16
Evergreen Trees	17.3
Deciduous Trees	13
Grass	7.9
Heath	20
Rape Seed	14
Built-up area	30

Table 1: Interception rate of different land cover classes (Miralles et al., 2010)

4.2.3.4. Defining hydraulic and storage parameters

The hydraulic conductivity parameters, which govern the water flow were defined for both unsaturated zone and saturated zone. The unsaturated zone hydraulic parameters are defined through the UZF package described in section 4.2.4.2. The saturated zone hydraulic parameters include horizontal (HK) and vertical hydraulic (VK) conductivity which are defined in the upstream weighting package (UPW package) described in section 4.2.4.5. The storage parameters in the saturated zone include specific yield (SY) and specific storage (SS) which also are defined in the UPW package.

To take into account the spatial variability of these storage and hydraulic parameters, a zoning approach was used which consist of partitioning the area into different small regions (zones) with different parameters. The initial zones and their corresponding parameters as previously defined by Emmanuel (2019) were initially used in the present model as demonstrated in Table 3 but later they were adjusted during the calibration process.

4.2.3.5. Initial heads

For transient model simulation, initial heads are very important. There are three approaches to define initial heads. The first option is to use the calibrated head from a steady-state model, however, this approach is inaccurate for a system that has high spatial and temporal variability of fluxes (Anderson et al., 2015c). The second approach is to sacrifice a part of your data in the warm-up of your model, the purpose to reduce errors as the simulation goes on. It works well if you have a long simulation period. The third approach which was used in this present model is to run the model with a long, realistic data set before the beginning of the actual simulation. The data of the driving forces for the first year (2012) were duplicated for the warm-up period to reduce errors in the state variables as the simulation progresses. In the Emmanuel's model, the warm-up period wasn't considered and it was noticed that it had a big impact on the simulation results. After the warm-up, the initial heads were obtained from the measurements and all other parameters were kept as they were.

4.2.4. Boundary conditions and model packages

The model boundaries describe how the water flows within or outside the model and consist of sources and sinks. They consist of external and internal model boundaries.

The external boundary defines the flow that enters or leaves the system at the model perimeter. In this study, a constant flow boundary (a fixed flow rate is known across the model perimeter) was used to define the flow entering the system through the external model boundary (described in section 4.2.4.1).

The internal boundaries describe the interactions between different units within the model. These interactions can be gaining water from the groundwater or sourcing the aquifer. For

instance, if the reservoir stage is high than the groundwater level then the aquifer is gaining and vice versa.

Packages can be used to define these interactions and they are integrated into MODFLOW-NWT (El-Zehairy et al., 2018). In the current model, the packages used are Flow and Head Boundary package (FHB), Unsaturated Zone package (UZF), Reservoir package, Drain package, and stream flow routing package (SFR package).

4.2.4.1. FHB package

The external model boundary in Aamsveen is a flow constant boundary and it was defined firstly by Nyarugwe, (2016). He assigned a no-flow boundary to the entire study area. Later, Emmanuel (2019) analyzed stream data of the Eastern part (The German side) and noticed that there is a gentle flow of around 0.005 m³/day enters the study area. This flux was assigned to the eastern perimeter of the model through the FHB package and a no-flow boundary was applied to the remaining perimeter. The current transient model uses the same external boundary conditions as Emmanuel (2019).

4.2.4.2. UZF package

The UZF package simulates the water flow in the unsaturated zone. The package replaces both the recharge and evapotranspiration packages of the previous versions of MODFLOW. In the model, the recharge in the UZF package is internally defined based on the spatial and temporal variability of ET_p , rainfall, and unsaturated zone parameters such as initial unsaturated water content, residual water content, saturated water content, etc. The recharge to the groundwater is estimated using simplified Richard's equation by kinematic wave approximation as demonstrated in equation 4-13 (Niswonger, 2005).

$$\frac{\partial \theta}{\partial t} + \frac{\partial K(\theta)}{\partial z} + i = 0 \tag{4-13}$$

Where:

 θ (m³.m⁻³) Volumetric water content

 $t ext{ (day)}$ Time

 $K(\theta)$ (m.day⁻¹) Unsaturated hydraulic conductivity

i (m. day⁻¹.day) Unsaturated zone ET (ET_{uz}) rate per unit depth

 $K(\theta)$ can be written as

$$K(\theta) = K_s \left[\frac{\theta - \theta_r}{\theta_s - \theta_r} \right]^{\varepsilon} \tag{4-14}$$

Where

 K_s (m.day⁻¹) Unsaturated vertical hydraulic conductivity

 θ_r (m³.m⁻³) Residual water content

$$heta_s$$
 (m³.m-³) Saturated water content $arepsilon$ (-) Brooks-Corey-Epsilon

ET extinction depth and ET extinction water content (θ_{ext}) are other input data that are required in The UZF package. ET extinction depth is the depth below which the ET stops while ET extinction water content is the minimum water content below which ET can't be removed from the unsaturated zone. ET_{uz} occurs as long as θ_{ext} is not reached. But when ET_{uz} is larger than what the unsaturated zone can deliver, then ET_g takes place but only if the water level is above the ET extinction depth.

These parameters were defined and values are shown in Table 3. The ET extinction depth was defined using the rooting depth map of Emmanuel (2019) shown in Figure 8.

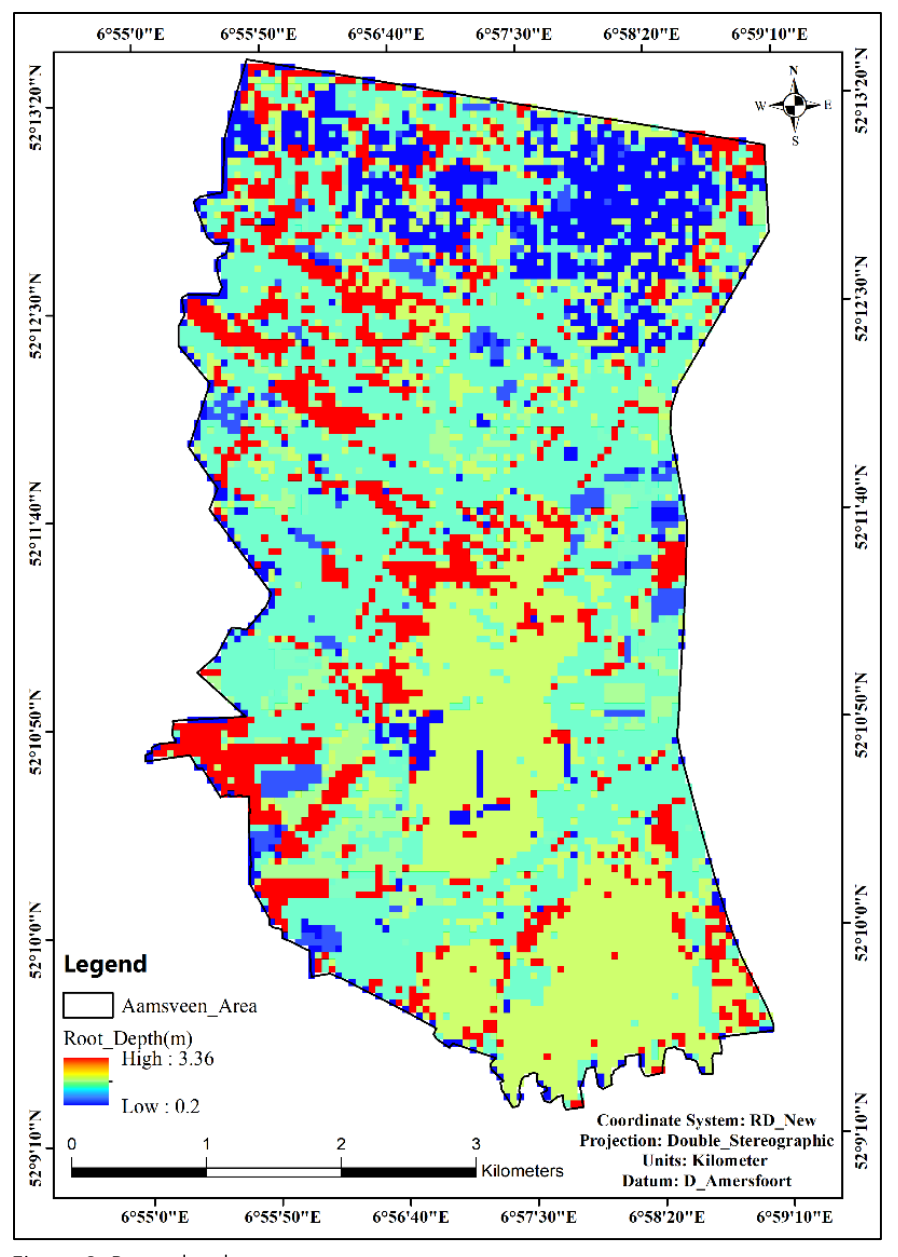


Figure 8: Root depth map

4.2.4.3. Reservoir package

The reservoir package simulates the interaction between the reservoir and the aquifer. Input data are reservoir bed thickness set to 0.2 m, reservoir hydraulic conductivity was set at 0.8 m.day⁻¹, and reservoir elevation was defined as "model top". The package requires the reservoir stages data which were made available from a water level gauge located near the reservoir.

4.2.4.4. Drain Package

The drain can only take water from the aquifer. When the water level is above the drain elevation, then the aquifer will lose water to the drain (equation 4-15). When the water level in the aquifer is below the drain elevation, then no flow in the drain (equation 4-16).

$$Q_d = C_d (H_a - H_d) \qquad \text{when } H_a > H_d$$
 (4-15)

$$Q_d = 0 when H_a \le H_d (4-16)$$

Where

Q_d(m³.day⁻¹) Flow from into the drain from the aquifer

C_d(m².day⁻¹) Drain conductance

 $H_a(m)$ Water head in the aquifer

 H_d (m) Drain elevation

In the model, C_d was assigned as 0.5 m².day⁻¹ and H_d was set as "Model Top -1".

4.2.4.5. Stream Flow Routing package (SFR package)

The SFR package was selected to simulate the interactions between streams (head-dependent boundary) and the aquifer (groundwater). Using the SFR package enables the user to calibrate the model using the streamflow measurements. Contrary to the river package, calibration is only done on the baseflow. The flow in the stream is governed by the manning equation while the interactions between groundwater and streams are governed by Darcy's law (equation 4-17)

$$Q = \frac{K_{stream}LW}{M} * (h_1 - h_2)$$
 (4-17)

Where

Q (m².day⁻¹) Volumetric flow between stream reaches and aquifer,

 K_{stream} (m.day⁻¹) Hydraulic conductivity of streambed material

L (m) Length of reach W (m) Width of river

M (m)	Thickness of river bed
h_2 (m)	Head in the stream
h_1 (m)	Head in the aquifer

In the model, the stream bed elevation was assigned to 1 or 2 m below the surface (top of the model) according to the stream location since they have different depths in the study area. All other inputs required in the SFR package can be found in Table 2.

Parameter	MODFLOW	Initial value	Unit
	Name		
K _{stream}	STRHC1	0.01 - 0.23	(mm.day ⁻¹)
L	RCHLEN	Object length	(m)
W	Stream width	1 - 4	(m)
M	STRTHICK	0.1 - 0.2	(m)
Roughness Coefficient	-	0.035	(-)
Slope	-	0.01 - 0.2	(-)
Saturated volumetric water content	THTS	0.3	(m ³ .m ⁻³)
Initial volumetric water content	THTI	0.2	(m³.m ⁻³)
Brooks-Corey-exponent	EPS	3.5	(-)
Maximum unsaturated vertical K	UHC	1	(m.day ⁻¹)

Table 2: SFR package input data

4.2.4.6. Upstream-weighting package (UPW)

The UPW is activated when the MODFLOW-NWT solver is used. This package estimates conductance between grids differently to other flow packages. Flow packages such as Block-Centered flow (BCF), Layer Property flow (LPF), or Hydro-geologic-Unit Flow (HUF) use a discrete approach when estimating conductance between grid cells. However, The UPW package uses average conductance for flow estimation between cells (Niswonger, 2005). The hydraulic and storage parameters in section 4.2.3.4 are defined through this package.

4.2.5. Model calibration

Model calibration consists of fine-tuning the model parameters to match simulated state variables (usually discharge and heads) to observed ones. The current model was calibrated with respect to observed groundwater head, streamflow, and MOD16A2 ET_a.

4.2.5.1. Groundwater head

The present model was calibrated using five piezometers (Appendix 1) while in the Emmanuel's model, four piezometers were used. Other piezometers available in the region were found to

be unfunctional and with a lot of gaps for both the calibration (2012-15) and validation periods (2016-18) as was also confirmed by Emmanuel (2019). B35A0178 is the new additional piezometer located just outside the wetland area. The other four piezometers are within the wetland area. In the model, the head observation package (HOB) was activated to provide a comparison between observed and simulated heads.

4.2.5.2. Streamflow

In Aamsveen, there are two stream gauges. Melodiestraat (located in the northern part of the study area) and Aamsveen camping gauge (Located in the wetland) as shown in Appendix 2. The latter was the only one used in the calibration because the Melodiestraat was found to be unreliable as it provides unrealistic streamflow measurements (Emmanuel, 2019).

4.2.5.3. Calibration with MOD16A2 ETa

An additional new method to calibrate the transient model of Aamsveen was adopted that consist of integrating satellite-based ET_a. It was done by matching the simulated ET_a that includes interception to the bias-corrected satellite-based ET_a for the calibration period of 4years (2012-15). The calibration was made on eight days average values of ET_a.

 ET_a was processed and bias-corrected the same way as ET_p as described in section 4.1.1 and the results are shown in Appendix 3.

The model provides daily volume of ET_a which includes ET_{uz} and ET_g . Interception defined separately in section 4.2.3.3 was added to the simulated ET_a . Daily total volume of canopy interception was obtained by multiplying daily rainfall to the canopy interception rates of different land cover classes to get the amount of rainfall intercepted by pixel. Then the interception of individual pixels were summed up to get the total volume of interception for the entire area.

4.2.5.4. Initial calibration parameters

The initial calibration parameters were obtained from the Emmanuel's model and they are shown in Table 3.

Parameter	NAME	initial values	Unit	Model
		range		package
HK	Horizontal	0.001 - 11	(m.day ⁻¹)	UPW
	hydraulic			
	conductivity			
VK	Vertical	0.0001 - 1.1	(m.day ⁻¹)	
	hydraulic			
	conductivity			
SS	Specific	0.00001 - 0.0001	(m ⁻¹)	
	storage			
SY	Specific yield	0.18 - 0.4	(-)	
θ_{i}	Initial	0.2	(m³.m ⁻³)	UZF
	unsaturated			
	water content			
$\theta_{ m r}$	Residual water	0.01	(m³.m ⁻³)	
	content			
$\theta_{\rm s}$	Saturated	0.3	$(m^3.m^{-3})$	
	water content			
θ_{ext}	ET extinction	0.1	(m³.m ⁻³)	
	water content			
K _s	Saturated	1	(m.day ⁻¹)	
	water content			

Table 3: Initial hydraulic and storage parameters of the present model

4.2.6. Model validation

The data of the period of 1^{st} January $2016-31^{st}$ December 2018) was used for the validation of the model. The driving forces (precipitation, $ET_{p,}$ and Interception) were processed and imported into the model as described in sub-section 4.2.3.3.

4.2.6.1. Heads for validation

The observed heads were made available for the validation period (Appendix 4). The observed head had no gaps for the validation period contrary in the calibration except piezometer B35A0836 that had stopped recording at the beginning of 2017.

4.2.6.2. Streamflow for validation

The streamflow measurements data for validation (Figure 9) was found to have no flow for long periods, especially when the rainfall is little. It can also be explained by the fact that the stream flow is not natural, it is controlled by the water managers of the region by blocking the stream bed above the gauge.

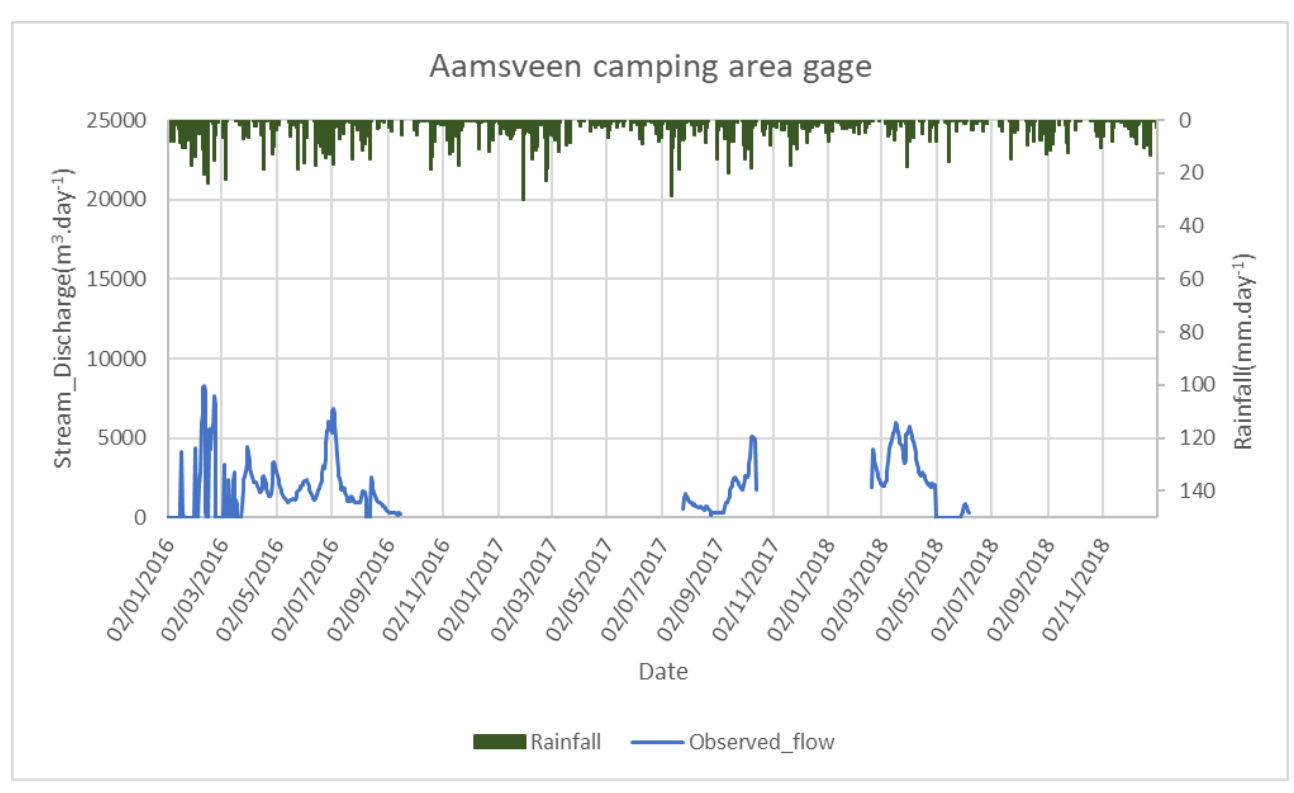


Figure 9: Observed stream flow for validation

4.2.6.3. MOD16A2 ET_a for validation

MOD16A2 data set for validation (Appendix 3) was processed the same way as for the calibration as described in section 4.2.6.3.

4.2.7. Error Measures

The modelling accuracy was estimated by using standard or global indicators. The following calibration targets were set; RMSE is <0.8m and MAE should be \leq 0.5m. The stream accuracy was assessed using volumetric error (VE) which is a flow measurement metric. The model was considered well-calibrated when VF is < 0.5%.

$$MAE = \frac{1}{n} \sum_{i=1}^{n} |(h_{obs} - h_{sim})_i|$$
 (4-19)

$$RMSE = \sqrt{\left(\frac{1}{n}\sum_{i=1}^{n}(h_{obs} - h_{sim})_{i}^{2}\right)}$$
 (4-20)

$$VE = 1 - \frac{\sum_{i=n}^{n} |(Q_{obs} - Q_{sim})|_{i}}{\sum_{i=1}^{n} Q_{obs}}$$
(4-21)

Where

Mean of errors ME (m)MAE (m) Mean absolute error RMSE (m)Root mean square error VE (%) Volumetric efficiency Observed head h_{obs} (m) h_{sim} (m) Simulated head Q_{obs} (m³.day⁻¹) Observed flow Q_{sim} (m³.day⁻¹) Simulated flow Number of records n(-)

4.2.8. Sensitivity Analysis

Sensitivity analysis was carried out on ET_a (including interception) and groundwater heads. It consisted of finding parameters that are most sensitive to ET_a and heads hence affecting the model performance. It was achieved by applying a certain magnitude of change to model parameters and analyze the effect on RMSE. The sensitivity analysis focused on parameters that had a significant impact during calibration and include HK, VK, SY, and θ_{ext} .

4.3. Comparison between current and Emmanuel's model

To assess the effects of the modifications of the model, it was interesting to make a comparison to the Emmanuel's model. The comparison was made on the groundwater heads, stream flows, and the water budget.

5. RESULTS AND DISCUSSIONS

5.1. Validation and bias correction for MOD16A2 product

Figure 10 shows that at TWENTHE and HUPSEL stations, there is a systematic error in MOD16A2 ET_p estimates. The MOD16A2 algorithm is not perfect as it overestimates the ET_p .

The systematic shift or bias is demonstrating periodicity due to the effect of the vegetation. Generally, it was noticed that the spring and summer months have the highest systematic bias.

Applying the average bias fixing factor from Table 4, the MOD16A2 ET_p values were re-scaled to match with the in situ measurements. The R^2 is 0.95 and 0.91 for TWENTHE and HUPSEL respectively (Table 10).

Season	TWENTHE station	HUPSEL station	Average Bias fixing factor
Winter	1.43	1.36	1.39
Spring	1.83	2.06	1.95
Summer	1.82	1.96	1.89
Autumn	1.60	1.77	1.68

Table 4: average bias fixing factor

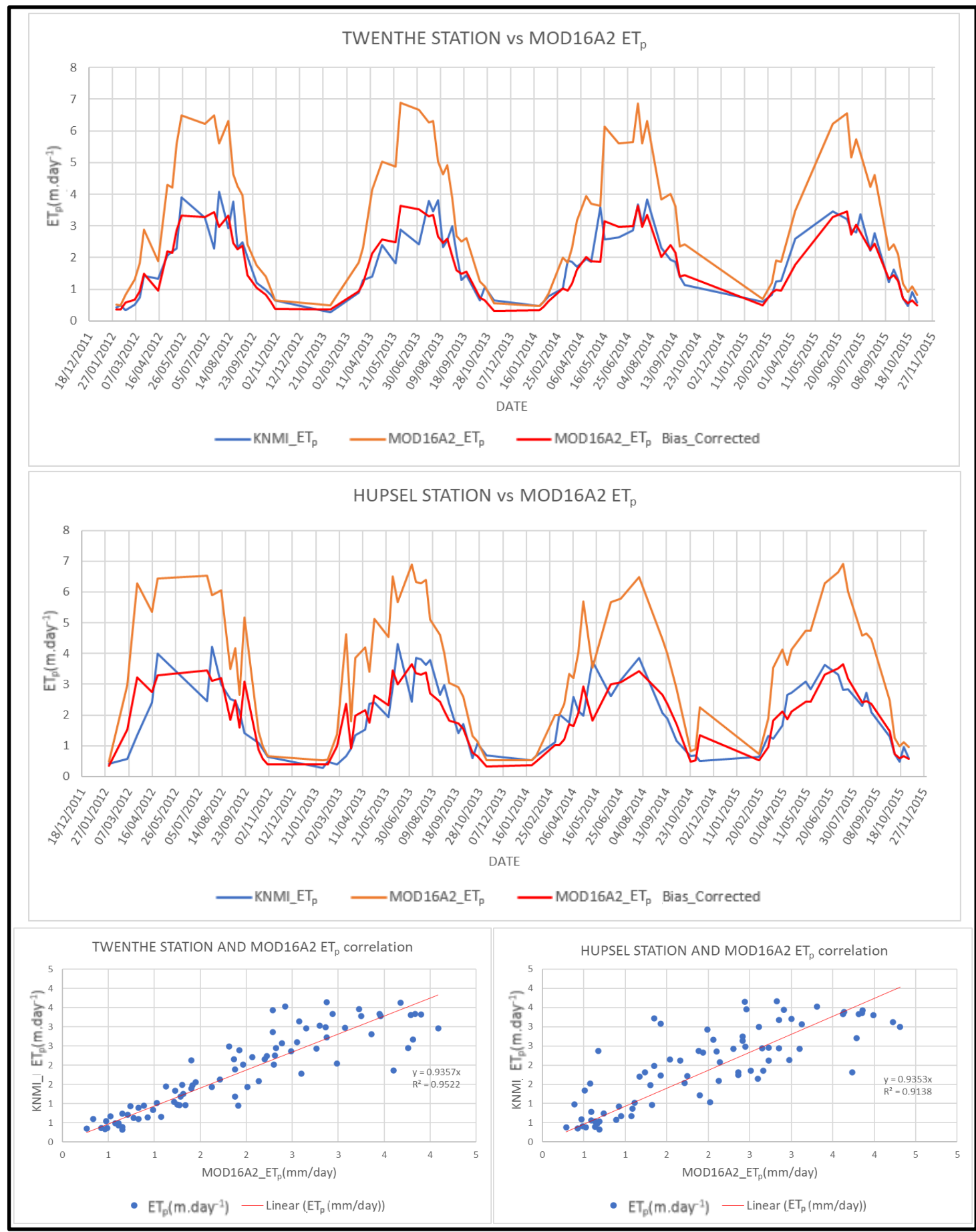


Figure 10: MOD16A2 ET_p validation results

5.2. ET₀

The simulated ET_0 (Figure 11) from the Penman-Monteith model demonstrated seasonal variation. High values of ET_0 were noticed in the summer (with annual maxima around 7mm.day⁻¹) while low values of ET_0 were seen in the winter (with annual minima around 0.08mm. day⁻¹).

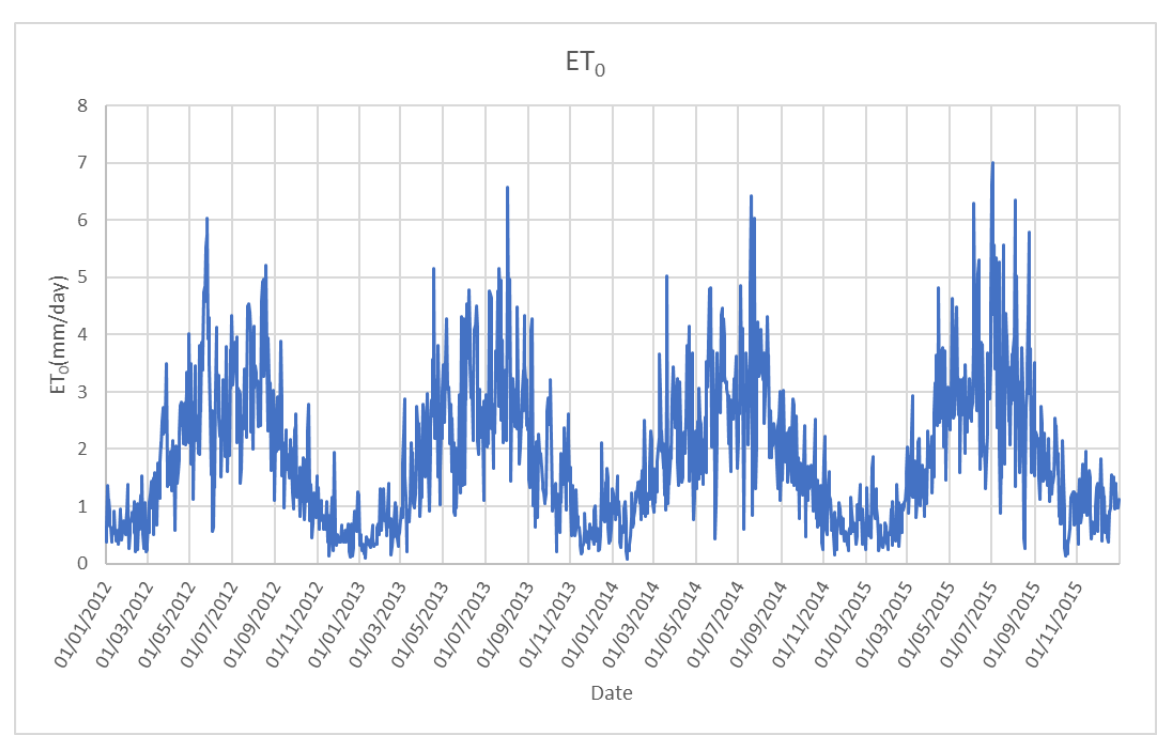


Figure 11: Time series ET₀ produce by Penman-Monteith model using ILWIS

5.3. Defining K_c

In the previous research, the K_c value of heath was considered constant throughout the simulation period disregarding the spatial and temporal variability. It covers a significant area in the region. Figure 12 shows a seasonal average NDVI change in the heathland that should be considered. During the winter season, heath is photosynthetically not as active as in the summer. The average NDVI of the heath can reach a minimum of around 0.35 in winter and a maximum of 0.84 in the summer. Jones, (1968) indicated that different heath types have different growth stages but in general Heath blooms or grows from mid-June to mid-September.

In Figure 13, the average NDVI value shows a slight increase in the heathland which is due to the bushland growing in the region and the slope is around 0.0028 in the summer, and in the winter, the slope is 0.0127. The K_c value of heath was estimated according to these changes in NDVI using Choudhury et al., (1994), and values are shown in tables 5 and 6.

In Figure 12, The mean NDVI values of the deciduous trees show a seasonal change and it was considered in the Emmanuel's model. Nevertheless, the growth of the forest (deciduous trees) resulting in high NDVI for both summer and winter was not incorporated in the Emmanuel's model. Figure 14 demonstrates an increase of the forest with a slope of 0.0138 in the winter and a slope decrease of -0.0075 in the summer for the NDVI values. This decrease is due to the drought that happened in the Netherlands in 2018 and has affected deciduous trees (Buitink et al., 2020). Before the drought, the NDVI of deciduous trees had a slope of 0.0038.

In the Emmanuel's model, a K_c value of zero was attributed to the Built-up area. However, Figure 12 shows that the NDVI in the built-up area represents not only buildings but also the vegetations of gardens and parks and so a variable K_c value should be considered. Choudhury et al., (1994) was also used to estimate the K_c values in the built-up area and it is shown in tables Table 5 and 6.

The agriculture fields (maize, wheat and rapeseed) are rotated in the area. These changes in crops were considered and values were from Allen et al., (1998). The K_c values for the remaining landcover classes (grass, water, bare soil, and evergreen trees) were taken from Allen et al., (1998) and it is demonstrated in Tables 5 and 6.

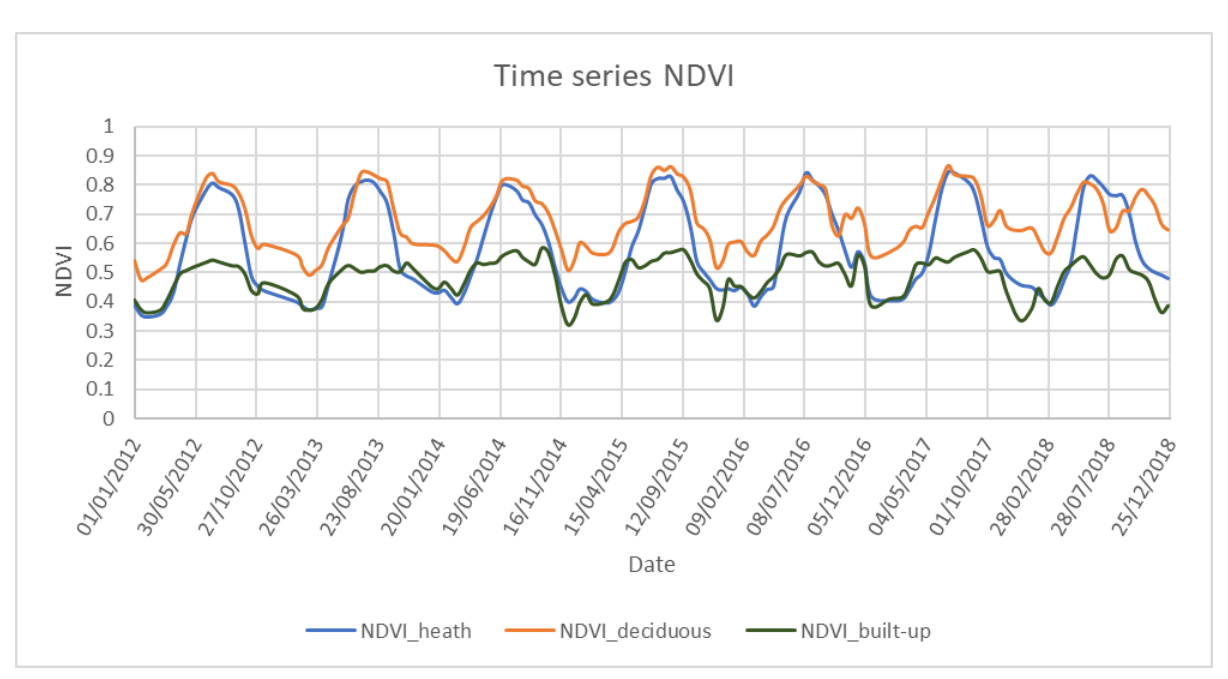


Figure 12: Time series average NDVI value for heath, Deciduous, and built-up area

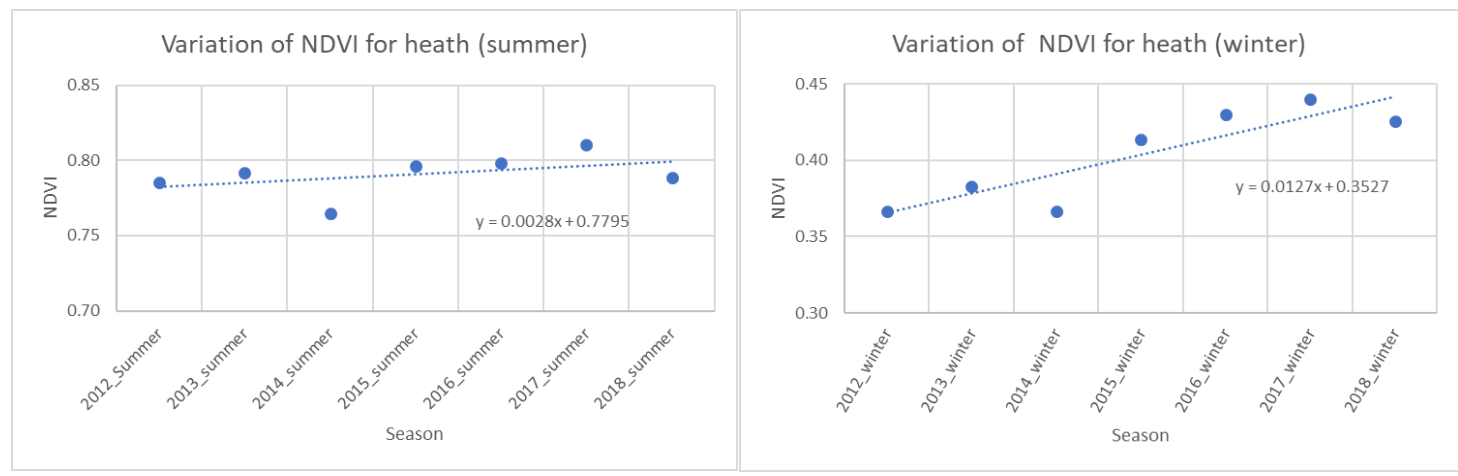


Figure 13: Summer (left) and winter (right) average variation of NDVI for heath

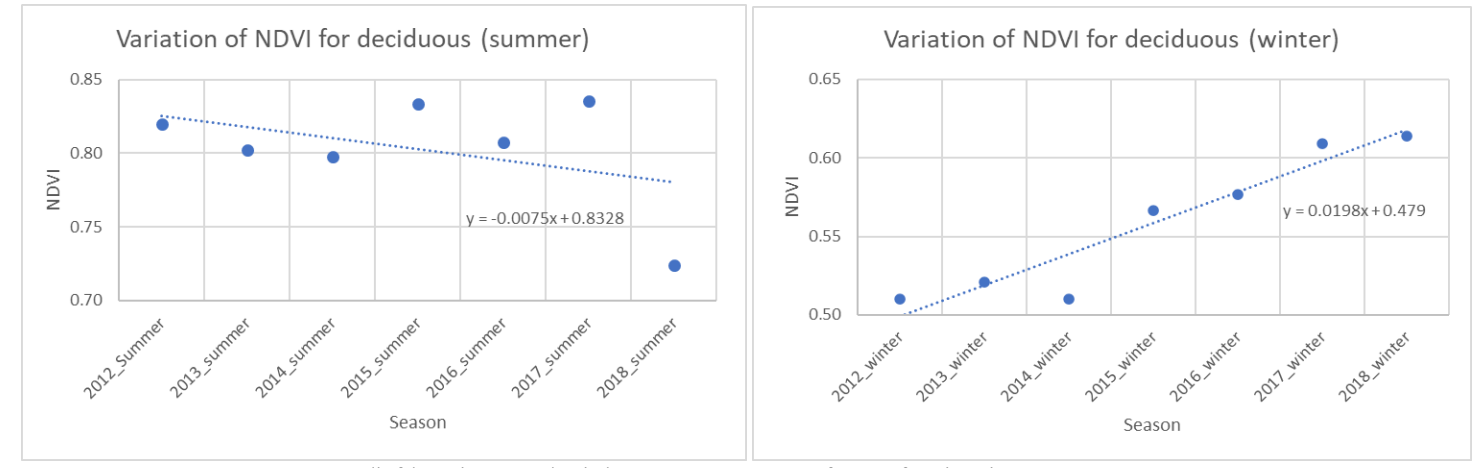


Figure 14: Summer (left) and winter (right) average variation of NDVI for deciduous

Year		Growing :	season (Ap	ril, May, J	une, July	, August, Sept	ember)	
	Heath	Deciduous	Built-up	Water	Grass	Evergreen	Bare soil	Rapeseed
2012	0.89	0.94	0.52	1.05	1.00	0.90	0.20	0.35
2013	0.90	0.91	0.49	1.05	1.00	0.90	0.20	0.35
2014	0.86	0.90	0.54	1.05	1.00	0.90	0.20	0.35
2015	0.90	0.96	0.54	1.05	1.00	0.90	0.20	0.35
2016	0.91	0.92	0.54	1.05	1.00	0.90	0.20	0.35
2017	0.92	0.96	0.55	1.05	1.00	0.90	0.20	0.35
2018	0.89	0.80	0.49	1.05	1.00	0.90	0.20	0.35
Reference	(Cho	oudhury et al.,	1994)		(Allen et al.,19	998)	

Table 5: K_c values for different land cover classes for the growing

Year		nactive seasoi	n (October,	Novembe	r, Decemb	per, January, F	ebruary, M	arch)
	Heath	Deciduous	Built-up	Water	Grass	Evergreen	Bare soil	Rapeseed
2012	0.27	0.48	0.30	1.05	1.00	0.90	0.20	0.35
2013	0.30	0.50	0.30	1.05	1.00	0.90	0.20	0.35
2014	0.27	0.48	0.30	1.05	1.00	0.90	0.20	0.35
2015	0.34	0.57	0.30	1.05	1.00	0.90	0.20	0.35
2016	0.37	0.58	0.35	1.05	1.00	0.90	0.20	0.35
2017	0.38	0.63	0.38	1.05	1.00	0.90	0.20	0.35
2018	0.36	0.64	0.33	1.05	1.00	0.90	0.20	0.35

Table 6: K_c values for different land cover classes for the inactive season

5.4. Comparison between MOD16A2 ET_p and K_c based ET_p

As demonstrated by Figure 15, the values of MOD16A2 ET_p after bias correction are in the range of the K_c -based ET_p , and Figure 16 shows that both have a strong correlation with an R^2 of 0.95 and RMSE of 0.8 mm. However, in terms of representing the spatial variability of the region, K_c -based ET_p is showing more details, as demonstrated in Figures 17 and 18. This difference in pattern is due to a landcover map used by MODIS in their algorithm indicated in Figure 4. The MOD16A2 ET_p product doesn't perfectly consider the spatial variations in the Aamsveen catchment due to the low spatial resolution and too generic land cover classes used in the land cover map.

The high correlation value shows that although the data sets are the results of physically independent measurements, both describe the temporal changes of the same physical process, although the spatial pattern differences prove the presence of uncertainties in the quantification. For the present groundwater modeling purposes, since ET_p is related to the land cover, and K_c -based ET_p is based on more detailed and accurate land cover information than MODIS-based, the K_c -based ET_p was used. However, in regions where in situ data are not available, MOD16A2 ET_p can be used as an alternative after bias correction. Furthermore, due to the consistency of the MODIS dataset, the MODIS-based ET_a values are suitable for representing the temporal variations of the regional ET_a in the modelled area.

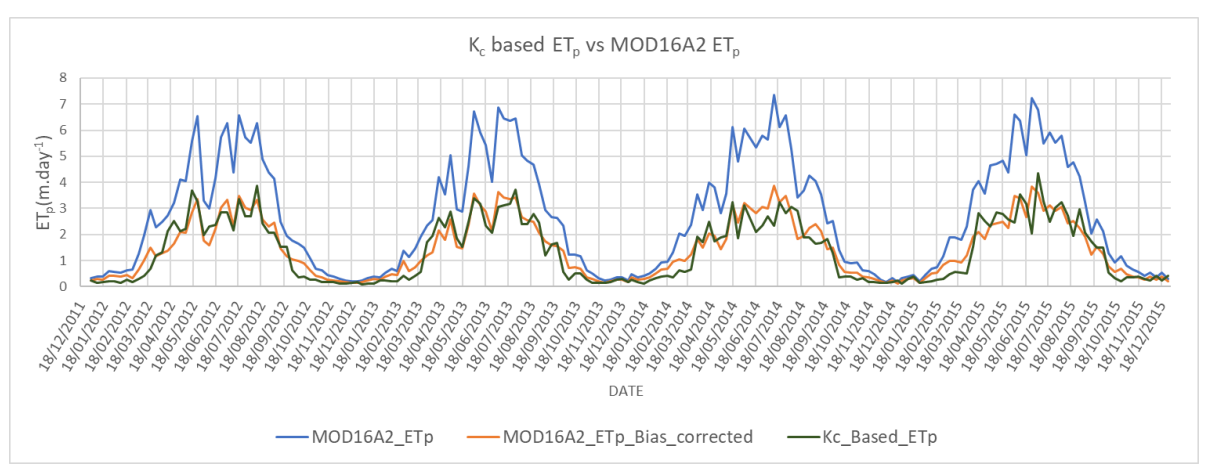


Figure 15: Time series pixel comparison between MOD16A2 and Kc based ETp (average daily ET_p values taken every eight days)

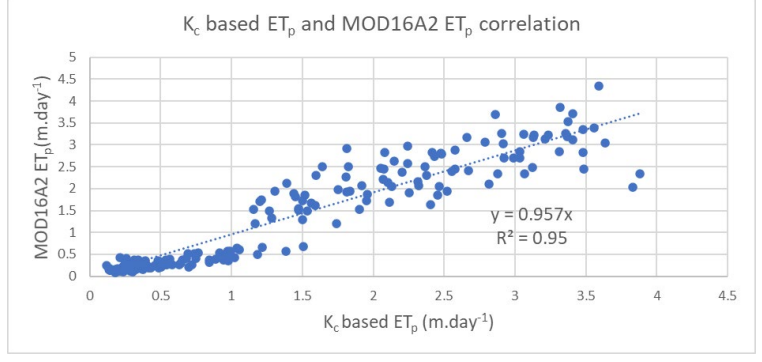


Figure 16: Correlation between MOD16A2 and K_c based ETp

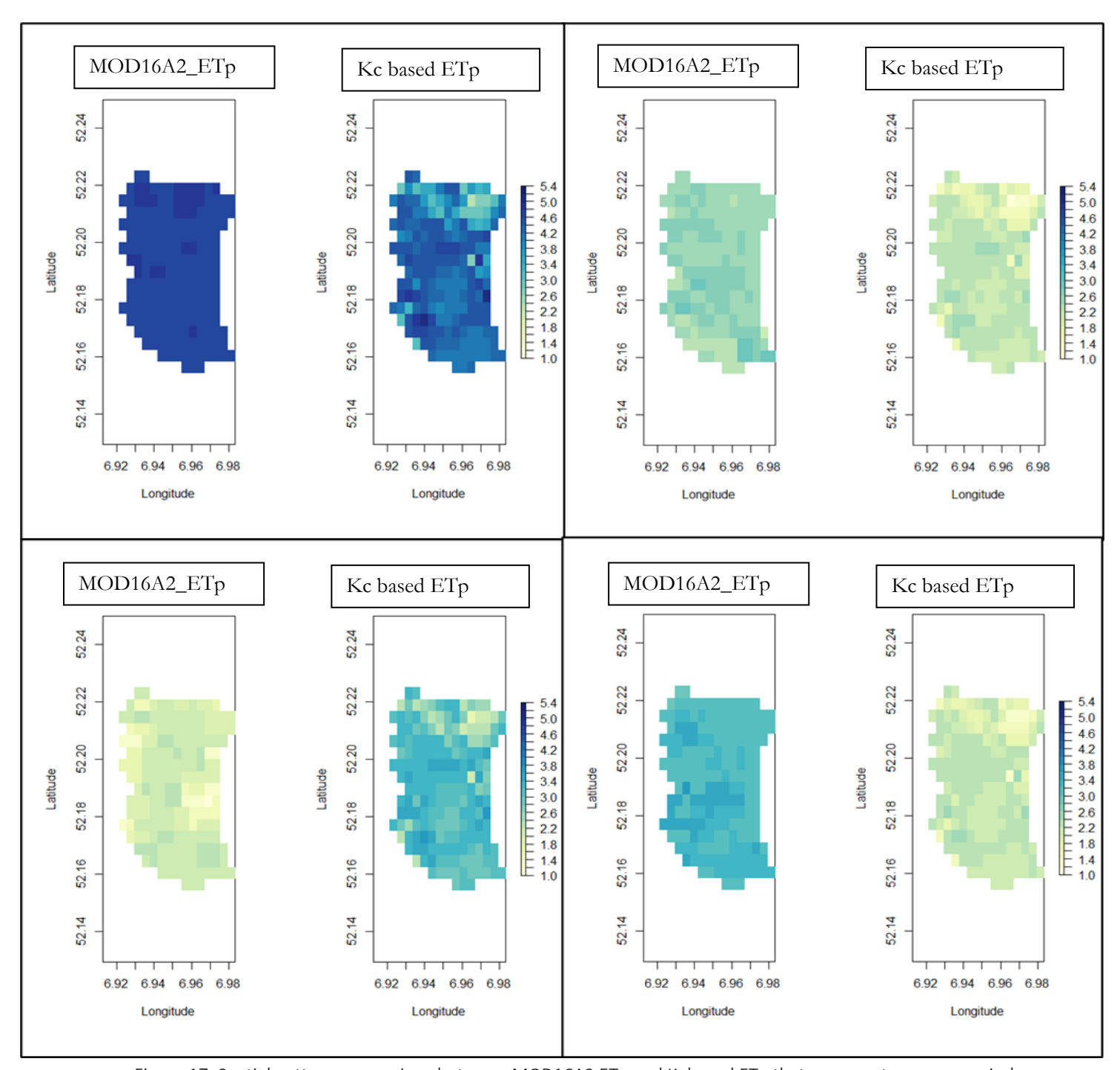


Figure 17: Spatial pattern comparison between MOD16A2 ETp and K_c based ETp that represent summer period (all images represent 12th of August each year from 2012 to 2015)

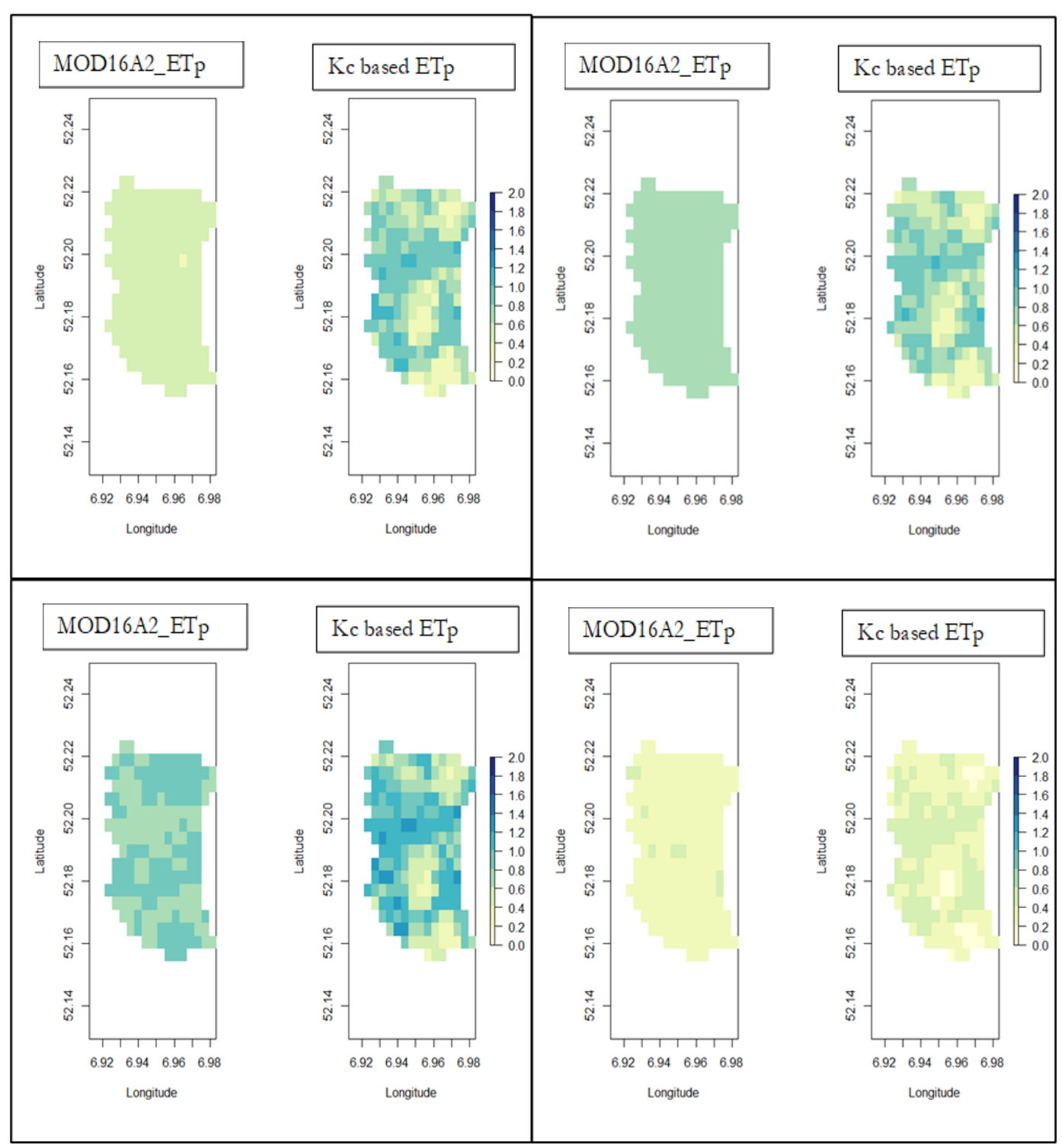


Figure 18: Spatial pattern comparison between MOD16A2 ETp and K_c based ETp that represent winter period (all images represent 2^{nd} of February each year from 2012 to 2015)

5.5. Interception rates

Figure 19 shows the interception rate of different landcover classes. The interception rate values presented in Table 1 were assigned to the Aamsveen land cover map of 20 m*20 m resolution (Figure 1). Two maps were considered as the deciduous trees completely lose leaves in the winter (Emmanuel, 2019). A summer map represents the summer and autumn months and a winter map that represents the winter and spring months.

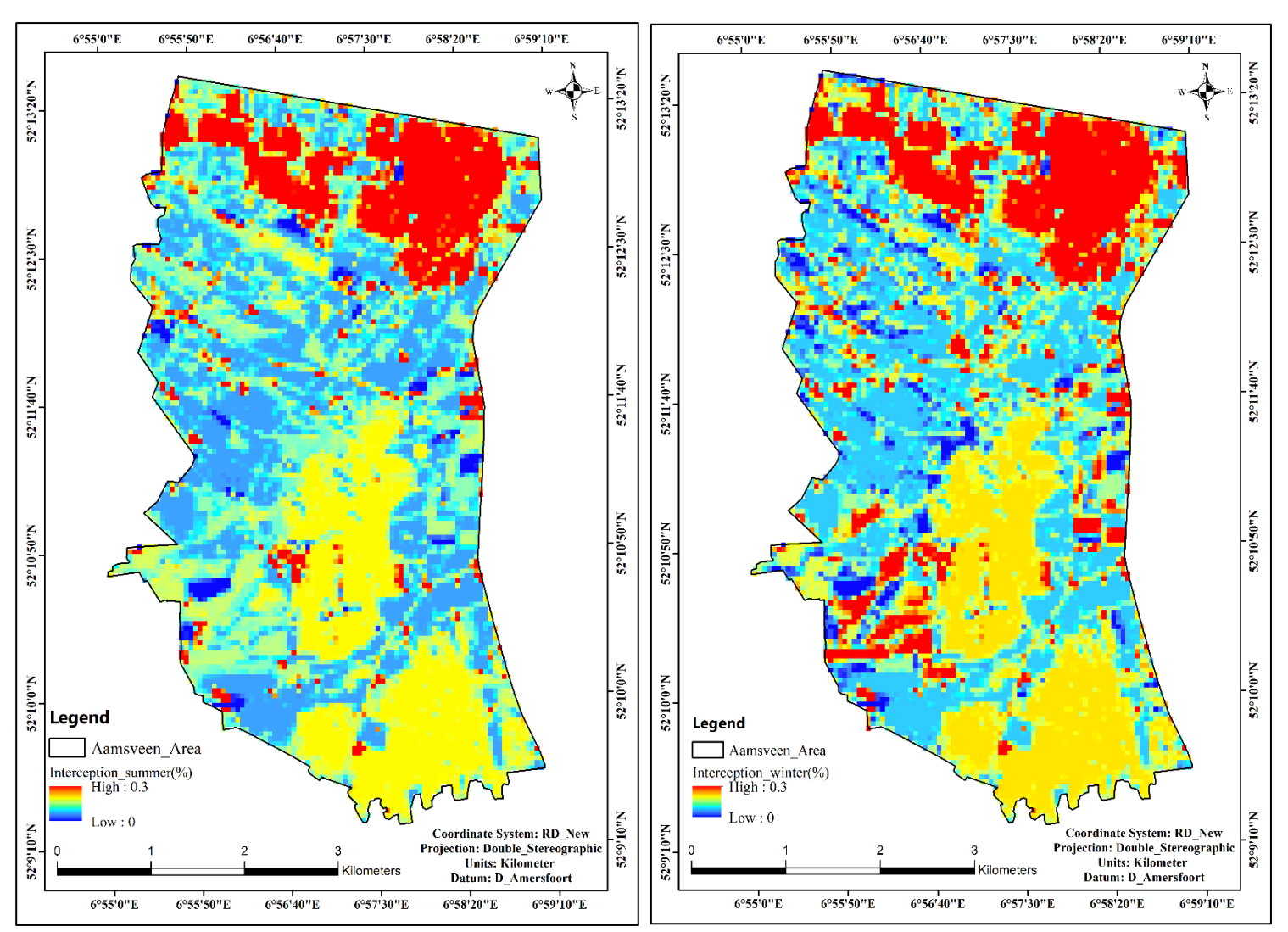


Figure 19: Interception rate for summer (left) and winter (right)

5.6. Calibration Results

5.6.1. Calibrated parameters

Table 7 presents the final calibrated parameters. Figures 20, 21, and 22 provide the spatial variability of some calibrated parameters (HK, VK, and SY)

Parameter	NAME	Calibrated	Unit	Model package
		Parameter		
HK	Horizontal	0.05 - 20	(m.day ⁻¹)	UPW
	hydraulic			
	conductivity			
VK	Vertical	0.2 - 0.9	(m.day ⁻¹)	
	hydraulic			
	conductivity			
SS	Specific	10 ⁻⁴ - 10 ⁻⁵	(m ⁻¹)	
	storage			
SY	Specific yield	0.02 - 0.4	[-]	
$\theta_{\rm i}$	Initial	0.2	(m ³ .m ⁻³)	UZF
	unsaturated			
	water content			
$\theta_{ m r}$	Residual water	0.01	(m ³ .m ⁻³)	
	content			
$\theta_{\rm s}$	Saturated	0.5	(m ³ .m ⁻³)	_
- 5	water content		(,	
θ_{ext}	ET extinction	0.03	(m³.m ⁻³)	
CAC	water content		,	
K _s	Saturated	1	(m.day ⁻¹)	7
	water content			
K _{stream}	Streambed	0.05 - 3.4	(m.day ⁻¹)	SFR
	vertical			
	hydraulic			
	conductivity			

Table 7: Results of calibrated parameters

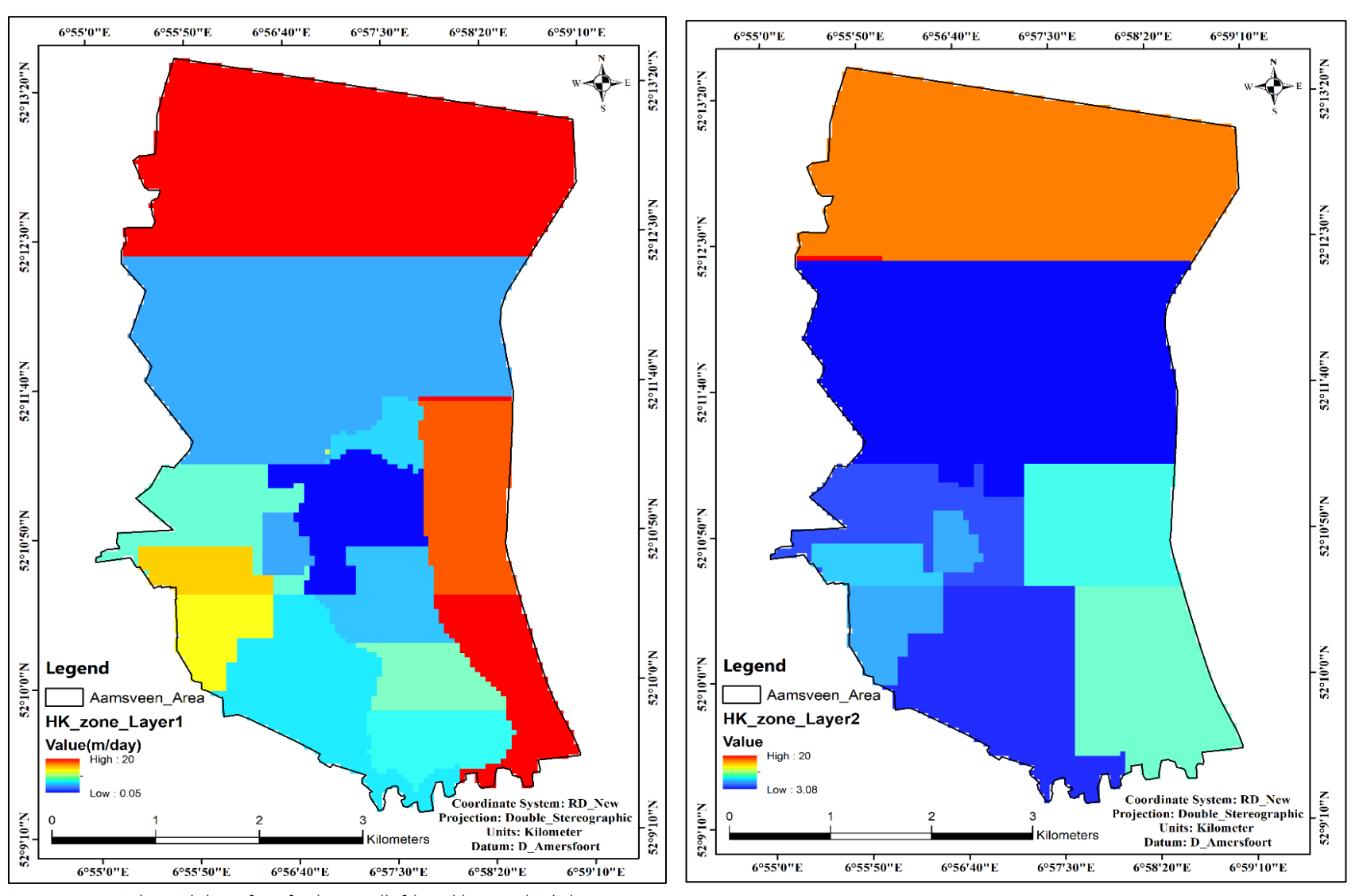


Figure 20: Spatial variability of HK for layer 1 (left) and layer 2 (right)

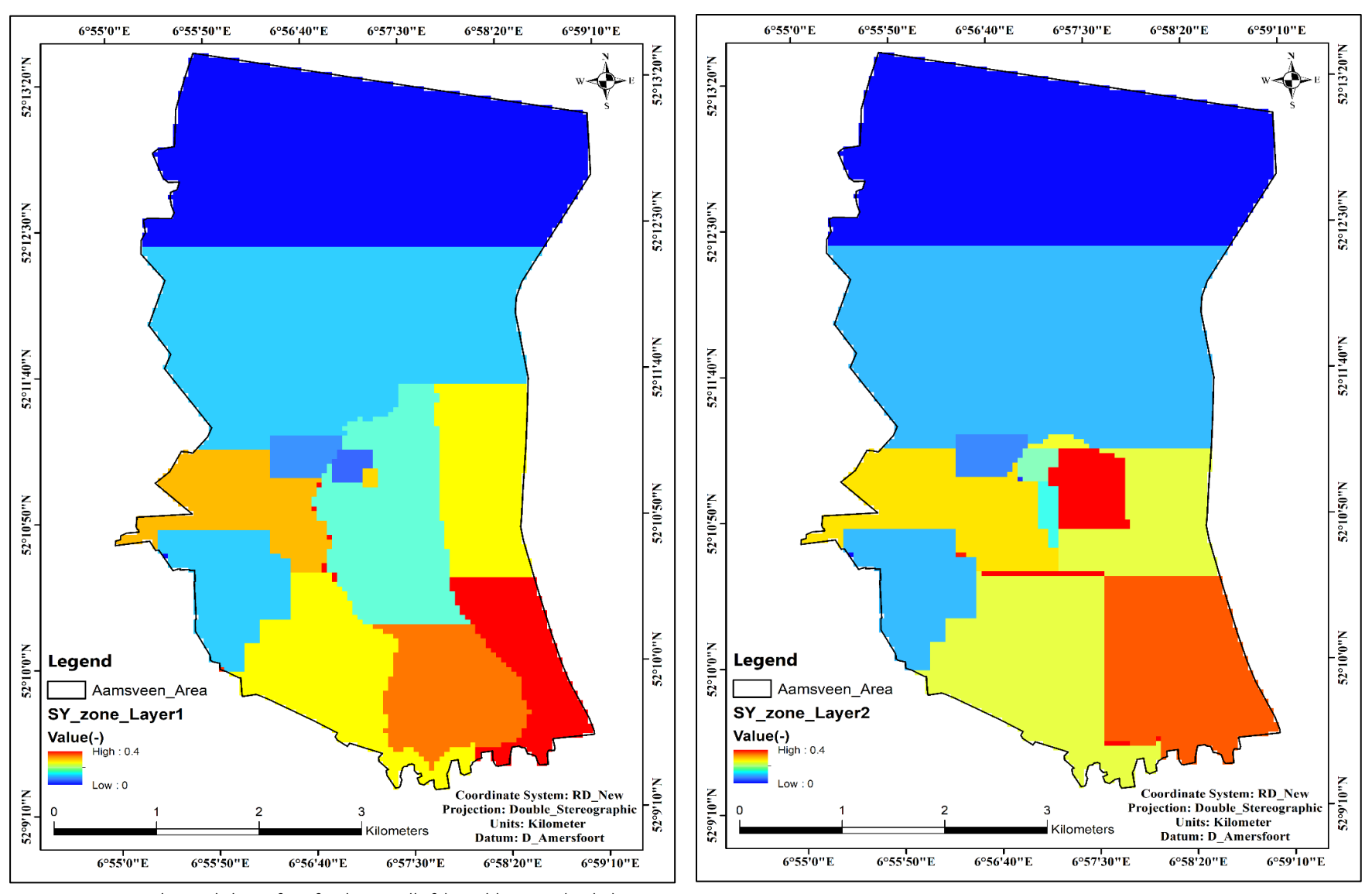
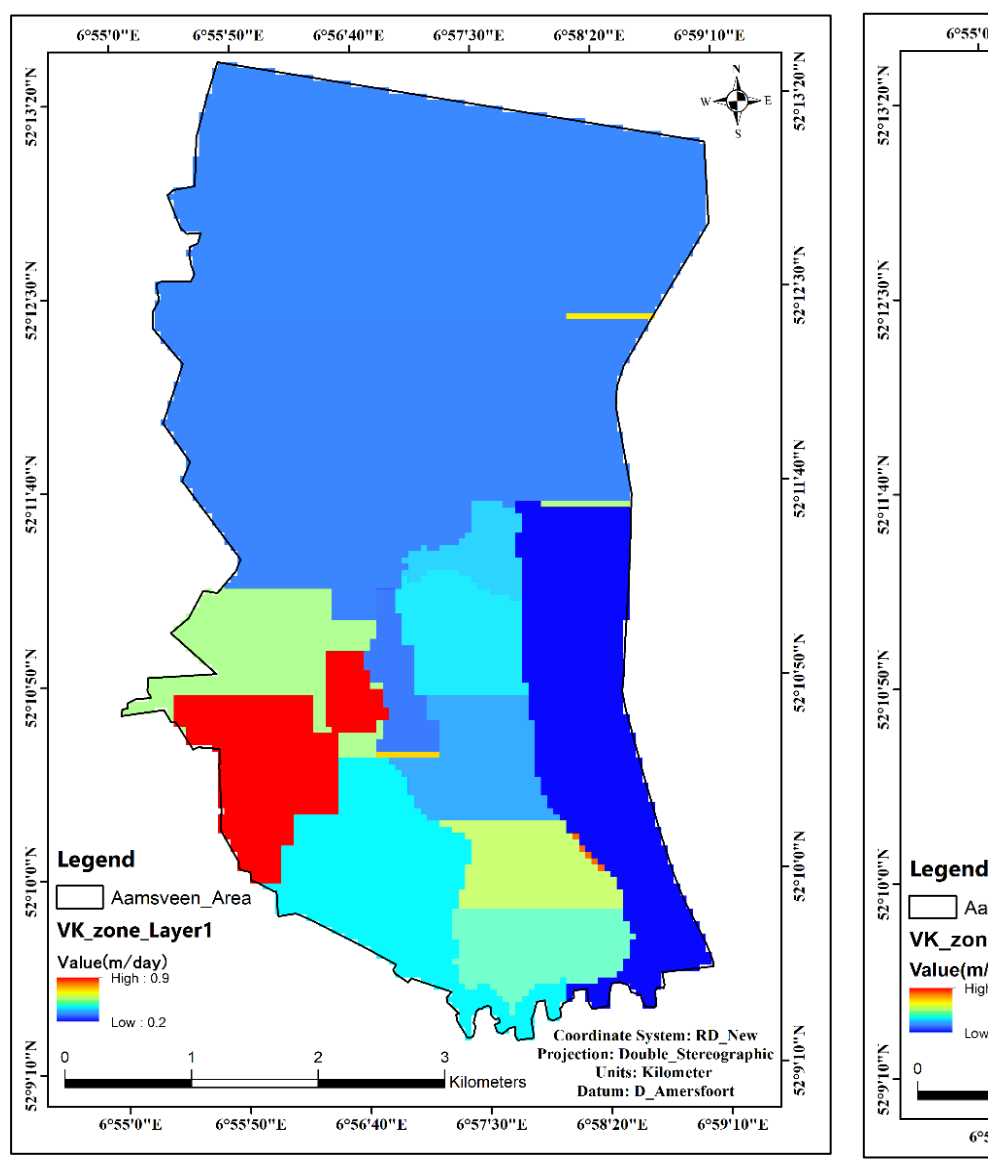


Figure 21: Spatial variability of SY for layer 1(left) and layer 2 (right)



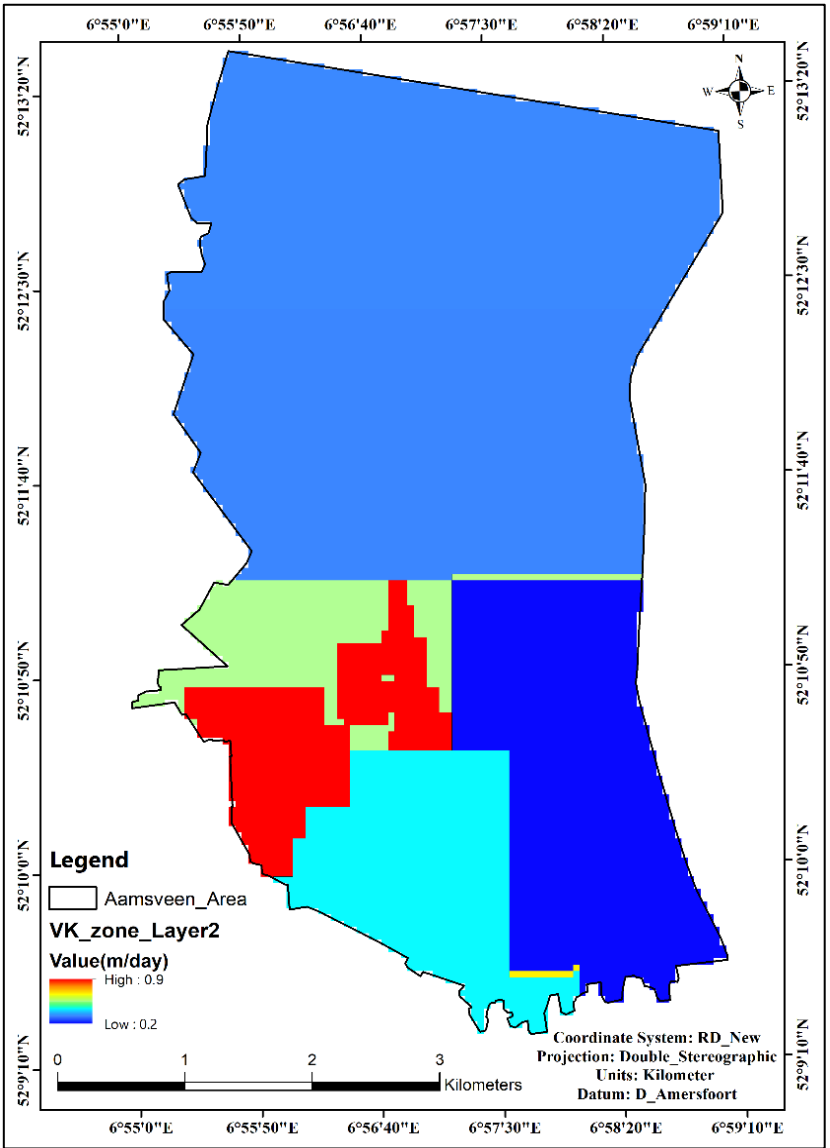


Figure 22: Spatial variability of VK for layer 1 (left) and layer 2 (right)

5.6.2. Calibrated groundwater heads

Figures 23, 24, 25, 26, and 27shows the comparison between simulated heads and observed heads of the piezometers used for the calibration and validation. The accuracy assessment is provided in Table 8. The accuracy parameter values met the calibration targets.

The simulated heads showed similar dynamics to the observed heads, meaning that the model responds quite well to the hydrological forcing.

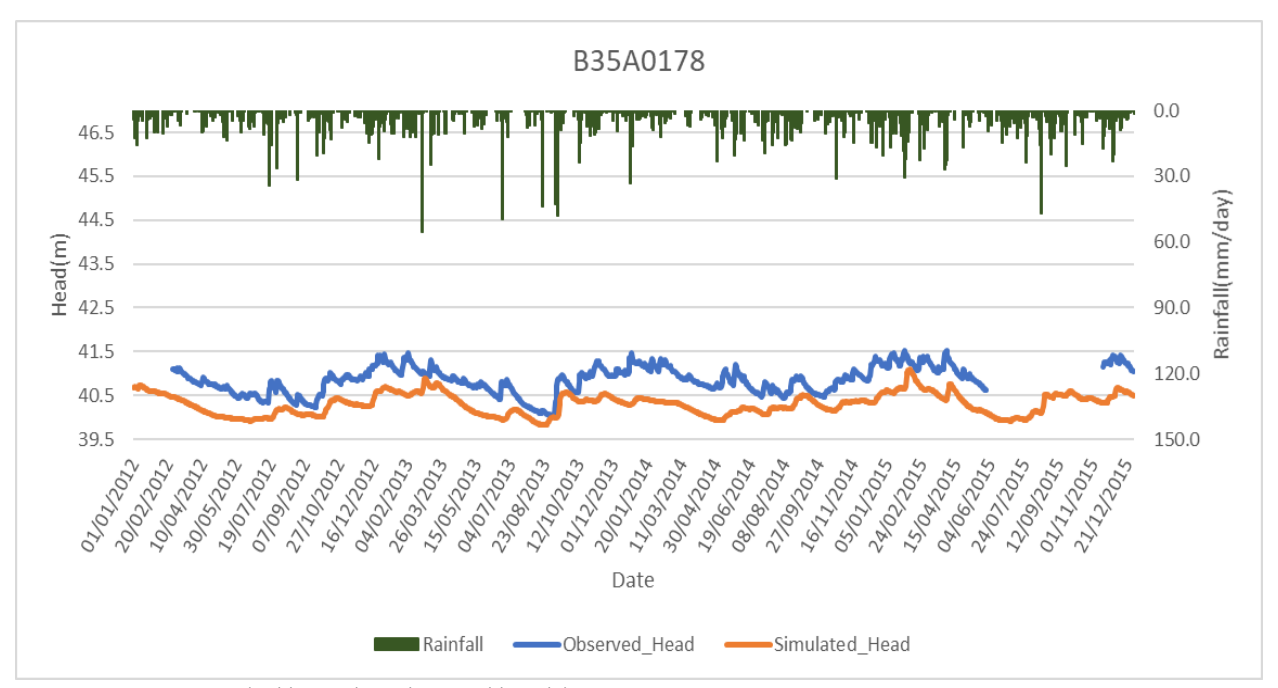


Figure 23: B35A0178 (calibrated vs observed heads)

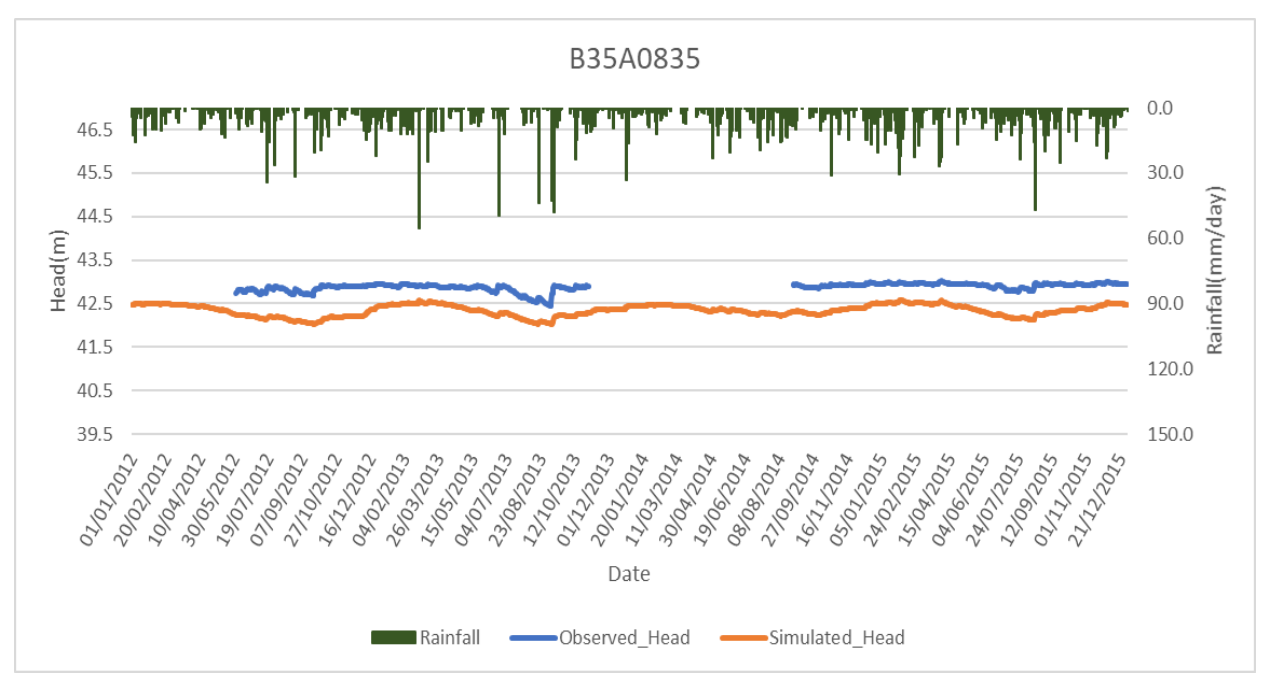


Figure 24: B35A0835 (calibrated vs observed heads)

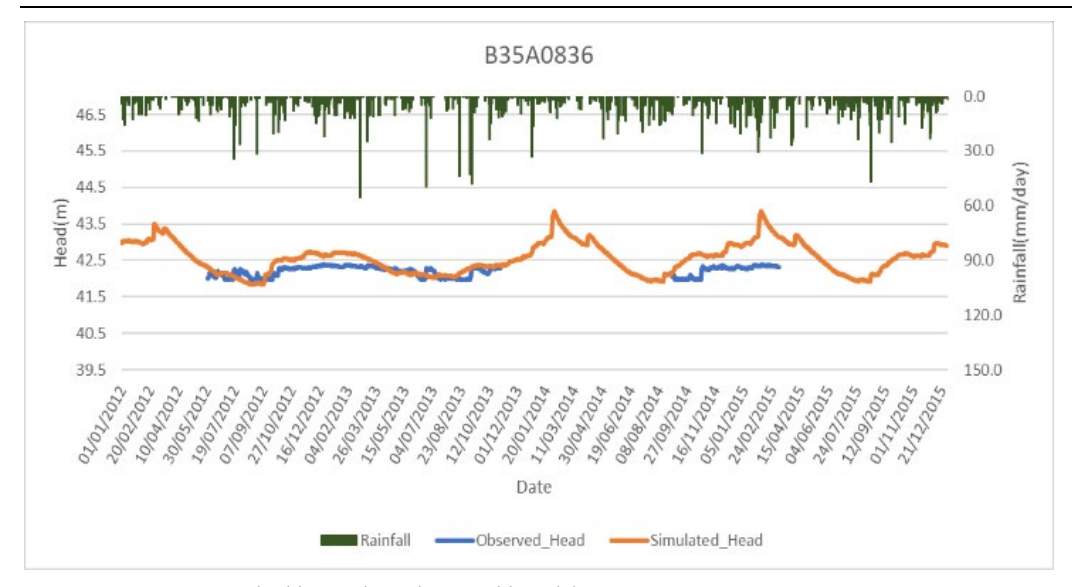


Figure 25: B35A0836 (calibrated vs observed heads)



Figure 26: B35A0837 (calibrated vs observed heads)



Figure 27: B35A0890 (calibrated vs observed heads)

Piezometer	RMSE	MAE
B35A0178	0.46	0.5
B35A0835	0.43	0.43
B35A0836	0.18	0.24
B35A0837	0.06	0.17
B35A0890	0.03	0.04

Table 8: Accuracy assessment between observed and simulated heads

5.6.3. Calibrated streamflow

Figure 28 shows the comparison of simulated and observed streamflow. The VE was found to be 0.48. Although the volumetric error met the calibration target, the temporal pattern of the simulated streamflow does not match in all details with the observed one. The major trends are similar, i.e., streamflow is simulated in the wet periods (e.g., 10/2014 - 04/2015) and dry periods were simulated without streamflow (e.g., 04/2015 - 09/2015), many peaks are missing from the simulation. This is most probably due to the management interventions of the flow directly from the upstream of the gauge.

In general, it can be concluded, that the overall temporal pattern is well simulated, but some details are lost and the model produces less streamflow than what was measured.

It should be noted that the observed streamflow represents only a small upstream part of the model, but this part can be considered to represent the whole model due to their similarity in geology and land cover.

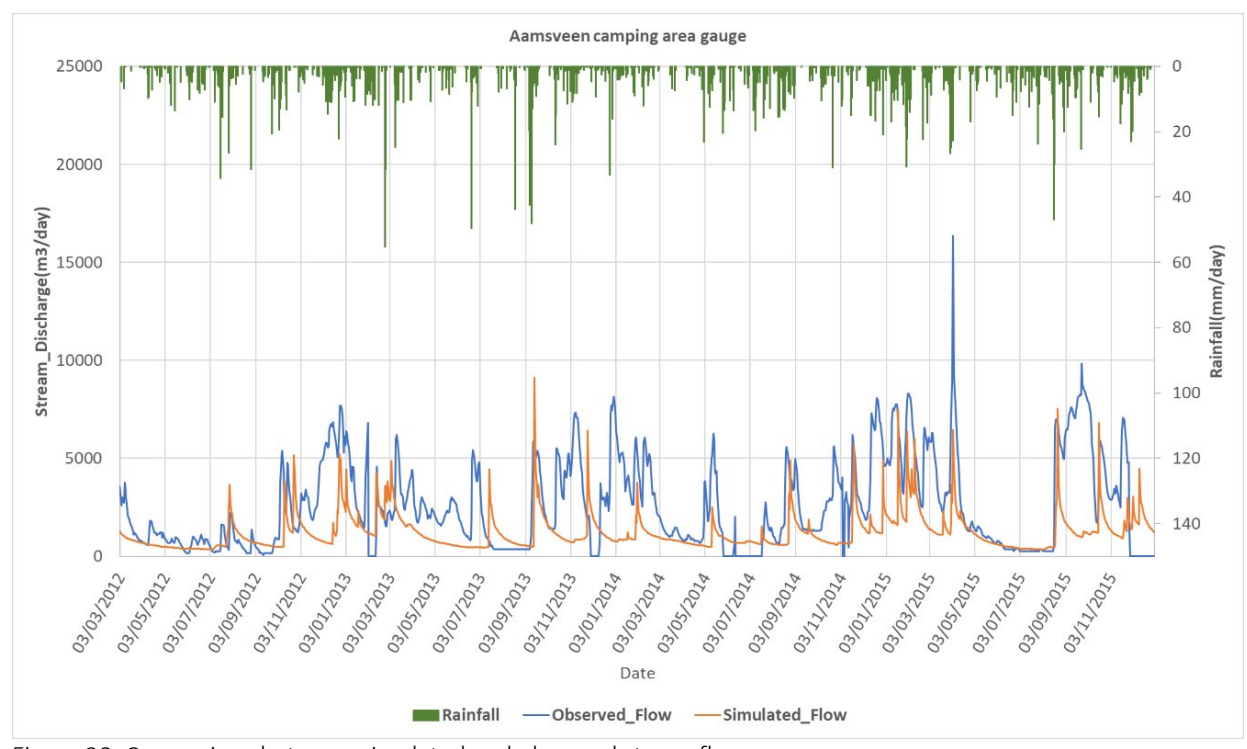


Figure 28: Comparison between simulated and observed streamflow

5.6.4. Calibrated ET_a

The calibration of the model using ET_a aimed at matching the simulated regional ET_a to the MOD16A2 ET_a for the entire calibration period (2012-15). Figures 29 and 30 show the comparison and correlation between the simulated ET_a plus canopy interception and MOD16A2 ET_a. The overall pattern is very similar, which is also proved by the high correlation coefficient. The satellite-based measurements show smaller temporal variations due to:(a) Those are downscaled from 8-day sums, and the simulation is based on daily rainfall events; (b) the vegetation cover is not considered in the satellite-based ET_a with as much detail as in the model.

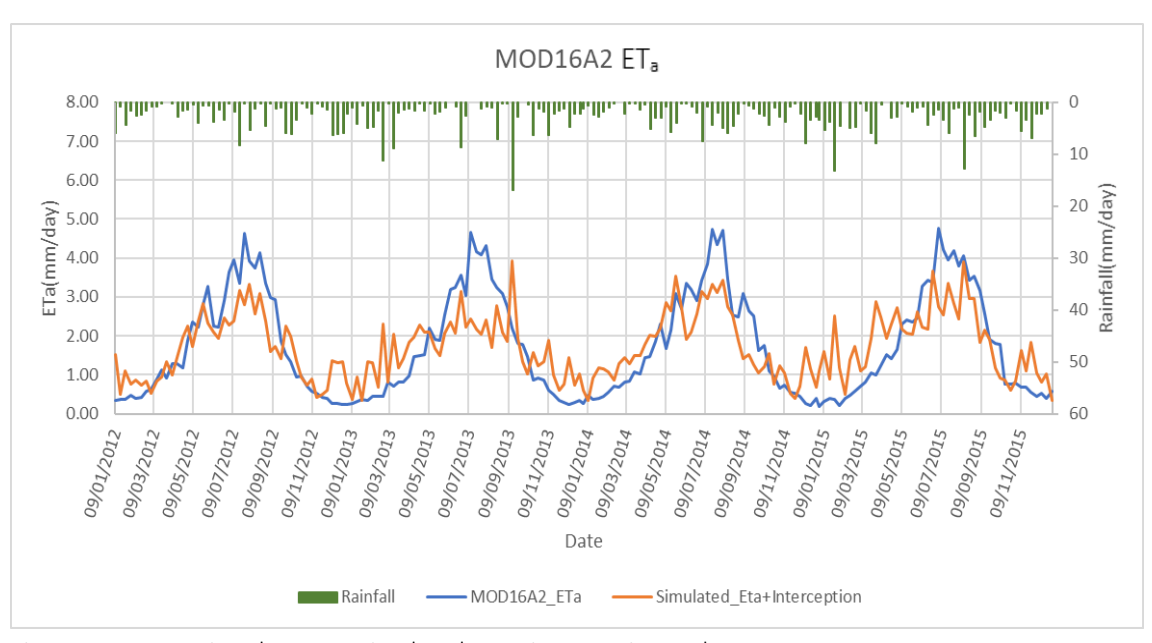


Figure 29: Comparison between simulated ET_a + interception and MODIS16A2 ET_a

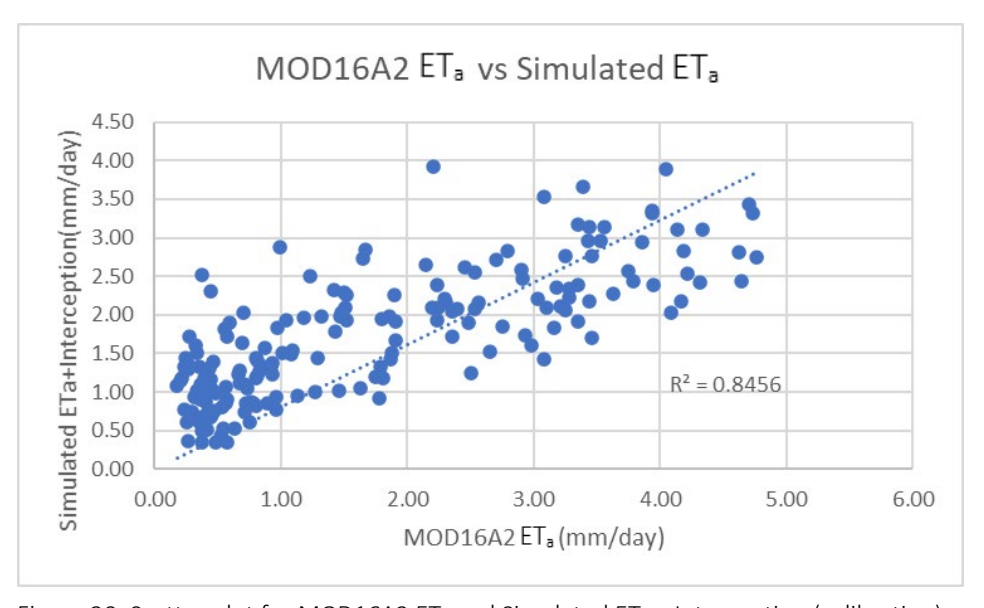


Figure 30: Scatter plot for MOD16A2 ET_a and Simulated ET_a + Interception (calibration)

5.7. Validation Results

5.7.1. Validated groundwater head

Figures 31, 32, 33, 34, and 35 show the comparison between simulated and observed heads during validation, and the accuracy assessment is provided in Table 9. The validation results meet the calibration target as well. The simulated heads are showing very similar patterns and dynamics with observed heads except for B35A0837 (Figure 33) which is demonstrating less dynamics but the same pattern with observed heads. Nevertheless, it is still in the range of the calibration target (RMSE of 0.27m).

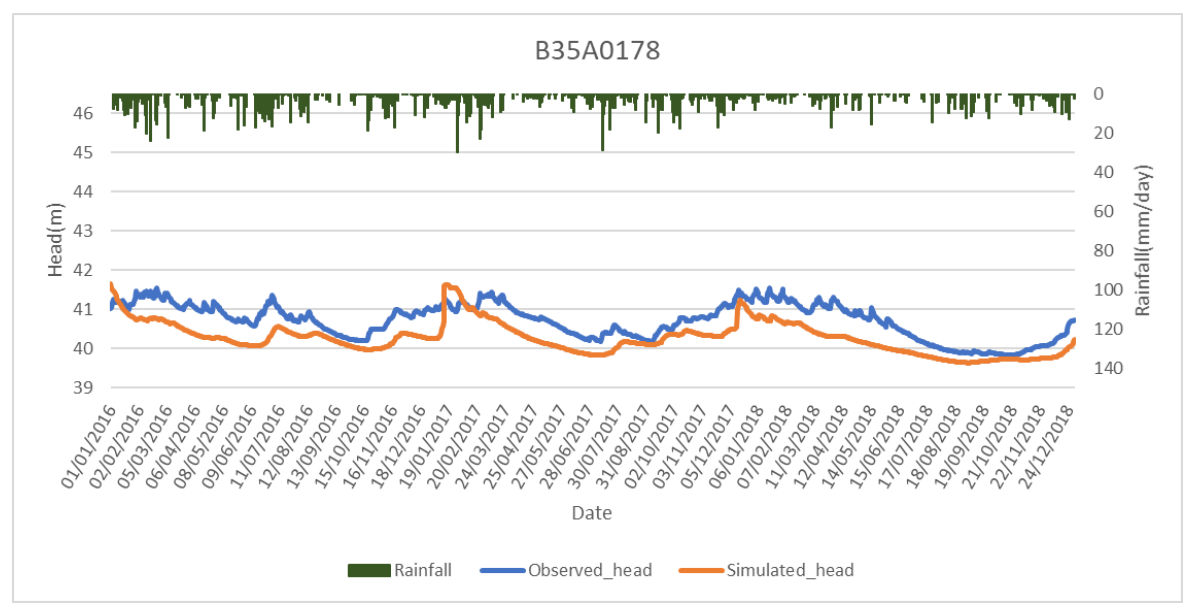


Figure 31: B35A0178 (validated and observed heads)

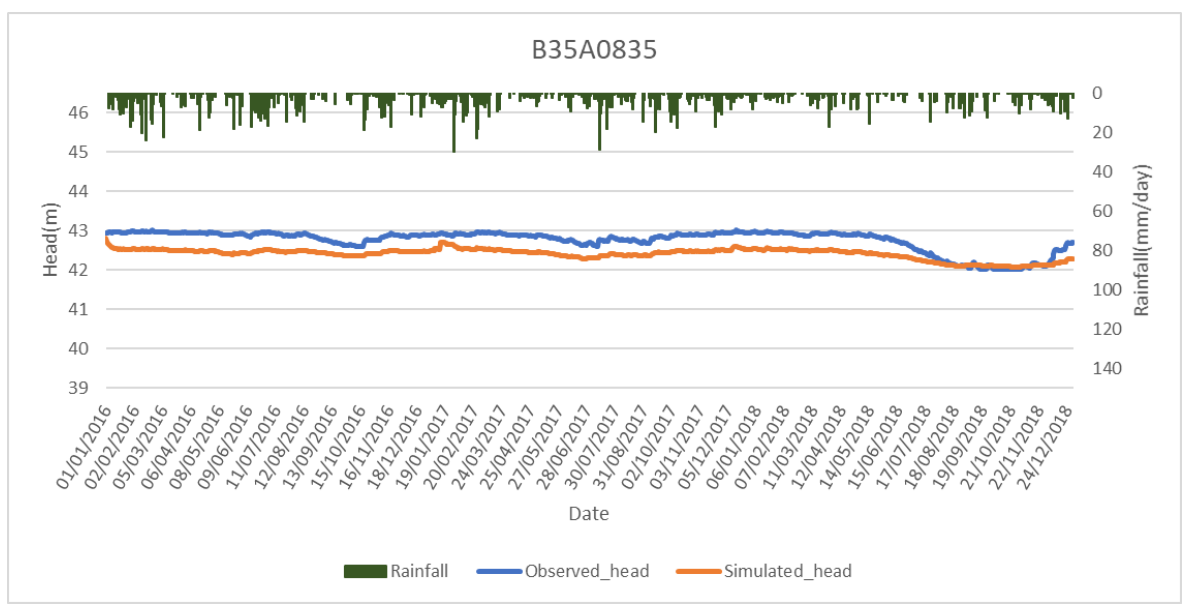


Figure 32: B35A0835 (validated and observed heads)



Figure 33: B35A0837 (validated and observed heads)



Figure 34: B35A0836 (validated and observed heads)



Figure 35: B35A0890 (validated and observed heads)

Piezometer	RMSE	MAE
B35A0178	0.43	0.45
B35A0835	0.34	0.35
B35A0836	0.49	0.56
B35A0837	0.29	0.27
B35A0890	0.68	0.60

Table 9: Accuracy assessment for the validated heads

5.7.2. Validated streamflow

Figure 36 shows the comparison of the simulated flow and validated flow. It can be concluded that the streamflow simulated showing the mean peaks, confirming that the model works pretty well, although further fine-tuning is still possible.

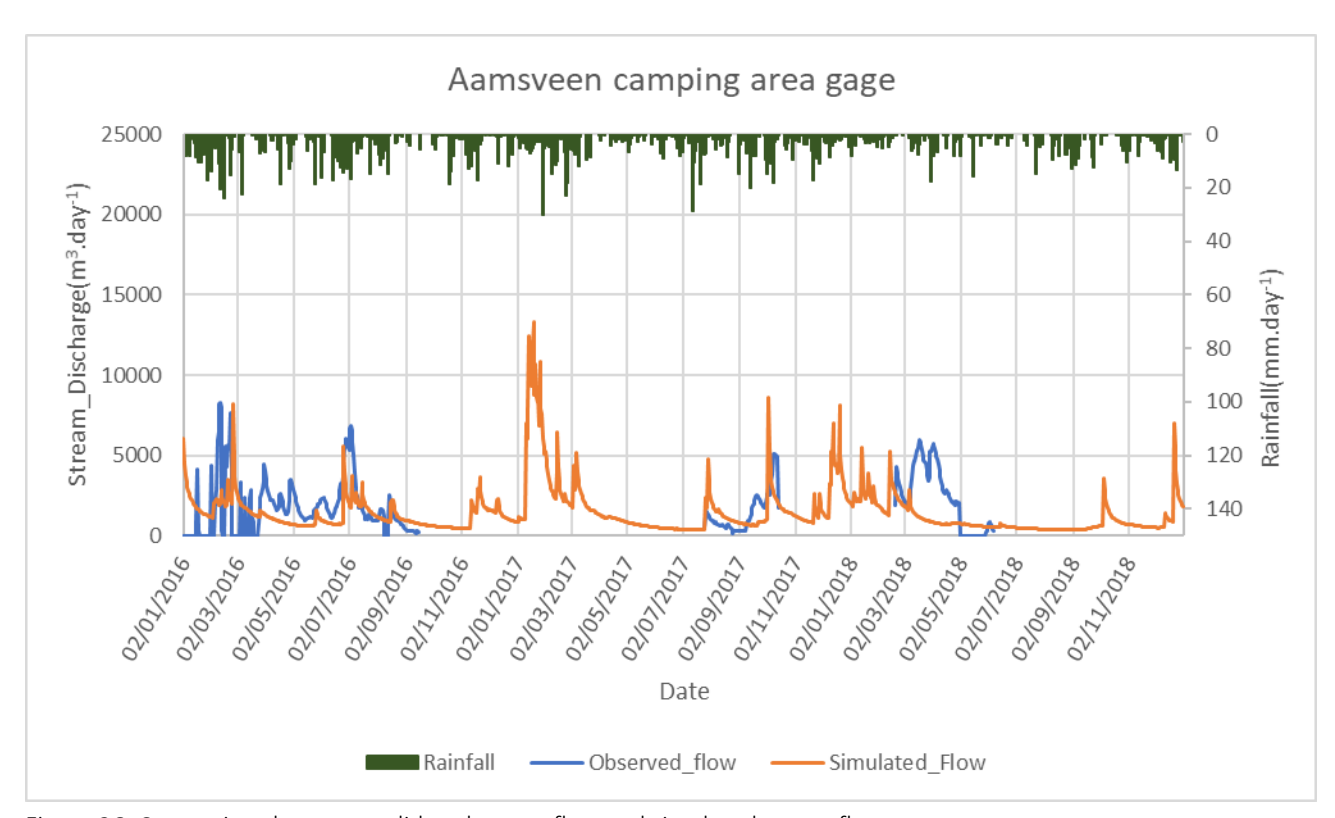


Figure 36: Comparison between validated streamflow and simulated streamflow

5.7.3. Validated ETa

Validation of the model was conducted with MOD16A2 ET_a and comparison results are shown in Figure 37. The correlation (R^2) is 0.78 (Figure 38). It can be concluded that the ET_a is well calculated and basically, the model was well-calibrated. However, further fine-tuning is still possible.

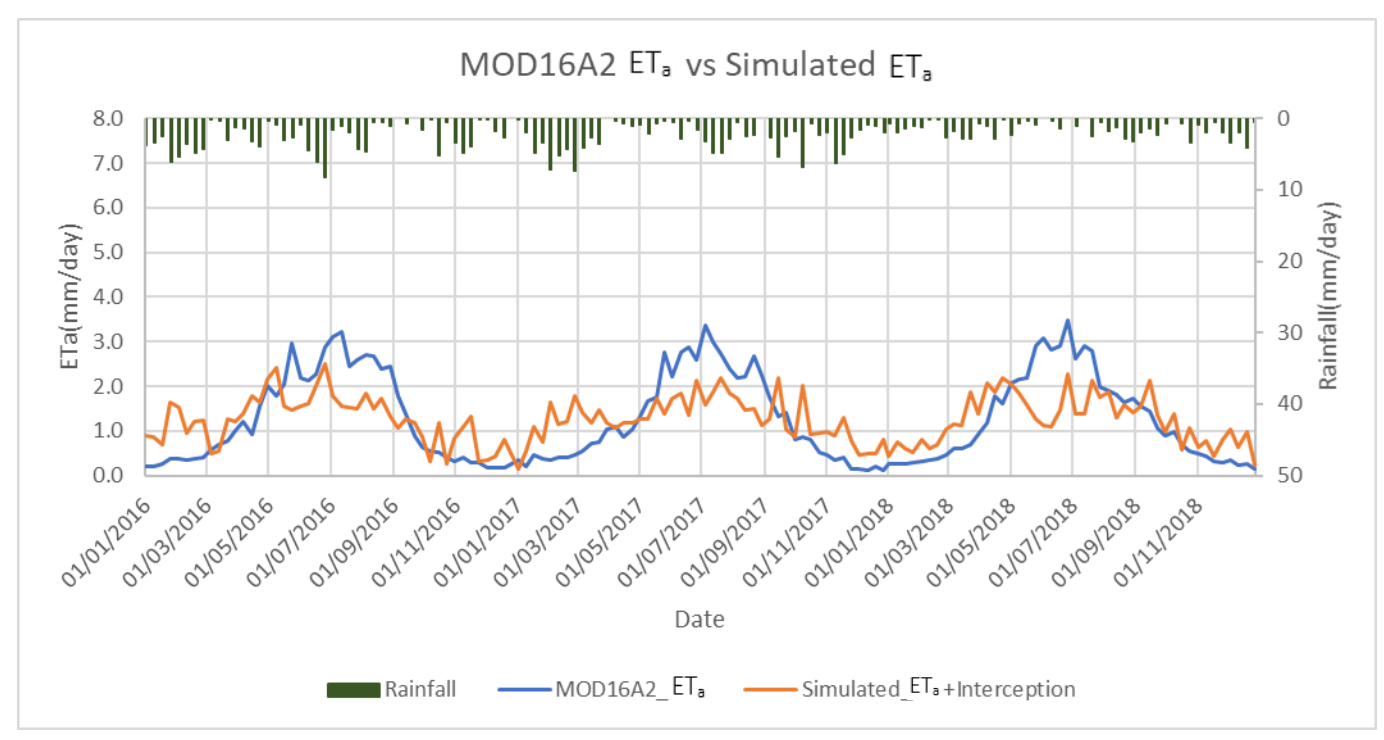


Figure 37: Comparison between MOD16A2 and simulated ET_a (validation)

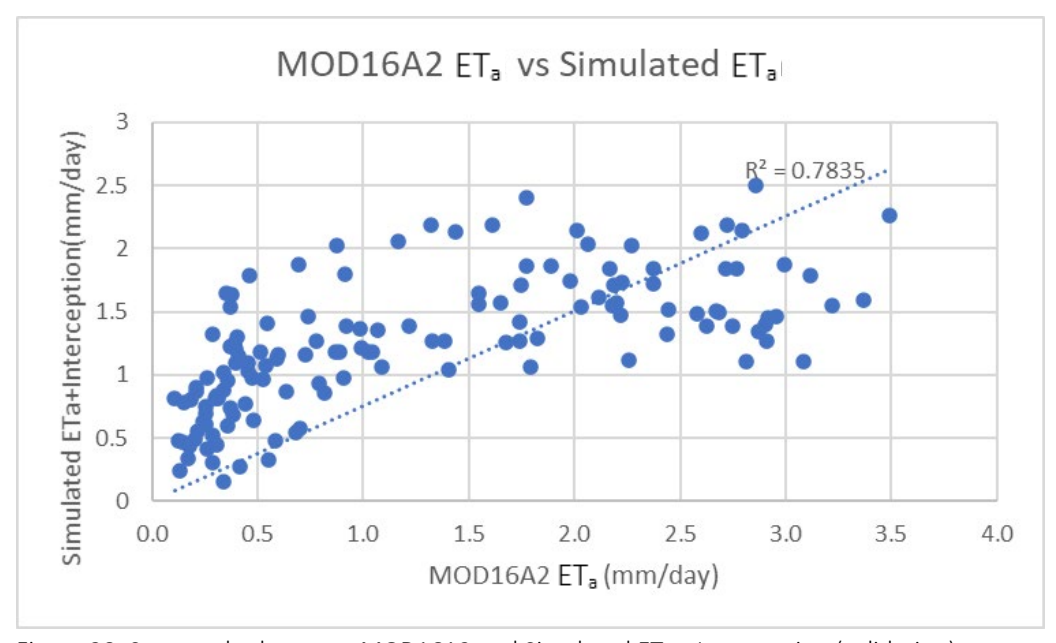


Figure 38: Scatter plot between MOD16A2 and Simulated ETa + Interception (validation)

5.8. Water balance

The water balance of the calibration period (1st January 2012 -31st December 2015) is presented in Table 10. P_e is the effective precipitation or actual infiltration while P_a is the gross infiltration. The main inflow to the entire catchment is Rainfall (P) which accounts an average of 89.56 Mm³(million-meter cube) for the entire calibration period. The major outflow fluxes from the catchment are ET_a that also includes I, flow through streams (Q_b) and drains (Q_{drain}) as well as hortonion and Dunnian runoff (Q_{H+D}). The highest outflow flux from the area is ET_a plus interception with 56.2% of P while the outflow at the catchment outlet (Q_s) accounts 40.5% of P. and (Q_b), (Q_{drain}) and (Q_{runoff}) account 14% of P, 2.5% of P, 1.9% of P respectively. It was noticed that the inflow and outflow are in balance as demonstrated in the water budget of differet zones in Table 11, 12 and 13 (All components are in Mm³.year¹¹).

Year	P	I	P _e	P _a	SF	Q_b	Q_{H+D}	$Q_{in(s)}$	Q _{out (s)}	Q_s	Q in (res)	Q out (res)	Q out (drain)	R_g	I _{exf}	ET_g	ET_{uz}	ETa	R_n	∂s_{uz}	∂s_g
2012	19.8	1.7	17.6	17.9	0.01	2.7	0.3	1.2	3.9	8.0	9.6	0.03	0.5	12.3	13.5	4.9	5.3	10.2	-6.11	0.04	-0.08
2013	22.5	2.1	19.9	20.4	0.01	3.5	0.5	1.2	4.8	9.2	10.5	0.05	0.6	15.8	16.2	5.7	4.1	9.9	-6.13	0.01	-0.06
2014	20.1	1.9	17.9	18.2	0.01	2.6	0.3	1.3	3.9	8.3	10.8	0.06	0.5	12.8	14.4	5.5	5.3	10.8	-7.01	-0.2	-0.4
2015	27.1	2.5	24.0	24.6	0.01	4.1	0.7	1.2	5.4	10.8	11.9	0.06	0.7	19.4	19.5	6.5	4.7	11.3	-6.67	-0.2	-0.2
Total	89.5	8.2	79.46	81.1	0.04	13.2	1.8	4.9	18.0	36.3	42.8	0.22	2.3	60.3	63.6	22.7	19.4	42.2	-25.93	-0.4	-0.8
Mean	22.4	2.1	19.86	20.3	0.01	3.2	0.4	1.2	4.5	9.07	10.7	0.05	0.6	15.10	15.9	5.6	4.8	10.5	-6.48	-0.1	-0.2
% of P		9.3	88.6	90.6	0.1	14.7	1.8	5.4	20.1	40.5	47.8	0.3	2.5	67.3	71.1	25.3	21.9	46.9	29.0	-0.5	0.0

Table 10: Water budget components of Aamsveen in Mm³.Year⁻¹

5.8.1. Surface and unsaturated zone budget

The surface and unsaturated zone budget was obtained by applying equation 4-10. Yearly averages of the water budget components in Table 10 were substituted in the equation and results are presented in Table 11. The negative sign means the outflow from the system while the positive sign means inflow to the system.

In			Out		Total_IN	Total_OUT	IN - OUT	Percentage Discrepancy
P _a	Q_{H+D}	ET_{uz}	R_g	∂s_{uz}				
20.3	-0.4	-4.8	-15.07	-0.1	20.3	-20.4	-0.1	-0.5%

Table 11: Surface and unsaturated zone budget in Mm³. Year⁻¹

5.8.2. Saturated zone budget

The saturated zone budget was estimated using equation 4-11. It was achieved by substituting yearly averages of the water budget components in Table 10 in the saturated zone equation and results are shown in Table 12.

		In	Out To							Total_IN	Total_OUT	IN- OUT	Percentage
R_g	Q in (res)	$Q_{in(s)}$	SF	ET_g	I_{exf}	Q out (res)	$Q_{out(s)}$	Q out (drain)	∂s_g				Discrepancy
15.10	10.7	1.2	0.01	-5.6	-15.9	-0.05	-4.5	-0.56	-0.2	27.01	-26.8	0.21	0.8%

Table 12: Saturated zone budget in Mm³. Year⁻¹

5.8.3. Entire Model

The yearly averages were used to estimate the entire model budget as well using equation (4-4) and outcomes are presented in Table 13.

li	า	Out				Total_IN	Total_OUT	IN - OUT	Percentage	
P	SF	ET _a	I	Q_s	Q_{drain}	дs				Discrepancy
22.4	0.01	-10.5	-2.1	-9.07	-0.6	-0.3	22.4	-22.5	-0.1	-0.44%

Table 13: Entire model budget Mm³. Year⁻¹

5.9. Temporal and spatial variability of water fluxes

Figure 40 demonstrates the temporal variability of groundwater fluxes of Aamsveen in mm/day. It was noticed that an increase in ET_g during the summer period results in a decrease of R_n due to low R_g as the rainfall reduces in the summer period. The I_{exf} is higher in the winter season when ET_g is considerably low.

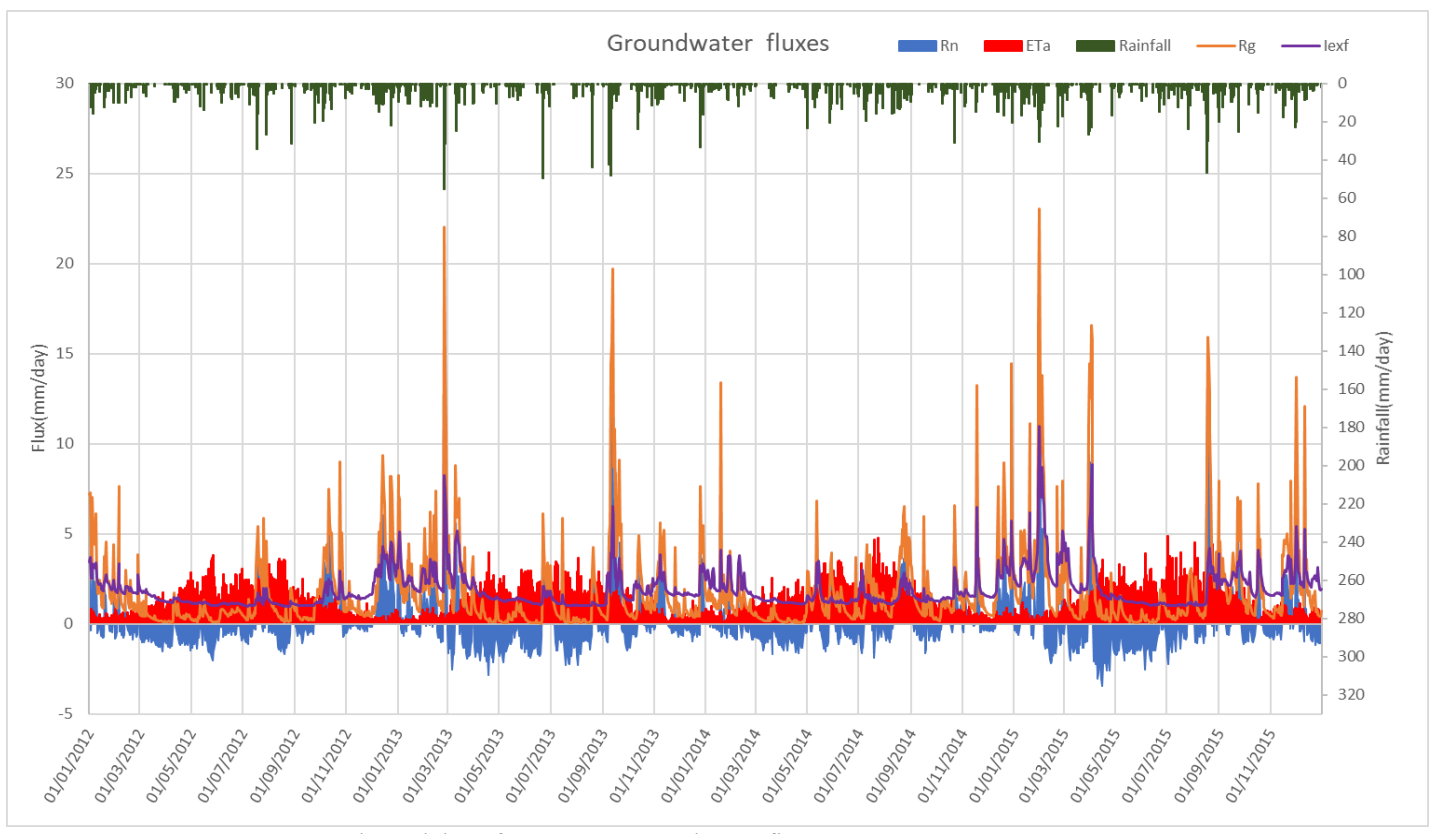


Figure 39: Temporal variability of important groundwater fluxes

5.9.1. Spatial variability

 R_g , I_{exf} , and ET_a were used to analyze the spatial variability of groundwater fluxes in Aamsveen. MODFLOW-NWT provides daily images of all water budget components. These three fluxes play the most important role in the hydrological changes of the wetland. Based on the temporal variability of these fluxes (Figure 40), characteristics dates with a high flow rate that is expected to result in high spatial variability were selected. Later, It was even noticed that the spatial pattern doesn't vary significantly with time. The selected dates selected are 29^{th} December 2014 for both R_g and I_{exf} and 5^{th} June 2015 for ET_a and the resulting images are shown in Figure 41. It can be observed that R_g follows the pattern of ET_a . In the wetland area where ET_a is high, R_g is also high and both decrease as we move towards the built-up area. I_{exf} is high in the wetland area and even higher in the reservoir area as more water.

It can also be noted that, although the calibration targets were met, the northern part (zone) is inconsistent compared to the rest of the model, a further fine-tuning will be needed for the region.

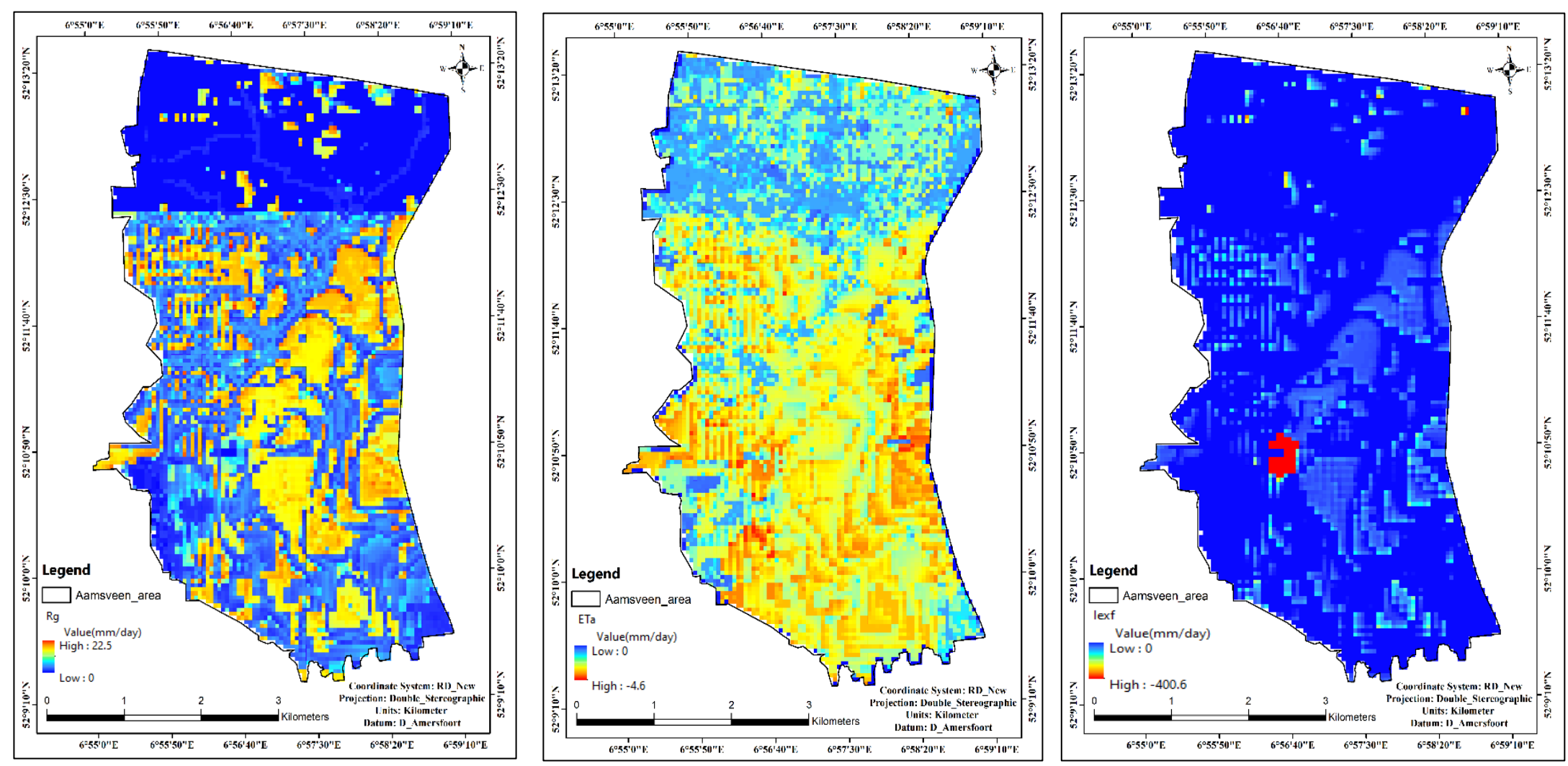


Figure 40: Spatial variability of Rg (left), ETa excluding interception (Middle) and Iexf (right) (the – sign refers only to the direction of the flow)

5.9.2. Sensitivity Analysis

5.9.2.1. Sensitivity on groundwater heads

Figure 42, demos that groundwater heads were more sensitive to changes in SY than to changes in HK, θ_{ext} , and VK, as has also been confirmed by Emmanuel (2019). HK was also more sensitive relatively to θ_{ext} and VK. These two parameters (SY and HK) were very important in the calibration

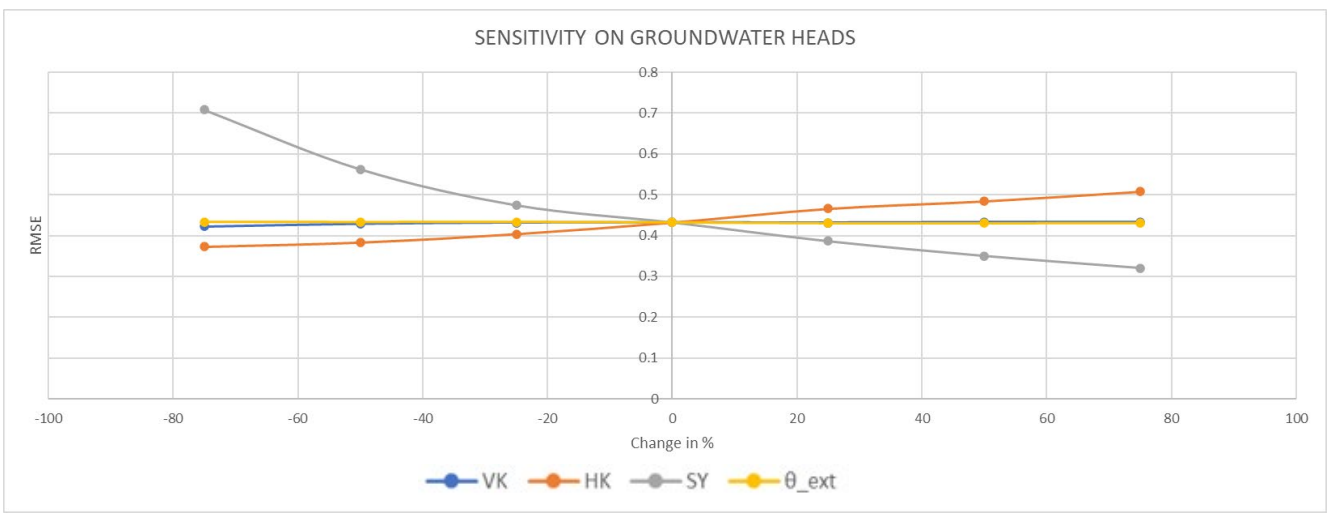


Figure 41: Sensitivity analysis on groundwater heads

5.9.2.2. Sensitivity on ETa

It was noticed that ET_a including interception was very sensitive to changes on SY and θ_{ext} than VK and HK as demonstrated in Figure 43. It is due to the fact that these two parameters (SY and θ_{ext}) control the amount of water that can be taken out from the aquifer.

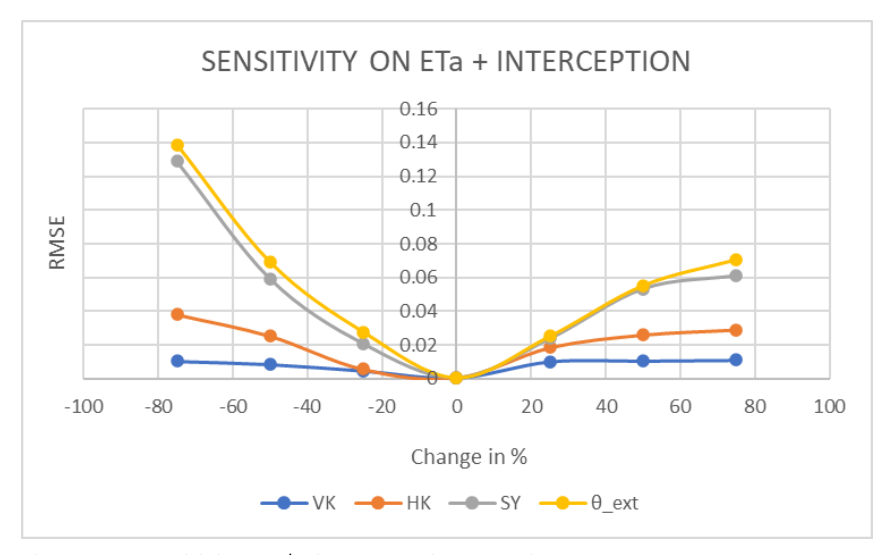


Figure 42: Sensitivity analysis on ET_a + interception

5.10. Comparison of the current study with the study Emmanuel (2019)

The comparison was based on calibrated groundwater head, streamflow, and water budget of the region. In general, the improved spatial and temporal ET_p was found to be crucial in providing dynamics for boreholes and streamflow in the region.

5.10.1. Groundwater head comparison

The Emmanuel's model was calibrated with four piezometers while the current model was calibrated with five piezometers (one additional piezometer). The additional piezometer was key in improving calibration hence providing a more reliable model. The accuracy of the calibrated heads for both models was found to be in the predefined range as described in section 4.2.7. Besides, the dynamics in groundwater heads were improved than in Emmanuel's model such as piezometer 35A0837 shown in Figure 44 compared to the current one demonstrated in Figure 26. It was achieved by considering time series vegetation changes of the region when defining ET_p (described in section 4.1). The HK values were significantly adjusted in the present model but the model zonations were slightly modified. The HK was varying from 0.08 to 11 m.day⁻¹ in the Emmanuel's model but with the current model, it is varying from 0.05 to 20 m.day⁻¹. The warm-up period was discarded in Emmanuel's model while in the current model it was considered. It was found that the warm-up period was very important in the calibration as the model start with more realistic state variables.



Figure 43: Previously calibrated groundwater head for piezometer B35A0837 by Emmanuel (2019)

5.10.2. Streamflow comparison

The streamflow was significantly improved because the model has significantly provided more or similar dynamics as observed streamflow. It was achieved by making sure that the model has enough water by redefining the canopy interception rate of different landcover classes in the region and introducing the warm-up period. Figure 45 demonstrates how the stream flow dynamics were not perfectly simulated in Emmanuel's model contrary to the current model which provides more dynamics (Figure 28).

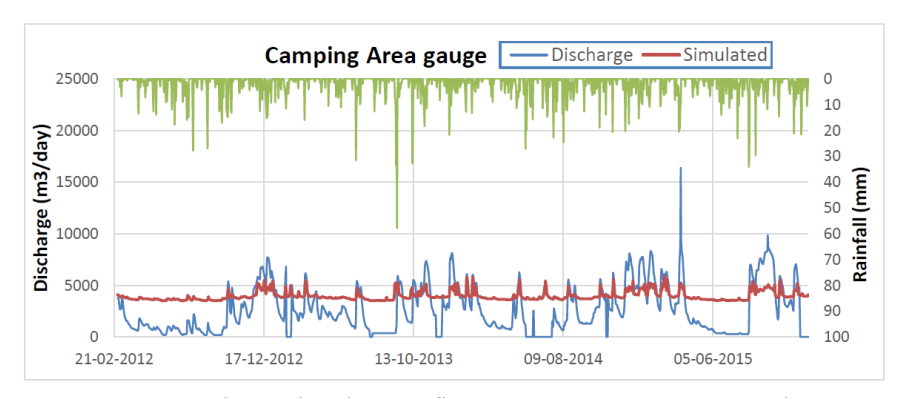


Figure 44: Previously simulated streamflow at Aamsveen camping Area by Emmanuel (2019)

5.10.3. Calibration with satellite ETa

 ET_a was produced in Emmanuel's model and it was the main outflow flux in Aamsveen. Yet it is not known how accurate it is. In the current model, the calibration was carried out using satellite-based ET_a (MOD16A2 ET_a). With this type of calibration, the parameters are more constrained hence providing a more reliable model. It was found that θ_{ext} and SY affect highly ET_a . In the previous θ_{ext} was set to 0.1 but in the current model was found to be 0.03. The specific yield in Emmanuel's model was varying from 0.18 to 0.45 while in the present model, it varies from 0 to 0.4.

5.10.4. Water budget comparison

Emmanuel (2019) concluded that the highest outflow flux from Aamsveen is ET_a with 63.2% of the total rainfall. This is the total ETa which was the sum of I with 25% of P and simulated ET_a with 37.8% of P where ET_g accounts 35.3% of P and ET_{uz} accounts 2.5% of P. The current model, ET_a was seen to be the highest outflow flux with 56.2% of P including I where interception, ETuz, and ET_g accounts 9.3, 21.9 and 25.3 % of P. In his model the I had a significant effect (25% of P) to the total ET_a contrary to the current model where Interception accounts 9.4 % of P . it can be explained by the fact that interception was refined considering global standard interception rate which resulted in reducing interception rate. The calibration with satellite-based ET_a resulted in increasing ET_{uz} relative to the Emmanuel's model. It is due to a decrease in extinction water content and specific yield as stated in section 5.10.3. Figure 46 demonstrates important water budget components which were produced using yearly averages of the whole calibration period (2012-15).

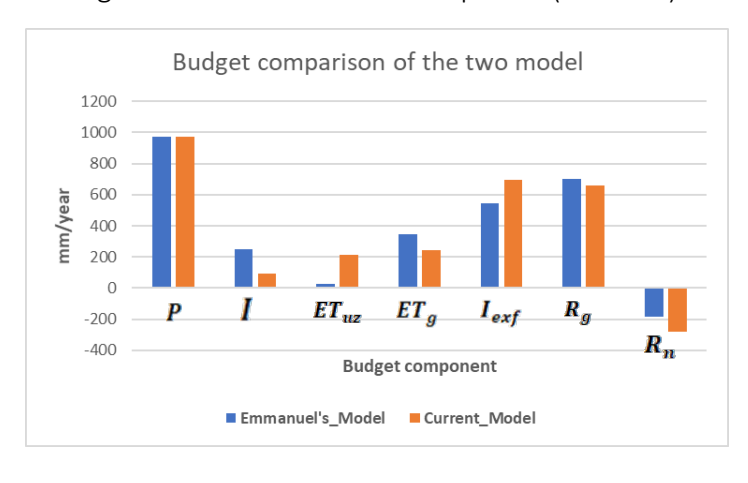


Figure 45: Budget comparison between Emmanuel's model and the current model of Aamsveen

5.11. calibration and validation experience with satellite-based ETa

This new approach of calibrating and validating the Aamsveen model with ET_a resulted in a more reliable model. It consisted of, in addition to calibrating and validating with groundwater heads and streamflow, matching the satellite-based ET_a the satellite-based ET_a (MOD16A2 product), and the simulated ET_a plus Interception time series.

For each run, the simulated components (heads, streamflow, and ET_a) were compared to the observed components (heads, streamflow, and satellite-based ET_a). A sensitivity analysis was used to define the parameter, which affects in one way or another all these three components. For instance, an increase in SY (allowing more water to be removed from the aquifer) resulted in an increase of ET_a and a decrease in GW head. An increase in θ_{ext} (limiting ET in the unsaturated zone) resulted in a decrease in ET_a and a slight increase in groundwater heads. All these changes have to be carried out taking into consideration realistic parameters

It was noticed that visualization of the spatial distribution of groundwater fluxes, especially ET_{uz} and ET_g in the MODFLOW-NWT interface was key for a good calibration. It helped to detect regions with unrealistic values. For instance, if an unrealistically higher was noticed in the built-up area than in the wetland area, then the most sensitive parameter was adjusted accordingly. This type of calibration gives the user more room for improvements and control of the model including groundwater fluxes (ET_{uz} and ET_g). Most integrated groundwater models provide ET_a but it is not exactly understood how accurate it is. The satellite-based ET_a time-series helped to keep the modelled ET_a in a realistic value range. For a precise and reliable model which can be used for forecasting purposes, this approach can be used.

6. CONCLUSION AND RECOMMANDATION

6.1. Conclusion

The main objective of this study was to develop a method that integrates satellite-based evapotranspiration time series in integrated groundwater modeling using the example of the Aamsveen for a calibration period of 4years (1st January2012-31st December 2015) and a validation period of 3years (1st January2012-31st December 2015). It was achieved by improving the existing transient model of Aamsveen towards spatial and temporal variable ETp. Besides, the model was calibrated and validated using satellite-based ETa (MOD16A2 product). This was a new approach to the commonly used method which consist of calibrating and validating the groundwater model with the state variables (observed groundwater heads and streamflow). The results of the current model were compared to the Emmanuel's model.

Referring to the specific objectives and research questions of this study, it can be concluded that:

1. To improve the ET_p of the existing integrated model of Aamsveen by defining the spatial and temporal distribution of the ET_p

In Emmanuel's model, the spatial and temporal variability of ET_p were not perfectly considered. A landcover map used to estimate ET_p did not consider the growth of bushes that have been increasingly growing in the wetland. In the current model, two different independent methods that provide spatial and temporal distributed ET_p (MODIS16A2, the satellite-based ET_p product, and K_c -based ET_p) were analyzed and compared to each other to define which one is suitable for improving the existing wetland model. MOD16A2 satellite-based ET_p provides spatial and temporal distributed ET_p defined with the help of a surface energy balance model. The K_c -based ET_p approach consists of multiply ET_a (obtained from in situ weather data) to K_c values of different vegetation species. The K_c was linked to NDVI values to account for the vegetation changes in the area. It was seen that the K_c -based ET_p approach is better at representing more spatial patterns details of the Aamsveen which is crucial for integrated groundwater modeling. However, MOD16A2 had a strong correlation with the K_c -based ET_p approach in terms of representing the temporal variability of ET_p . In regions where in situ data are insufficient, it can be an alternative option.

It was noticed that these changes had a significant effect at representing the dynamics of water fluxes, heads, and streamflow which wasn't perfectly simulated in the Emmanuel's model.

2. To calibrate and validate the integrated groundwater model with satellite-based ETp

The wetland model was calibrated and validated using the MODIS16A2 ET_a product. It was achieved by more or less matching the simulated ET_a that includes interception to the satellite-based ETa. Average daily values of ET_a taken every eight days (MODIS16A2 temporal resolution) in mm.day⁻¹ were used for the calibration and validation processes. It was noticed that extinction water content (θ_{ext}) and specific yield (SY) parameters influence ET_a considerably. The calibration and validation of integrated groundwater modeling with satellite-based ET_a is possible and can provide more reliable results. This is because the model is subject to less degree of freedom and parameters are further constrained which was also confirmed by Li et al. (2009). This approach was new in the study area but can also be applied in other regions where in situ data are insufficient and accuracy in ET_a is required.

3. Comparison with Emmanuel (2019)

The simulation results of the current model and the Emmanuel's model were compared. The comparison was made to groundwater heads, streamflow, and water budget. In general, the improvement made were essential and made a significant effect on the simulation of the wetland dynamics.

6.2. Recommendation

The interception was found to be an important flux for the wetland modeling. An appropriate method is needed for accurate estimation. In the current model, It was assumed that all the water intercepted was evaporated. However, in reality, they might be a throughfall or wind might blow and causes leaves to shake hence some amount of intercepted rainfall by a canopy might fall on the ground. Besides the rain characteristics, these processes also influence the interception and might be considered when proper meteorological data is available.

The k_c -NDVI relationship applied in this research was obtained from the literature. It has been developed in an area with more or less similar characteristics to Aamsveen. However, a relationship developed specifically for Aamsveen would provide more accurate results.

It was found that the observed data (groundwater heads and streamflow) are insufficient and not well distributed in the Aamsveen catchment. Some piezometers and stream gauges were having gaps due to poor maintenance. Therefore, the installation of new piezometers and stream gauges that are evenly distributed is required in the area.

- Al, A. et. (1998). FAO Irrigation and Drainage Paper Crop by. *Irrigation and Drainage*, 300(56), 300. https://doi.org/10.1016/j.eja.2010.12.001
- Allen, R. G., Pereira, L. S., Raes, D., & Smith, M. (1998). FAO Irrigation and Drainage Paper No. 56 Crop Evapotranspiration. March.
- Anderson, M. P., Woessner, W. W., & Hunt, R. J. (2015a). *Chapter 1 Introduction* (M. P. Anderson, W. W. Woessner, & R. J. B. T.-A. G. M. (Second E. Hunt (eds.); pp. 3–25). Academic Press. https://doi.org/https://doi.org/10.1016/B978-0-08-091638-5.00001-8
- Anderson, M. P., Woessner, W. W., & Hunt, R. J. (2015b). *Chapter 2 Modeling Purpose and Conceptual Model* (M. P. Anderson, W. W. Woessner, & R. J. B. T.-A. G. M. (Second E. Hunt (eds.); pp. 27–67). Academic Press. https://doi.org/https://doi.org/10.1016/B978-0-08-091638-5.00002-X
- Anderson, M. P., Woessner, W. W., & Hunt, R. J. (2015c). Model Calibration. In *Applied Groundwater Modeling*. https://doi.org/10.1016/b978-0-08-091638-5.00009-2
- Anderson, M. P., Woessner, W. W., & Hunt, R. J. (2015d). More on Sources and Sinks. In *Applied Groundwater Modeling*. https://doi.org/10.1016/b978-0-08-091638-5.00006-7
- Ayyad, S., Al Zayed, I. S., Ha, V. T. T., & Ribbe, L. (2019). The performance of satellite-based actual evapotranspiration products and the assessment of irrigation efficiency in Egypt. *Water* (*Switzerland*), 11(9). https://doi.org/10.3390/w11091913
- Bakhtiyari, S. G. (2017). Analysis And Modeling Of Groundwater System For Wetland Management With The Example Of The Aamsveen Wetland In The Analysis And Modeling Of Groundwater System For Wetland Management. [Masters' thesis]. https://library.itc.utwente.nl/login/2017/msc/wrem/ghasemi.pdf
- Bell, J. ., Hullenaar, van 't J. W., Jansen, A. J. ., Linden, M., & Sevink, J. (2018). Ecohydrologische systeemanalyse Aamsveen. *Bell Hullenaar Ecohydrologisch Adviesbureau*, 1–118.
- Buitink, J., Swank, A. M., van der Ploeg, M., Smith, N. E., Benninga, H.-J. F., van der Bolt, F., Carranza, C. D. U., Koren, G., van der Velde, R., & Teuling, A. J. (2020). Anatomy of the 2018 agricultural drought in The Netherlands using in situ soil moisture and canopy nearinfrared reflectance satellite imagery. *Hydrology and Earth System Sciences, August*, 1–17.
- Choudhury, B. J., Ahmed, N. U., Idso, S. B., Reginato, R. J., & Daughtry, C. S. T. (1994). Relations between evaporation coefficients and vegetation indices studied by model simulations. *Remote Sensing of Environment*, *50*(1), 1–17. https://doi.org/10.1016/0034-4257(94)90090-6
- Doorenbos, J., & Pruitt, W. O. (1977). *Guidelines for predicting crop water requirements*. Food and Agriculture Organization of the United Nations.
- El-Zehairy, A. A., Lubczynski, M. W., & Gurwin, J. (2018). Interactions of artificial lakes with groundwater applying an integrated MODFLOW solution. *Hydrogeology Journal*, *26*(1), 109–132. https://doi.org/10.1007/s10040-017-1641-x
- Emmanuel, S. G. (2019). Modeling of groundwater systems in a wetland: a case study of the aamsveen, the netherlands (Issue February) [Masters' Thesis].

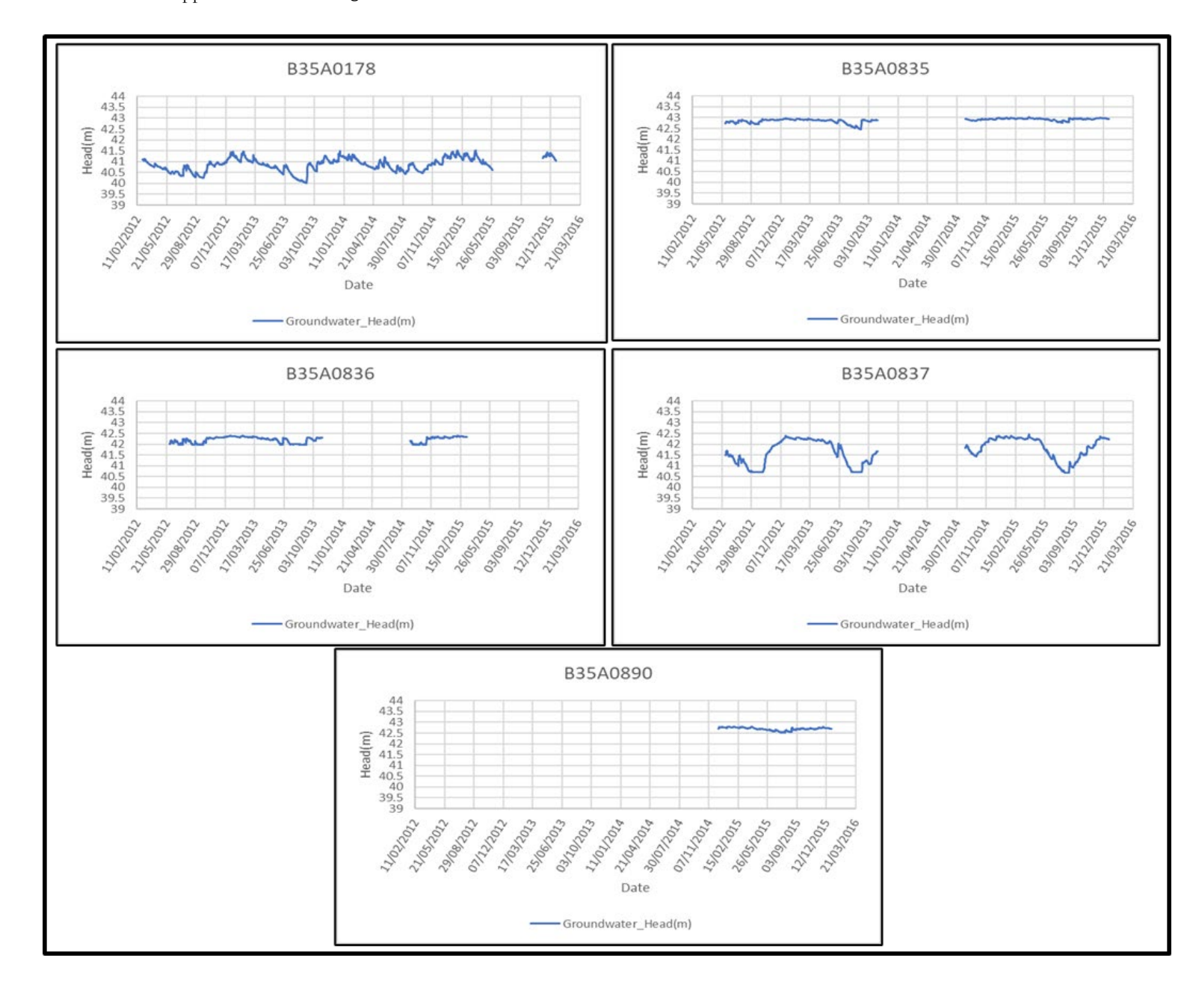
 https://library.itc.utwente.nl/papers 2019/msc/wrem/emmanuel.pdf
- Fensholt, R., & Sandholt, I. (2005). Evaluation of MODIS and NOAA AVHRR vegetation indices with in situ measurements in a semi-arid environment. *International Journal of Remote Sensing*, 26(12), 2561–2594. https://doi.org/10.1080/01431160500033724
- G. Pypker, T., S. Tarasoff, C., & Koh, H.-S. (2012). Assessing the Efficacy of Two Indirect Methods for Quantifying Canopy Variables Associated with the Interception Loss of Rainfall in Temperate Hardwood Forests. *Open Journal of Modern Hydrology*, *02*(02), 29–40. https://doi.org/10.4236/ojmh.2012.22005
- Jones, R. (1968). Productivity studies on heath vegetation in southern Australia the use of fertilizer in studies of production processes. *Folia Geobotanica et Phytotaxonomica*, *3*(4), 355–362. https://doi.org/10.1007/BF02851815
- Kamble, B., Kilic, A., & Hubbard, K. (2013). Estimating crop coefficients using remote sensing-based vegetation index. *Remote Sensing*, 5(4), 1588–1602. https://doi.org/10.3390/rs5041588
- Lekula, M., & Lubczynski, M. W. (2019). Use of remote sensing and long-term in-situ time-series data in an integrated hydrological model of the Central Kalahari Basin, Southern Africa. *Hydrogeology*

- Journal, 27(5), 1541-1562. https://doi.org/10.1007/s10040-019-01954-9
- Lekula, M., Lubczynski, M. W., Shemang, E. M., & Verhoef, W. (2018). Validation of satellite-based rainfall in Kalahari. *Physics and Chemistry of the Earth*, *105*(January), 84–97. https://doi.org/10.1016/j.pce.2018.02.010
- Li, H. T., Brunner, P., Kinzelbach, W., Li, W. P., & Dong, X. G. (2009). Calibration of a groundwater model using pattern information from remote sensing data. *Journal of Hydrology*, *377*(1–2), 120–130. https://doi.org/10.1016/j.jhydrol.2009.08.012
- Lianghui, X. (2015). Wetland reconstruction by controlling water level in Aamsveen: the effects on variation of vegetation and nutrients. [Masters' Thesis]. https://pure.tue.nl/ws/portalfiles/portal/46984283/685278-1.pdf
- Liu, D., Chen, W., Menz, G., & Dubovyk, O. (2020). Development of integrated wetland change detection approach: In case of Erdos Larus Relictus National Nature Reserve, China. *Science of the Total Environment*, 731(August 2016), 139166. https://doi.org/10.1016/j.scitotenv.2020.139166
- Lopez, J. R., Erickson, J. E., Asseng, S., & Bobeda, E. L. (2017). Modification of the CERES grain sorghum model to simulate optimum sweet sorghum rooting depth for rainfed production on coarse textured soils in a sub-tropical environment. *Agricultural Water Management*, 181, 47–55. https://doi.org/10.1016/j.agwat.2016.11.023
- Miralles, D. G., Gash, J. H., Holmes, T. R. H., De Jeu, R. A. M., & Dolman, A. J. (2010). Global canopy interception from satellite observations. *Journal of Geophysical Research Atmospheres*, 115(16), 1–8. https://doi.org/10.1029/2009JD013530
- Mitsch, W. J., & Gossilink, J. G. (2000). The value of wetlands: Importance of scale and landscape setting. *Ecological Economics*, 35(1), 25–33. https://doi.org/10.1016/S0921-8009(00)00165-8
- Návar, J., & Bryan, R. B. (1994). Fitting the analytical model of rainfall interception of Gash to individual shrubs of semi-arid vegetation in northeastern México. *Agricultural and Forest Meteorology*, 68(3–4), 133–143. https://doi.org/10.1016/0168-1923(94)90032-9
- Niswonger, R. G. (2005). MODFLOW-NWT, A Newton Formulation for MODFLOW-2005.
- Nyarugwe, K. P. (2016). Effect of surface water management measures on a groundwater fed wetland [Masters' Thesis]. https://library.itc.utwente.nl/papers_2016/msc/wrem/nyarugwe.pdf
- Park, J., Baik, J., & Choi, M. (2017). Satellite-based crop coefficient and evapotranspiration using surface soil moisture and vegetation indices in Northeast Asia. *Catena*, *156*(April), 305–314. https://doi.org/10.1016/j.catena.2017.04.013
- Perry, C., Steduto, P., Allen, R. G., & Burt, C. M. (2009). Increasing productivity in irrigated agriculture: Agronomic constraints and hydrological realities. *Agricultural Water Management*, *96*(11), 1517–1524. https://doi.org/10.1016/j.agwat.2009.05.005
- Rientjes, T. H. M. (2016). Hydrologic modelling for Integrated Water Resource Assessments. *Lecture Book for Modules 9-10 Surface Water Stream, March*, 255.
- Running, S., Mu, Q., Zhao, M., & Moreno, A. (2019). *User's Guide NASA Earth Observing System MODIS Land Algorithm (For Collection 6*). 1–38. https://www.ntsg.umt.edu/project/modis/mod17.php
- Sophocleous, M. (2002). Interactions between groundwater and surface water: the state of the science. *Hydrogeology Journal*, *10*(2), 348–348. https://doi.org/10.1007/s10040-002-0204-x
- Teutschbein, C., & Seibert, J. (2012). Bias correction of regional climate model simulations for hydrological climate-change impact studies: Review and evaluation of different methods. *Journal of Hydrology*, 456–457, 12–29. https://doi.org/10.1016/j.jhydrol.2012.05.052
- Tian, J., Zhu, X., Wu, J., Shen, M., & Chen, J. (2020). Coarse-Resolution Satellite Images Overestimate Urbanization Effects on Vegetation Spring Phenology. *Remote Sensing*, *12*(1), 117. https://doi.org/10.3390/rs12010117
- Van Meter, K., Thompson, S. E., & Basu, N. B. (2016). Chapter 11 Human Impacts on Stream Hydrology and Water Quality. In J. B. Jones & E. H. Stanley (Eds.), *Stream Ecosystems in a Changing Environment* (pp. 441–490). Academic Press. https://doi.org/https://doi.org/10.1016/B978-0-12-405890-3.00011-7
- Wu, C., & Chen, W. (2020). Indicator system construction and health assessment of wetland ecosystem—Taking Hongze Lake Wetland, China as an example. *Ecological Indicators*, 112(June 2019), 106164. https://doi.org/10.1016/j.ecolind.2020.106164
- Wu, Y., Zhang, G., Rousseau, A. N., Xu, Y. J., & Foulon, É. (2020). On how wetlands can provide flood resilience in a large river basin: A case study in Nenjiang river Basin, China. *Journal of Hydrology*,

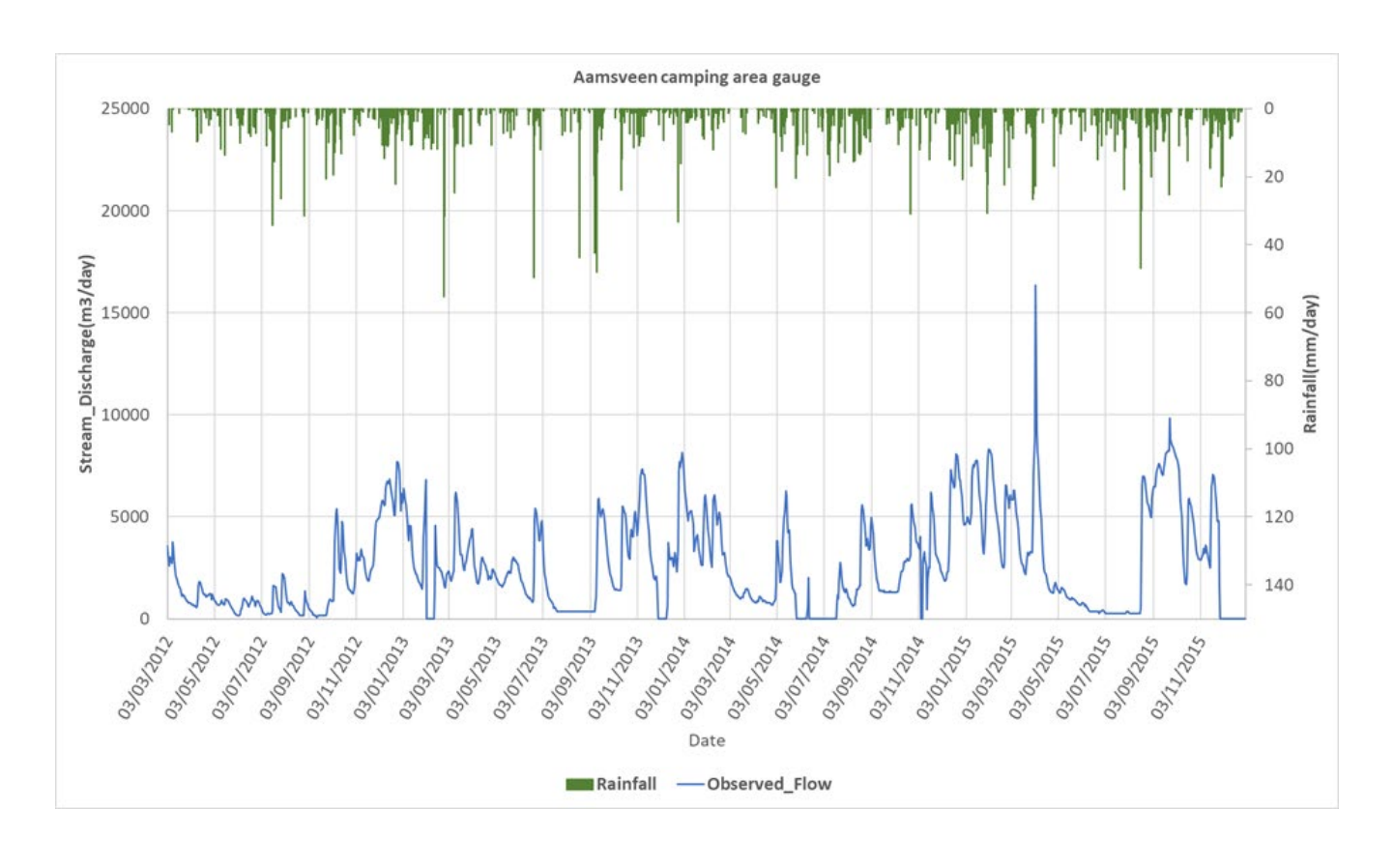
587(December 2019), 125012. https://doi.org/10.1016/j.jhydrol.2020.125012

Zedler, J. B., & Kercher, S. (2005). Wetlands resources: Status, Trends, Ecosystem Services, and Restorability. Annual Review of Environment and Resources, 30(1), 39–74. https://doi.org/10.1146/annurev.energy.30.050504.144248

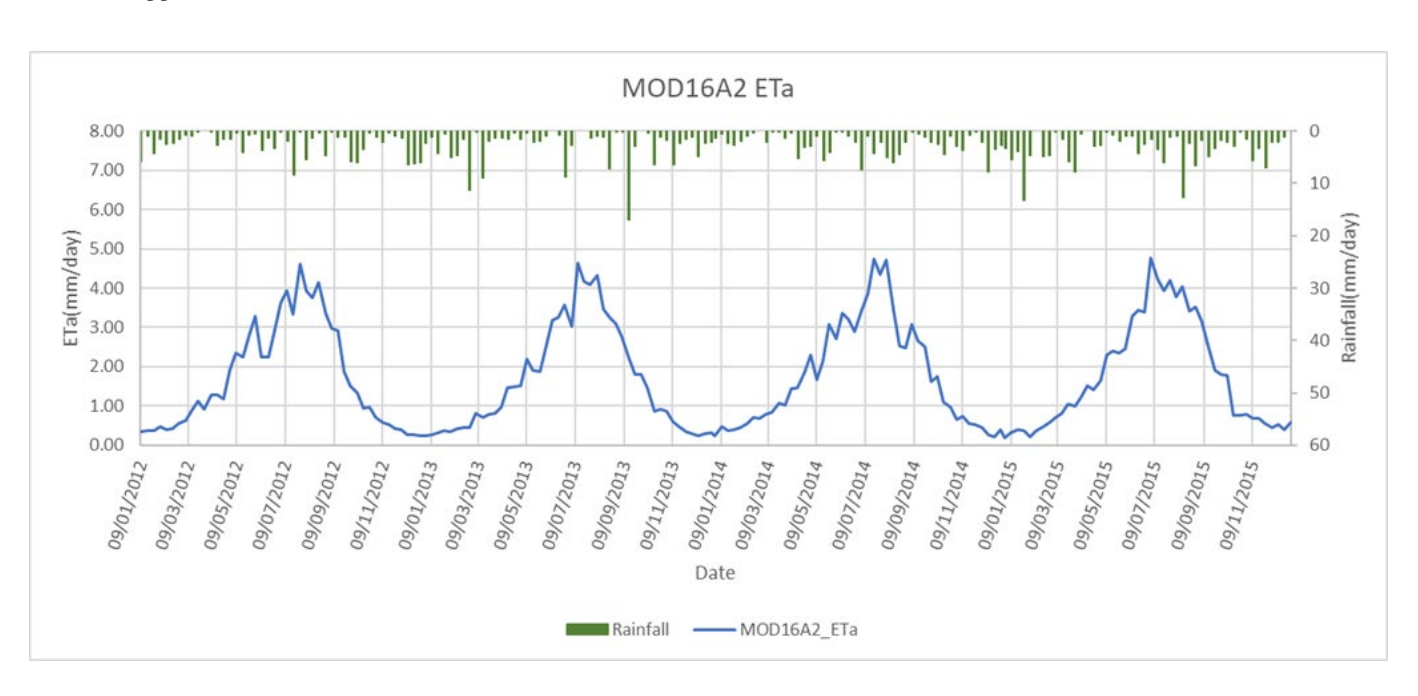
Appendix 1: Observed groundwater head for calibration



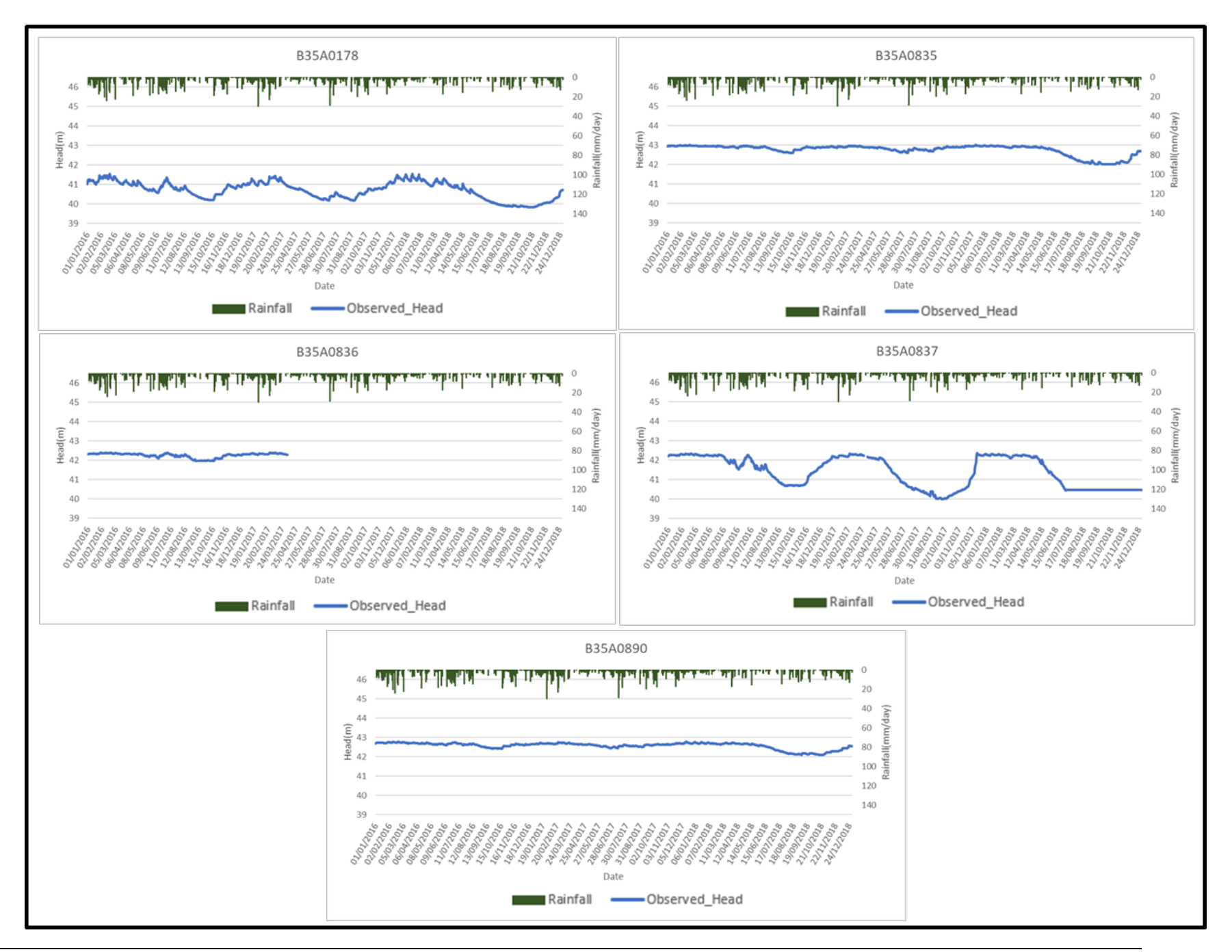
Appendix 2: Aamsveen camping area gauge



Appendix 3: MOD16A2 ETa (averages over 8-days periods)



Appendix 4: Observed groundwater head for validation



Appendix 5: MOD16A2 ET_a for validation

